The Structure-Property Relationships in Drying Polystyrene/Acrylic Latex Films

Ryan Seabright

Thesis submitted in partial fulfilment for the degree of
Doctor of Philosophy

The University of Sheffield,

Faculty of Engineering,

Department of Mechanical Engineering

2019

I.   Acknowledgments

Firstly I would like to thank my supervisor Prof. Patrick Fairclough for all his support over the last 6 years. Without his constant guidance, technical input and patience I would not be where I am today. I would also like to thank my second supervisor Dr. Candice Majewski who was always there to give me encouragement and valuable advice.

I'd like to thank AkzoNobel for providing funding for this project, without which no of this project would be possible. In particular I would like to thank Neal Williams and Ron Schmidt for the expert advice on all areas involving the project. I would also like to thank Martin Murray for his expertise in film cracking.

Thanks, should also go out to the Fairclough group as a whole and the numerous members that have helped me throughout my time in Sheffield. Thanks, should go to Dr. Christine Fernyhough for her help in the lab, I'd also like to thank Dr Antonio Bianco and Dr Tom Sydney for their help from the very start 6 long years ago. I'd like to also take time to thank the Physics contingency with special thanks going out to Dr Andrew Parnell for his help with numerous SAXS, AFM and Microscopy assistance. Dr Mike Weir, Dr Adam Washington and Dr Stephanie Burg should also get a mention for their invaluable physics advice during numerous group meetings. I'd also like to thank Kurt and Wendy for their assistance during my numerous ventures into the world of additive manufacture, albeit limited to the MakerBot

I'd also like to give special thanks to the motley crew of office D14: Ste Knox, Alec Shackleford, Rhys Williams, Luke Fox and Ryan Brown. My time in Sheffield would not have been the same without all the fun and games both in and out of the office.

Special thanks should go out to my family. If it was not for my Mother answering all of my 'Whys' as a child I'm not sure I would be so interested in science today. I'd also like to thank my Father who would admit that he is not the most 'book-smart' person but he is honestly the cleverest person that I know. Without the things that he has taught me I'm not sure I would be the man I am today.

Finally, I would like to thank Thomasin Mary Robinson, my amazing girlfriend, for her endless patience with me throughout my time doing my PhD. Without her support and words of encouragement I would not have been able to finish this.

II.   Abstract

This investigation initially set out to study the potential use of a number of additives as humidifying agents for the purpose of modifying the drying properties of water-borne paints. A gravimetric study was used to analyse the rate of evaporation during the early stages of film formation. A Styrene/Acrylic latex was used with varying concentrations of Pluronic PE9200, Methylcellulose *(MC)* and Hydroxypropyl Methylcellulose *(HPMC)*. It was found that the effect that the additives had on the rate of evaporation was small and, in comparison to the impact of humidity, negligible. Despite this, during this investigation it was observed that the cellulose-derived additives appeared to reduce levels of cracking. This phenomenon was investigated further using a number of techniques, in particular AFM, DMA and Optical Microscopy. Using these methods it was possible to observe how, unlike a conventional coalescent solvent such as Texanol™, the cellulose-derived additives appeared not to plasticise the latex, which raised the question as to how the additives were reducing cracking in the film. Having observed the lack of particle coalescence on the surface of the film, it was hypothesised that the cellulose-derived additives created a network that surrounded the latex particles enabling the formation of a crack-free film. In order to investigate this further, Small Angle X-ray Scattering *(SAXS)* was used to study particle packing within the film. As predicted, increasing concentrations of the cellulose-derived additives gave rise to increased particle spacing. This confirmed the presence of an additive network surrounding the particles, providing an alternative method for stress-relaxation other than cracking. Due to increasing legislative pressure to eliminate VOCs, coupled with heightened environmental and health concerns, the future use of cellulose-derived additives as a replacement for standard coalescent solvents should be the subject of further investigation.

III.   Table of Contents

IV.   Table of Figures

11

Chapter 1:   Introduction

Paint as a medium has evolved throughout history. Its importance primarily derived from a fascination in art and decoration; it is now used on a commercial scale. The composition of paint has necessarily evolved in parallel with its use. From as early as 32,000 B.P. (*Before Present*), humans used both pigments and dyes to create art.[1] One of the earliest examples of this comes from the Chauvet cave in the Ardèche valley located in the south of France. In this example of Upper Palaeolithic cave art, carbon derived from wood charcoal was primarily used to portray a number of different animal species. The image below (Figure 1:1) shows what is considered to be one of the best early examples of cave art in the world.[2] The image is part of the 'Horse' panel located in the Hillaire chamber of the aforementioned Chauvet cave; the image shows a painting of two rhinoceroses from a larger piece of art containing drawings of horse-like creatures as well as lions, mammoths and bison.[3]

Figure 1:1 – Shows a replica of cave art from the 'Horse' panel, located in the Hillaire chamber of the Chauvet cave located in the Ardèche valley in the south of France. (Image Available from: <https://www.ancient.eu/image/6350/panel-of-the-rhinos-chauvet-cave-replica/> [viewed 17th of September 2019] original image by Emma Groeneveld). The image shown is a depiction of two rhinoceroses painted using wood charcoal. Using radiocarbon dating of the charcoal from the original paintings, the age of the art is estimated to be over 30,000 years old.

Despite this being the earliest form of art, the materials used to create it are not those that we would recognise in modern decorative paints. The materials used by the ancient Greeks (*c. 2400 B.P*) are more familiar. In this period paints had been developed using a number of natural binders including honey, starch and most commonly tree or plant sap/gum. In a study conducted by Colombini et al. a number of paint samples from a Macedonian tomb were analysed using high-performance anion-exchange chromatography with pulsed amperometric detection (*HPAEC-PAD*). Using this technique a number of tree and plant gums were identified, including locust bean, guar, cherry and, most interestingly, acacia tree or 'Gum Arabic'. Paints based on the gum of the acacia tree are still used amongst artists today, forming the bases for most modern-day watercolour paints.[4]

Moving forward, the next noteworthy step in the development of modern paints occurred during the second industrial revolution (*c. 1860*). At this time the development of large machines and mass production meant that linseed oil was being produced on an industrial scale. This, alongside an abundance of pigment grade zinc oxide, allowed the first washable white paint to be produced. This paint was marketed as "Charlton White" and was sold ready-mixed, something that had previously not been achieved on a commercial scale. The company behind this product was the Averill Chemical Paint Company and was patented by their founder D. R. Averill in 1867.[5] In 1879 the Sherwin-William paint company filed a patent protecting the innovation of a resealable paint can.[6] This innovative technology enabled them to begin developing a reusable pre-mixed paint. Over a 10-year period a product was developed resulting in a paint that far exceeded other commercial paints on the market. In 1880 they had managed to formulate a product which they referred to as an "oil bound distemper"; this product was available in a number of different colours and was shipped globally.

Jumping forward a few years to 1906 is when we really start to see the development of waterborne paints as we know them today. Whilst working at Bayer AG, Fritz Hoffmann led a research group that was focusing on the commercialization of synthetic rubber, during the period from 1906 -1912

Hoffmann led his group to the filing of several key patents in this area, publishing a review of the work around this area in 1912.[7] One of the key piece of work that laid the foundations for modern waterborne paints was the invention of emulsion polymerisation of diene monomers that was carried out by Kurt Gottlob and Hoffmann.[8] This method is one of the key processes in the production of modern-day waterborne paints however, it was not until World War II when a shortage of linseed oil led to the increased use waterborne paints along with further development of synthetic lattices. It was reported that waterborne paint similar to PVA was being used in the manufacture of the German Tiger Tank, along with alternative waterborne paint technology for their military rolling stock.[9] In 1943 the USA led a collaborative project involving a number of universities and large companies to produce a synthetic latex that was not based on an isoprene but rather a mix of styrene and butadiene, however it was not until after the war that an architectural waterborne paint was commercially available. In 1948 Glidden's "Spread Satin" came to market as the first commercial styrene-butadiene architectural paint, selling nearly 500,000 litres in its first year on sale with total sales reaching over 15 million litres just two years later.[10] In 1964 Eastman Chemical company began to produce the paint additive Texanol™ on an industrial scale. Texanol™ is added to paint as a coalescence aid and allowed the use of waterborne latex paints over a much broader range of environmental conditions.[11]

In recent years the global paint sector has experienced significant growth compared to the "early era" of waterborne paints, with an average rise of 5.4% annually over the last decade. This resulted in the annual sales volume in 2013 exceeding 40 Million tonnes, worth over 100 Billion U.S. dollars. Growth in the paint sector has been driven by increased demand as a result of the continued recovery of the global economy. With this recovery came renewed industrialization, in particular in the Asia-Pacific region, with 48% of global sales in 2013 accounted for in this region. However, despite this constant growth, the paint sector has had a number of challenges to overcome. In particular as a result of the EU directive 2004/42/CE which has set out target levels of volatile organic compounds (*VOCs*) in paints and coatings.

1.1. Modern Legislation Affecting Water-Based Paint

Due to a number of VOCs in use in the UK paint and coating sector being either toxic and/or environmentally damaging, the UK government implemented the aforementioned EU directive in 2005 under "Volatile Organic Compounds in Paints, Varnishes and Vehicle Refinishing Products Regulations 2005" (S.I. 2005/2773). These regulations provided for the implementation of a phased incentive: the first phase set upper limits on the levels of VOCs allowed in products, the second phase further reduced these limits. The first phase was implemented in 2007, the second followed in 2010. This initiative to eliminate VOCs in paints and coatings has resulted in research and development into the area of water-borne coatings. In order to understand the challenges that arise in as a result of the enforced reduction of VOCs, the following section sets out the definition of a VOC and explains the extent to which the directive 2004/42/ CE requires a reduction in their use.

1.1.1. What Defines a VOC?

As previously mentioned, directive 2004/42/CE requires the reduction in VOCs in most decorative paints and varnishes. In order to control the levels of VOC in these systems it was necessary to first decide what constitutes a VOC. According to the directive 2004/42/CE the following two statements outline the definition of a VOC:

- "*Volatile organic compound (VOC) means any organic compound having an initial boiling point less than or equal to 250 °C measured at a standard pressure of 101.3 kPa.*"
- "*Organic compound' means any compound containing at least the element carbon and one or more of hydrogen, oxygen, sulphur, phosphorus, silicon, nitrogen, or a halogen, with the exception of carbon oxides and inorganic carbonates and bicarbonates.*"

The levels of VOC that allowed in a paint or coating, in other words the VOC content, are also defined as follows:

- "'*VOC content' means the mass of volatile organic compounds, expressed in grams/litre (g/l), in the formulation of the product in its ready to use condition. The mass of volatile organic compounds in a given product which react chemically during drying to form part of the coating shall not be considered part of the VOC content.*"

The final thing to note regarding VOCs in paints and coatings is that the levels of VOC permitted within a system is dependent on the system itself. The biggest factor that effects the amount of permitted VOC is whether the system is solvent-borne (SB) or water-borne (WB) and then where the system is used and on what type of substrate. Table 1:1 shows a number of different systems and the restrictions on VOC content for both, phase I and phase II of 2004/42/CE.

Table 1:1 – Permitted VOC Levels in Various Classes of Paints

System	Type	Phase I (g/l)	Phase II (g/l)
Interior matt for walls and ceiling	*WB*	*75*	*30*
	SB	*400*	*30*
Interior gloss for walls and ceiling	*WB*	*150*	*100*
	SB	*400*	*100*
Exterior walls for mineral substrate	*WB*	*75*	*40*
	SB	*450*	*430*
Exterior/Interior trim and cladding for wood, metal and plastic	*WB*	*150*	*130*
	SB	*400*	*300*

On reviewing Table 1:1 it can be seen that in phase I of the directive there is a clear difference between the permitted levels of VOC in WB and SB coatings regardless of the substrate and application. In contrast, at phase II it can be seen that for interior wall and ceiling paints the level of permitted VOC for both SB and WB systems are the same. This essentially means that for all large surface area interior applications such as walls and ceilings, coatings are required to be water-borne. In contrast, exterior and trim paints are currently not required to have as much of a reduction in VOCs, although with the current trend in VOC reduction, along with the possible health and environmental effects of VOCs, many manufactures are drastically reducing VOC levels in these systems in any event. This trend towards water-borne paints has driven the development of a pre-existing technology which relies on the use of a latex dispersion. Latex is most commonly associated with the non-vulcanised rubber material used to make rubber gloves. However, it gets its name from the raw material used in their production - natural rubber latex. Natural rubber latex is the sap of the *Hevea brasiliensis* plant, more commonly known as the rubber tree. This product is a milky white liquid that is made of polymer microparticles suspended in an aqueous medium. Latex can also be produced synthetically, this allows the properties of the polymers to be tailored for the desired application.

Materials, such as a latex, that are made of two or more immiscible components mixed on a microscopic level are called a colloid. In the next section colloids will be discussed in order to provide a sufficient background to support the discussion of how latex can be used to produce a system that is applicable for use in water-borne paints.

1.2. What is a Colloid?

A colloid is a heterogeneous mixture of one material dispersed within another. In general for a material to be classified as a colloid, the particulate size needs to be below 1000 nm and larger than 10 nm - more typically around 100 nm. As mentioned colloids are typically made of a mixture of two different materials: the dispersed phase and the dispersion medium. Colloids can be subdivided into a number of different classes depending upon the state of these two materials. Table 1:*2* provides a full list of all the colloid classes along with an example of each.[12]

Table 1:2 – Different Classes of Colloid with Examples

		Dispersed Phase		
		Gas	*Liquid*	*Solid*
Dispersion Medium	*Gas*	*None* *All gasses are miscible*	*Liquid Aerosol* *Fog – Water dispersed in air*	*Solid Aerosol* *Smoke – Soot Particles dispersed in air*
	Liquid	*Foam* *Whipped Cream – Air dispersed in cream*	*Emulsion* *Milk – Butterfat globules dispersed with an aqueous medium*	*Sol* *Ink – Solid Pigment dispersed within a liquid medium*
	Solid	*Solid Foam* *Meringue – Air dispersed in dried egg albumin*	*Gel* *Jelly – Water dispersed within a Gelatine network*	*Solid Sol* *Opal – Silica spheres arranged as colloidal crystal*

.

In this section there will be a focus on two classes of colloid: Emulsions and Sols. The reason being that modern paint technology falls under these classifications. Whilst they are not relevant to this review, the other classes of colloids are in themselves an interesting area of discussion. If you are interested in further reading into the other areas of Colloid Science the book "Introduction to Colloid and Surface Chemistry" by Biggs *et al.* provides a good starting point.[13]

As previously mentioned, the typical size of a colloidal particle is around 100 nm. It is the small particulate size of colloids that result in most, if not all, of their interesting properties. At an interface between materials, molecules can behave differently to the molecules in the bulk of the material. If one imagines a theoretical cube of solid material (*Solid A)* with sides of 1 cm, the surface area and volume of the cube would be 6 cm^2 and 1 cm^3 respectively. If Solid A is mixed with a liquid material (*Liquid A)* the properties would be governed by the bulk properties of each constituent material. If Solid A is divided into individual cubes with sides of 100 nm (*A typical size for a colloidal particle*) it creates a new material (*Solid B*). By adding the resulting Solid B to Liquid A this forms a mixture with vastly different properties. Changes in the property of the material arise as a result of the drastically increased surface area of the solid/liquid interface. In the first example the surface area to volume area of Solid A is 6 meaning that any interactions between Solid A and Liquid A would not have any noticeable influences on the properties of the material. However, in the second example the surface area of Solid B is 60m^2 this results in a surface area to volume ratio of 6x10^5. With such a large interface any molecular interactions between Solid B and Liquid A dominate the overall properties of the material.

The following section comments on how the properties of colloidal systems, in particular emulsions and sols, are affected by the interactions at these interfaces, and how these interactions ultimately define the properties of the system.

1.3. Colloidal Physics

Emulsions and sols are both comprised of small particulates dispersed within a liquid medium. Due to the inherent properties of these colloidal systems, they are thermodynamically unstable with respect to the bulk liquid phase. This instability can be expressed thermodynamically by the change in the Gibbs free energy of the system (dG) as the surface area of the colloidal system (dσ) changes at constant temperature and pressure. Combining these terms to create an expression yields the following:

$$dG = \gamma d\sigma$$

$(\ 1\ )$

Where γ is the interfacial surface tension, studying this expression, dG < 0 if dσ < 0; therefore, decreasing the surface area in the colloid through particle coalescence creates a more thermodynamically stable system. Therefore, in order for colloids to exist they must be stabilised.

Colloidal stability is governed by the total interparticle potential energy (V_{tot}). V_{tot} can be expressed as the sum of the individual components that make up the total potential energy within the system; this is shown below.

$$V_{tot} = V_{vdW} + V_{elec}$$

$(\ 2\ )$

In this expression V_{vdW} is the attractive potential energy caused by the long range Van der Waal interactions. V_{elec} is the repulsive electrostatic potential that results from the interactions between particles of like charge. These first two terms in equation (2) make up part of the DLVO theory, as developed by Derjaguin and Landau, with Verwey and Overbeek in the 1940s. Although this theory does not provide an extensive model for the stability of colloids, it will provide an understanding that will allow us to discuss the majority of cases we encounter.

The first term of equation (2) describes the attractive Van der Waal interaction energy. This attractive force is always present between two like particles. Van der Waal interactions are dependent upon both the surface of the particle and the media of suspension. We can define the Van der Waal attraction using the following expression:

$$V_{vdW} = -\frac{Ar}{12x}$$

(3)

In the above expression x represents the separation between the particles surfaces, r is the particle radius and A is the Hamaker constant.

The theory of electric double-layers forms the basis for the second term in equation (2). Below is the expression for the interaction energy of two hard spheres.

$$V_{elec} = 2\pi\varepsilon\varepsilon_0 r\zeta^2 e^{-kx}$$

(4)

Where ε is the dielectric constant of the dispersion medium, ε_0 is the vacuum permittivity, r is the radius of the particle, ζ is the zeta potential and k is a function of the ionic concentration. In relation to the value k, k^{-1} represents the Debye screening length. The Debye screening length is the distance from a particle where the electrostatic force is significantly reduced. It can be seen as x approaches the Debye screening length, the exponent tends towards e^{-1}. By plotting the above two interaction energies (V_{vdW} and V_{elec}) we can combine the two to produce a graphical representation of equation as a function of particle separation Figure 1:2.
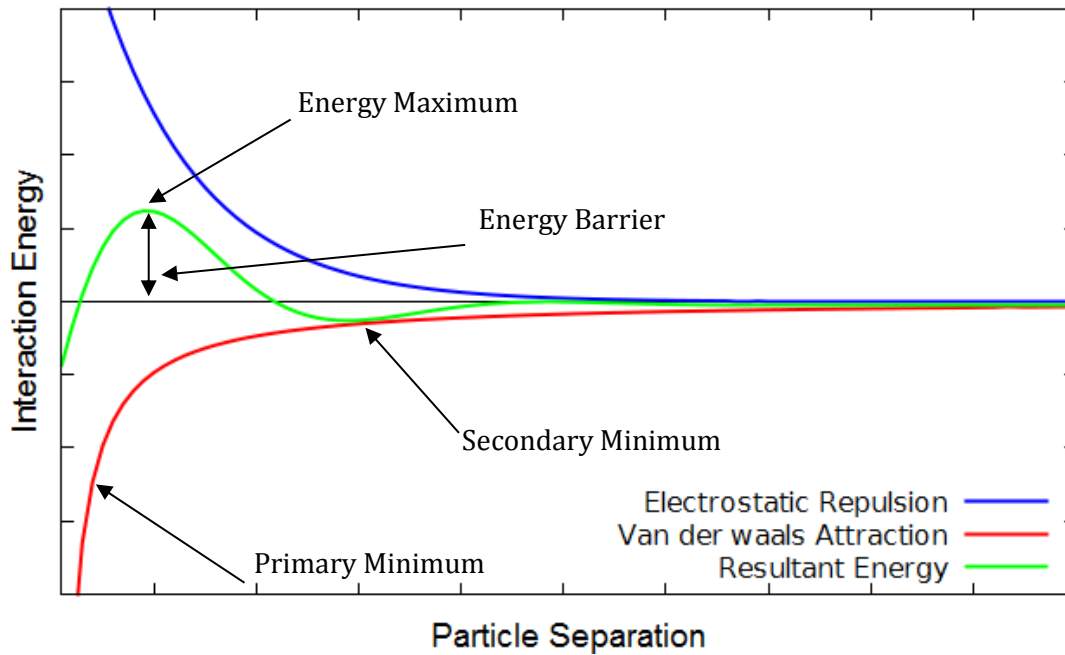
Figure 1:2 - Schematic illustration of the total energy curve as a result of the combination of electrostatic repulsions and Van der waals attractions. The main features of the energy profile have been labeled. All curves represent theoretical data produced from the basic DLVO equations.

It can be seen from the graphical representation of the interaction energies that at low interparticle separation the dominating force is Van der Waal interactions, resulting in a strong energy minima. However at larger separation the dominant force becomes the electrostatic interaction. From the above plot it can clearly be seen that there are two distinct energy minima. The first, as previously mentioned, is due to the dominance of the Van der Waal interactions at close particle separation, when particles enter this minimum they are said to have coagulated, due to the low energy state of this primary minimum this is typically seen as an irreversible process. The secondary minimum usually arises as a result of increasing ionic strength of the dispersion medium; altering ionic strength of the dispersion medium has a large effect on the stability of the colloidal system. Increasing the ionic strength of the dispersion medium screens the surface charge of the particles. This screening effect means that the relative influence of the Van der Waal interaction increases; as is shown in Figure 1:3.

28
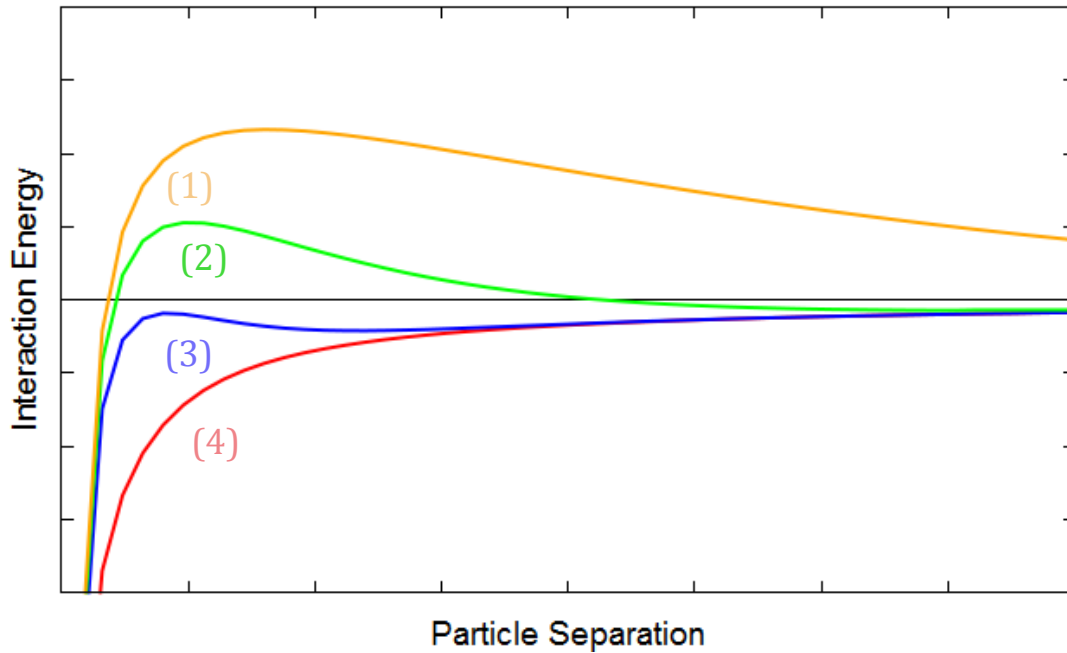
Figure 1:3 - Illustrates the effect on the potential energy curve with increasing salt concentration. With curve (1) being the lowest salt concentration through to (4) being the highest. All curves represent theoretical data produced from the basic DLVO equations.

When Particles enter this secondary minimum they are said to have *flocculated*, meaning that particles are weakly bound together. However, with the addition of a small amount of energy e.g. stirring, these clusters of particles can be redispersed. Figure 1:3 shows how the interaction energy changes as the ionic strength of the dispersion medium is increased. Curve 1 and 2 illustrate how the secondary minimum develops with increasing ion concentration. Curve 3 has gone through the *Critical Coagulation Concentration,* at this point the energy barrier has become zero and the particles can enter the primary energy minimum, resulting in the colloid becoming unstable. Finally curve 4 illustrates the potential energy curve when the ion concentration is so high that the only noticeable force acting on the particles is Van der Waals, this results in an unstable colloid in which rapid coagulation occurs. This phenomenon can be seen in nature in the formation of river deltas. As a river runs its course to the sea it picks up very small particles of clay and dirt through erosion. These particles are so small that they are considered colloidal and form stable suspensions. However, as the river nears the sea the ionic concentration of the water increases. As the water reaches the critical coagulation

concentration the colloidal clay and dirt become unstable and coagulate. As the size of these coagulants reaches a certain size they undergo sedimentation, hence forming a river delta. One of the best examples of this is the "bird-foot' delta at the estuary of the Mississippi river in the continent of North America. In order for liquid paint to be converted into a dry film, it must undergo a number of transitions. Unlike the formation of river deltas, where the formation is driven by changing ionic strength, the formation of colloidal films is primarily driven through the evaporation of water. In the next section this process, along with a number of factors that affect film formation, will be discussed.

1.4.　　　An Introduction to Latex Film Formation

Due to the current relevance of latex film formation in a number of different industries, including inkjet printing and the paint and coating sector, research into the factors affecting latex film formation is at an all-time high. Figure 1:4 shows the amount of citations each year with the topic "Latex Film Formation". Initial research in this field began with the work carried out by Dillon *et al.* in 1951.[14] Dillon *et al.* stated that film drying and particle deformation/sintering occur separately and that sintering of the particles is driven by polymer-air interfacial tension. In 1956 Brown observed that both evaporation and film formation finish at the same time. Therefore, he stated that both the water-air and polymer-water interface play a key role in latex film formation.[15] By the 1960s Sheetz *et al.* had introduced a model of film formation driven by osmotic pressure.[16] Sheetz noted that horizontal drying fronts could be seen when films of polymer particles dried. The physics behind this was further studied by Deegan *et al* in the late 1990s.[17] Deegan provided an explanation to the "coffee-ring effect", where a drying drop of coffee results in a ring like deposit forming. He based his explanation on the capillary flow created within a system as water evaporates, hence driving the suspended coffee particles to the edge of the droplet. In the work of Sheetz it was these capillary forces that created the horizontal drying front in the film. Since this work was carried there has been a number of models and theories created to explain a wide range of phenomena in this area of research. Before discussing these more complex models a basic model of film formation needs to be discussed.
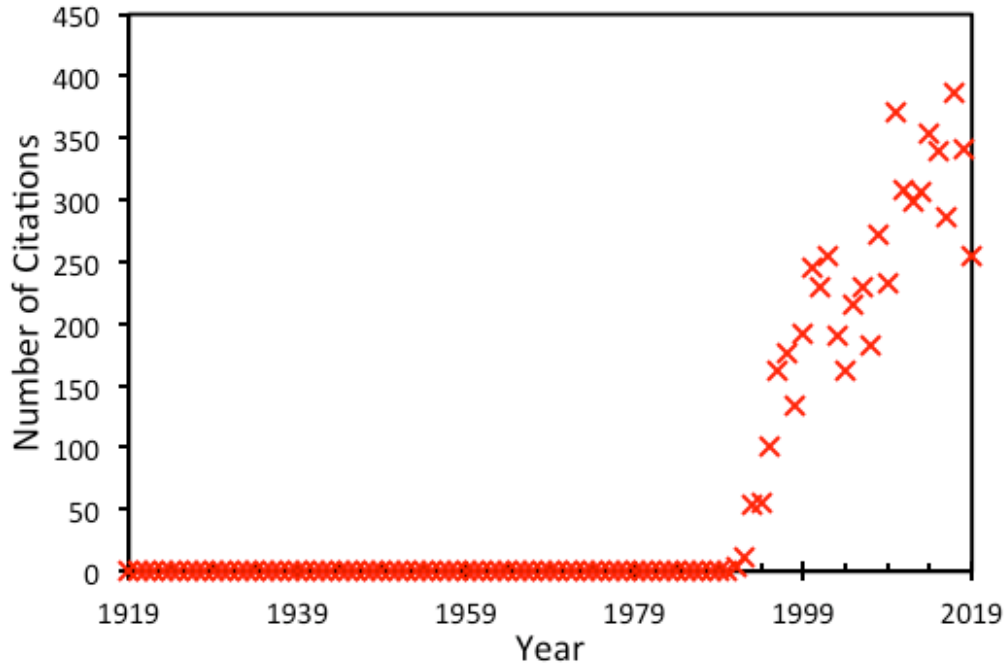
Figure 1:4 - Shows the number of citations each year since 1919 on the topic "Latex film formation". It can be seen that in recent years this area of research is at an all-time high. Citation report produced by 'Web of Science'.

At its most basic colloidal film formation, and hence latex film formation, can be split into three stages: drying, deformation and diffusion. For ease of explanation these stages have been split into distinct steps, in reality they can overlap. Variations in this film formation process can cause dramatic difference in both the property and appearance of the final film. Figure 1:5 has been produced to facilitate the explanation of the different stages of latex film formation and how changes in film formation can influence the properties of the final film.
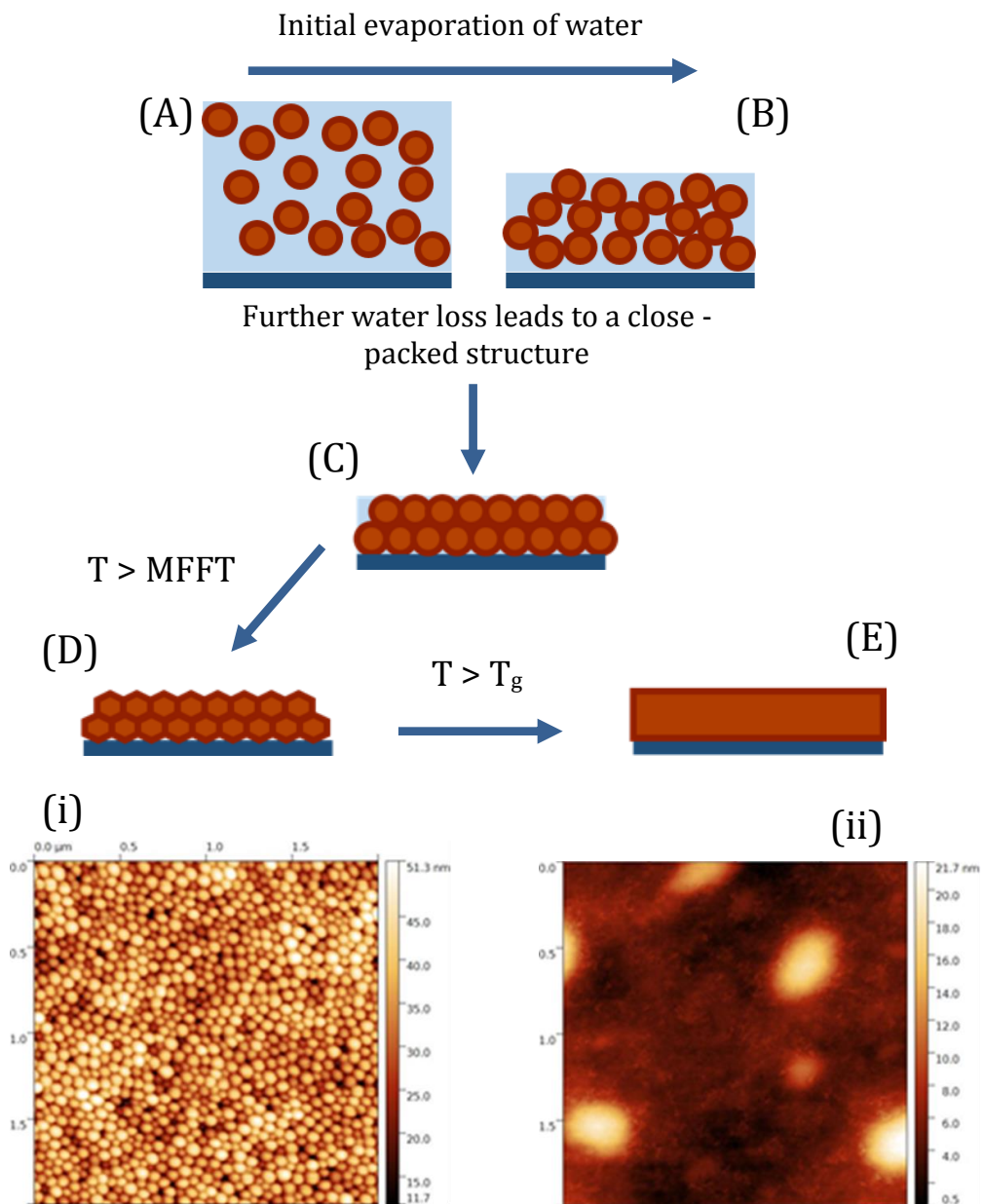
Figure 1:5 – (A) – (E) gives an overview of the latex film formation. (i) and (ii) shows an AFM image of a film at both stage (D) and Stage (E) of the film formation process. The first stage of latex film formation involves the evaporation water from the dilute latex dispersion, (A) – (B). As the volumes concentration of particles increases then they interact more, until eventually they form a close packed array of particles,(C). If the particles are soft enough then they will begin to deform and through polymer interdiffusion the particles will coalesce, (D). Finally if the particle is above its T_g then significant polymer interdiffusion can occur and the system will form a homogeneous film.

The first step in latex film formation starts with the latex in its most dilute state (Figure 1:5 – A). When the latex is applied to the substrate the first thing to occur is the evaporation of water. During this step the evaporation of water causes the latex to become more concentrated. There are a number of things that can affect the rate of evaporation during this step, these factors include both temperature and relative humidity. These factors will be discussed in greater detail, along with the factors that affect the other steps, in a later section. As the solution becomes more concentrated the interactions between the particles begin to increase (Figure 1:5 – B) and their movement becomes more restricted. As more water is lost from the film the particles begin to pack further. However, the drying of the latex film is typically not homogeneous. As previously mentioned, the coffee ring effect induces a drying front to form. After the drying front has passed, the particles begin to consolidate into a packed array of particles (Figure 1:5 – C). The type of particle packing is dependent on a number of factors. Typically the particles will exhibit random close packing with a volume fraction of 0.64, however, if the rate of drying is slow enough, the particles can form a colloidal crystal - a regular array of ordered particles.[18,19]

Further progression of the film formation is dependent on the properties of the particles themselves. If the particles are non-deformable then the film will be fragile and brittle due to the low adhesion between particles. If the particles are soft then after stage C the particles can begin to deform and coalesce (Figure 1:5 – D). An AFM image of a film that has begun to coalesce is shown in Figure 1:5 – i. During the deformation the inter-particle voids shrink, this reduces the light scattering within the film and hence the film becomes more transparent. Due to this deformation the film also has more resilience to cracking. The temperature above which the film exhibits no cracking can be defined as the minimum film formation temperature (MFFT). This temperature is one of particular importance to the paint and coatings sector, as a film must be formed above its MFFT to provide the desired barrier properties required in its application.

If the particles in the film have a T_g that is below the ambient temperature then the film can form a homogeneous structure, this is shown in Figure 1:5 – E. An

Atomic Force Microscope *(AFM)* image of a film that has formed above its T_g has also been shown in Figure 1:5 – ii. This homogeneity is important for both the barrier properties and the final appearance of the film. In the literature there are a number of useful reference books and reviews that cover all areas of latex film formation (Routh 2013, Keddie and Routh 2010, Steward 2000 and Keddie 1997).[20–23]

In the next section the first stages of film formation will be discussed, Figure 1:5 - A – C, the stages involving the loss of water. In later sections the rest of the film formation will be discussed in greater detail.

1.5.   Drying of Latex Films

As mentioned in section 1.4 the first stage of film formation involves the evaporation of water from the dilute latex. The rate at which water evaporates from a latex film can be affected by a number of factors. The main factor that affects the rate of evaporation in paint is humidity. Temperature increases the rate of evaporation but it also alters film formation in later stages - its effect will be discussed later in the chapter. Before discussing the science behind the evaporation of both pure water and in turn water form latex dispersions, humidity and humidity variation across the UK will be discussed.

1.5.1.   Humidity and Humidity Variation Across the UK

The Earth's atmosphere is composed of 78% Nitrogen 21% Oxygen and 1% trace gasses including CO_2, Argon and Methane. Alongside these gases, water vapour also makes up part of the earth's atmosphere. The concentration of water vapour is unique as concentration varies from 0-4% of the Earth's atmosphere depending on the time of year, time of day and location. Cold regions such as the Antarctic will typically maintain less than 1% water vapour whereas in the tropics there will typically be around 4% atmospheric water vapour year round.

The amount of water vapour in the atmosphere is called the *Humidity (H)*. The amount of water vapour that the atmosphere can hold depends on a number of factors, such as temperature and atmospheric pressure. Therefore looking at the temperature and pressure of the system we can predict the maximum amount of water vapour that could be present in the atmosphere. Comparing this maximum value to the actual amount of water vapour gives the *Relative Humidity (RH)* of the system. To be more exact Relative Humidity can be defined as;

$$RH = \frac{p_{H_2O}}{p^*_{H_2O}}$$

(5)

Where p_{H_2O} is the partial pressure of water vapor in the atmosphere and $p_{H_2O}^*$ is the equilibrium vapour pressure of water just above flat surface of water at any given temperature. Although this gives a fraction *RH* is typically quoted as a percentage.

The rate of evaporation of water is directly affected by the humidity of the environment. This phenomenon can be felt when trying to keep cool in humid conditions. The human body uses the evaporation of sweat to regulate body temperature; the evaporation of water actively cools the body during exercise or in hot climates. However, in high humidity the rate of evaporation is retarded, hence the body struggles to maintain a constant temperature.

1.5.1.1.　　Humidity Variation in the UK

Relative humidity varies across the UK with both seasonal and geographical factors affecting the observed humidity values. In order to gain a better understanding of the humidity variation observed across the UK, seasonal maps available on the MET office website were studied (http://www.metoffice. gov.uk/public/weather/climate/maps). Looking at Figure 1:6 it can be seen that there is a wide variation caused by the geographical location across the UK. Typically rural coastal regions have the highest recorded humidity, with urban areas experiencing the lowest recorded values, with clear regions of lower humidity observed around London, Birmingham and Manchester.
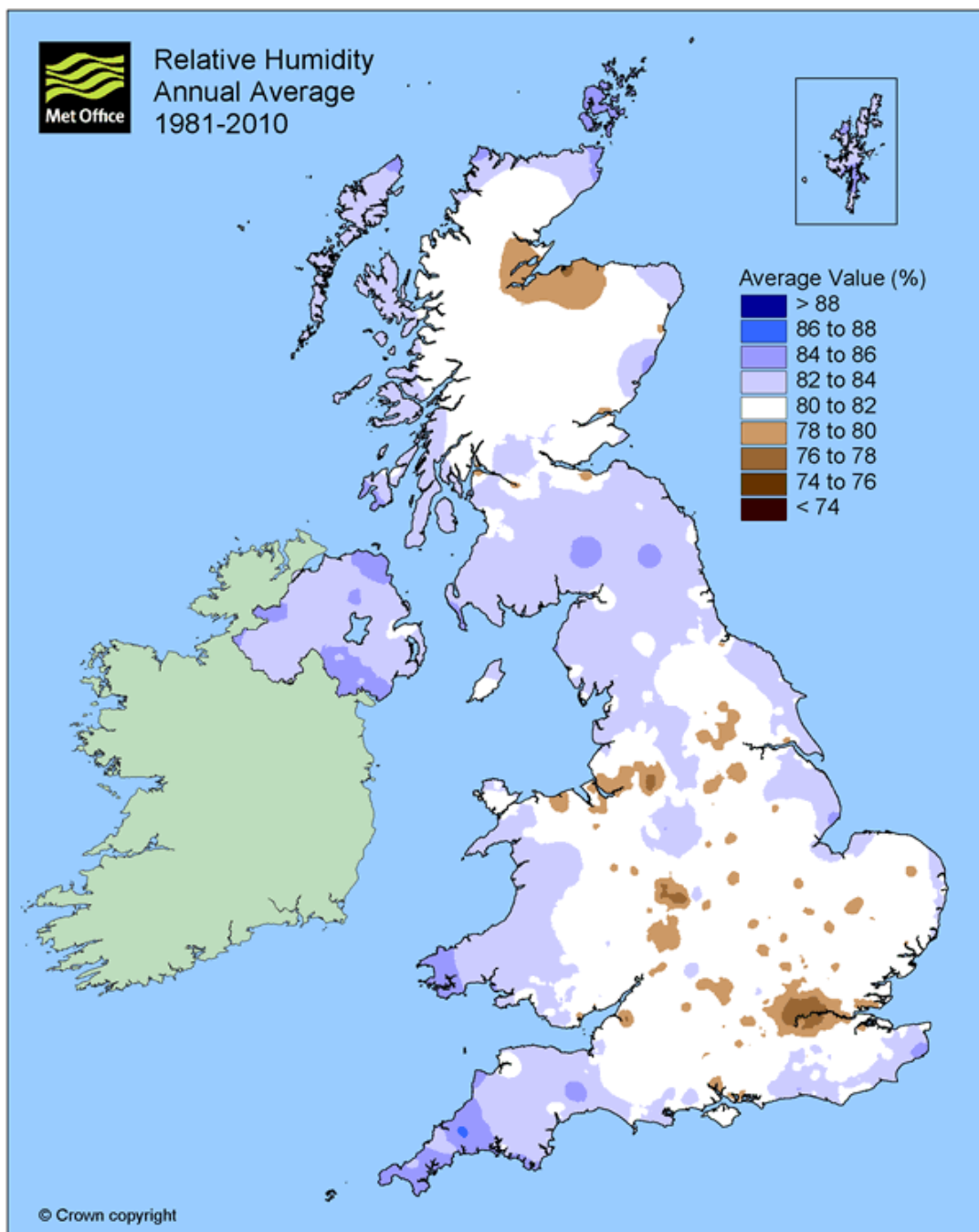
Figure 1:6 – Shows the annual average humidity in the UK. (Image available from: <http://www.metoffice. gov.uk/public/weather/climate/maps> [accessed 16th of September 2019]. It can clearly be se that urban areas such as London, Birmingham and Manchester the average humidity is lower than in rural areas in particular coastal rural areas such as Cornwall and the Pembrokeshire coastline.

of relative humidity on a shorter time scale is of greater interest to this investigation. In order to investigate the fluctuations in atmospheric humidity on a shorter time scale, MET office data on the daily average humidity at 4 locations across the UK was obtained. The weather stations used were London – St James Park, Plymouth, Sheffield (Leek) and Edinburgh (Cairnwell). This data is presented below in Figure 1:7.
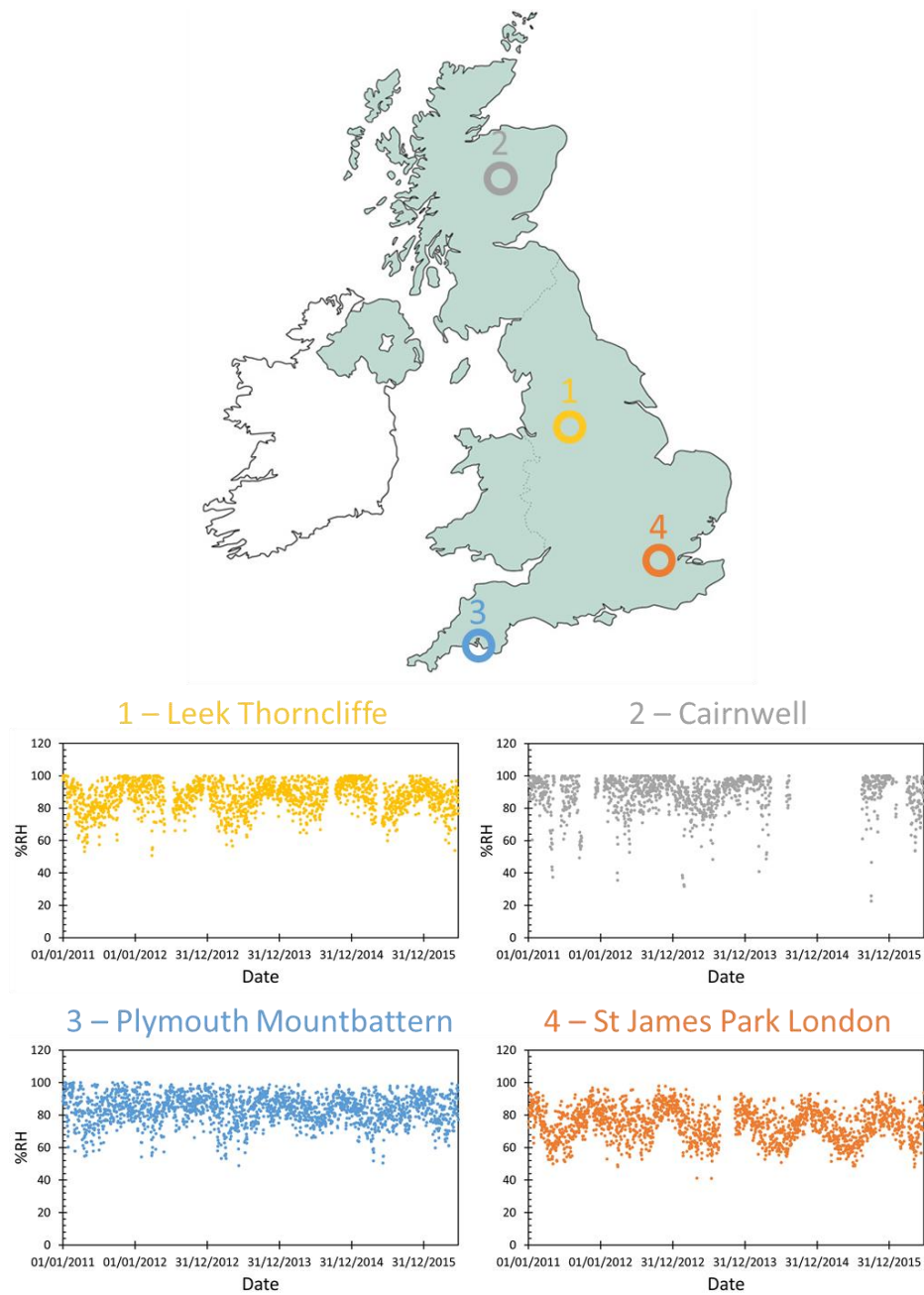
Figure 1:7 - Shows the daily humidity fluctuation across a number of different weather stations in the UK from 2011 – 2016. Data supplied by the MET office.

Looking at the data presented in Figure 1:7. we must first note that the gaps in the data are caused by the affiliated weather stations losing the ability to collect data for various reasons. Looking at the daily averages it can clearly be seen that there are seasonal fluctuations in humidity, with London – St James Park showing the strongest cyclic trend in recorded relative humidity across the 5-year period. Despite this seasonal trend, significant, random fluctuations do occur from day to day. The humidity varies from around 60 %RH up to 100 %RH. This fluctuation in humidity could cause the rate of evaporation of a water-borne paint to vary drastically. Having said that, these values derive from a weather station. Although this data provides a good indication of the possible range of humidity that may be experienced in the UK, interior paints are exposed to different conditions due to their use within the home. The humidity in a house is bound to vary from the humidity of the atmosphere. In order to explore the humidity variation that an interior paint may be exposed to, the humidity and temperature of a number of houses across the UK has been monitored. The humidity and temperature distributions over a 3 month period, for a three bed bungalow on the south coast has been displayed in Figure 1:8.
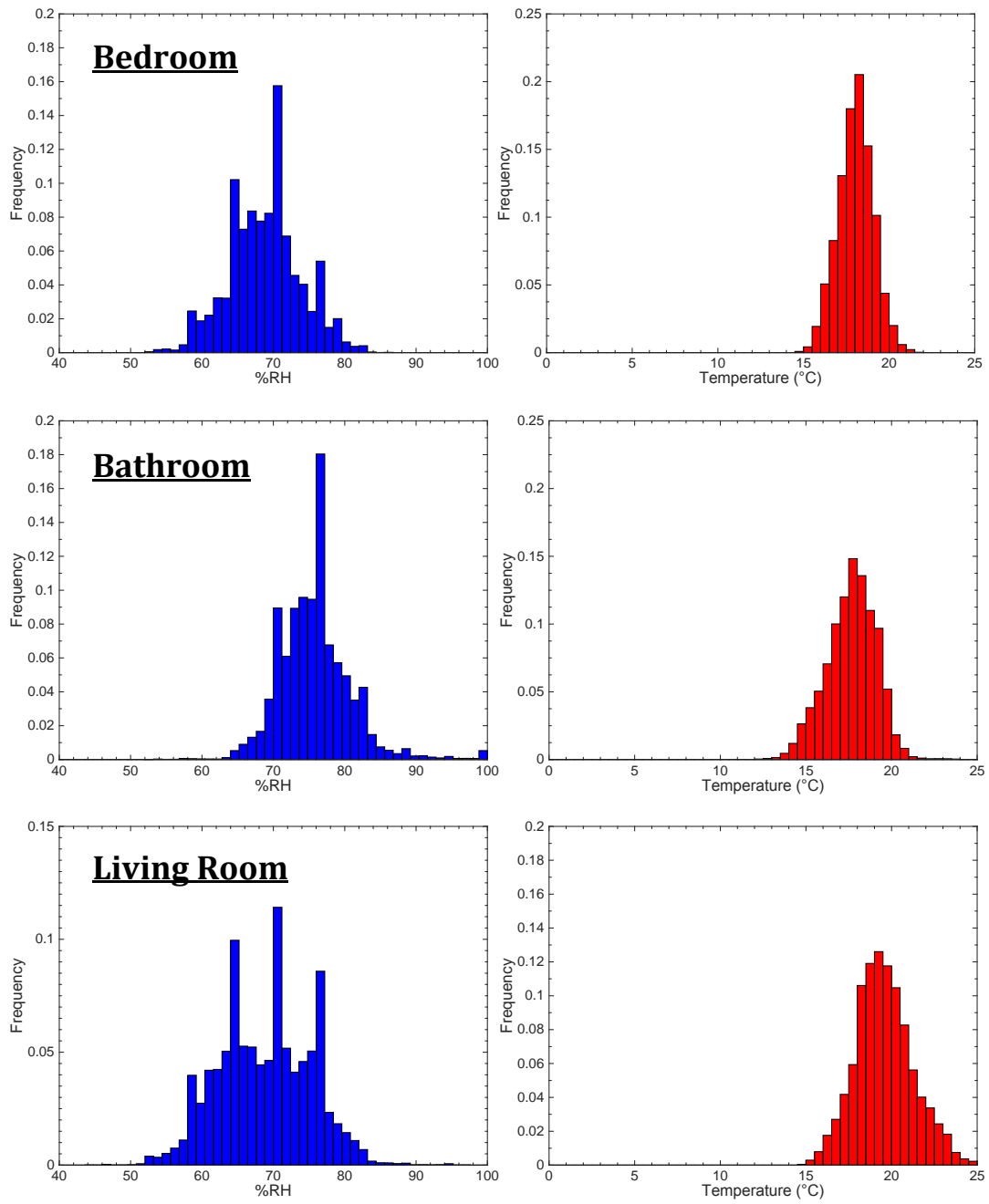
Figure 1:8 – Shows histograms of the hourly humidity and temperature values for a 3 bed bungalow in Bournemouth over a three month period from November 2017 to March 2018.

On reviewing the histograms in Figure 1:8 it can be seen that the recorded humidity values measured inside a house are typically lower than atmospheric humidity. The range of humidity observed is around 40 %RH from around 50 %RH to 90 %RH. This data along with data from the other two houses monitored will be used when selecting the desired experimental parameters later on in this thesis. As previously mentioned, the level of humidity directly impacts the rate of evaporation during the first stage of film formation. Before evaporation of water from a latex film is examined, evaporation of pure water will be briefly discussed.

1.5.2.   Evaporation of Pure Water

The evaporation rate of water *(E)* can be expressed either by of mass per unit area of surface or, in some cases, as a velocity *(Ė)* representing the distance that the surface recedes per unit time. $\dot{E}$ can easily be calculated using the below relationship:

$$\dot{E} = \frac{E}{\rho}$$

(6)

Where ρ is the density of the liquid. Hence in the case of pure water where the density is 1 g cm^{-3} the calculation is trivial. The evaporation rate of a pure water system is related to the difference in $p^*_{H_2O}$ and p_{H_2O} through the below equation:

$$E = k_m(p^*_{H_2O} - p_{H_2O})\frac{M_{H_2O}}{RT}$$

(7)

Where k_m is the mass transfer coefficient, M_{H_2O} is the molar mass of water. Since we have already established a relationship between *RH*, $p^*_{H_2O}$ and p_{H_2O} we are able to rearrange the above equation to put it in terms of RH. This equation is shown below:

$$E = k_m\, p^*_{H_2O}\,\frac{(100 - RH)}{100}\frac{M_{H_2O}}{R\,T}$$

(8)

From the above equation, it is apparent that we can alter the rate of evaporation by changing either the *RH* or the temperature of the system. However, one less

obvious change that can be made to alter E is to alter the airflow of the system. If we imagine a boundary layer of thickness L_b above the liquid surface in which the partial pressure varies linearly from $p_{H_2O}^*$ to p_{H_2O} across its thickness, Figure 1:9, under these conditions the mass transfer coefficient can be defined with the below equation:

$$k_m = \frac{D_{vap}}{L_b}$$

(9)

Where D_{vap} is the diffusion coefficient of water through air, if we then consider the above statement in which airflow is increased in the system we can imagine that with an increase in airflow the boundary layer above the water could be altered. Therefore altering L_b would result in a change in k_m and hence altering the evaporation rate, E. Although the work of Croll has shown that in some cases the initial rate of evaporation is similar to the rate of evaporation of pure water, as the film formation progresses and particles becomes more concentrated this fails to be the case.[24,25] In the next section the evaporation of water from latex films will be discussed before the final stages of film formation will be explored.
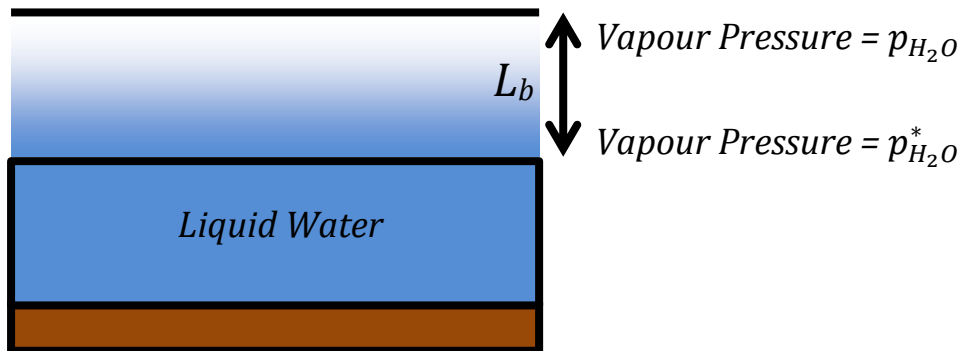
Figure 1:9 – Shows a schematic diagram of a boundary layer over a pool of liquid water. Over the thickness of the boundary layer L_b the vapour pressure varies linearly from $p_{H_2O}^*$ to p_{H_2O}. However, if airflow caused an alteration to the vapour pressure in the region it could be imagined that the rate of evaporation, E, could increase.

1.5.3. Evaporation of Water from Latex Dispersions

The first few stages of latex film formation, as discussed in section 1.4, involve the evaporation of water. Monitoring the loss of water is most commonly done gravimetrically. However, there are a number of studies that have used alternative techniques both stand alone and in conjunction with gravimetric techniques to study the loss of water. Some examples include; Ellipsometry, Rheology, Adaptive Speckle Imaging and Environmental Scanning Electron Microscopy *(ESEM)*.[26–29] Due to the ease of use of gravimetric techniques, they seem to prevail in the literature. One problem with the use of gravimetric techniques is caused by the no uniform nature of film formation. As previously mentioned, capillary forces during drying can lead to a drying front. This means that at any one time the film being monitored gravimetrically will be in multiple stages of the film formation. Despite this, there has been significant work on trying to produce a model for film formation that fits the gravimetric data. This work started with Vanderhoff *et al.* in 1973; they observed a three stage drying profile.[30]

Stage I involves a constant rate of evaporation close to the rate of evaporation from pure water.[16] This stage can last until the polymer reaches around 70 % volume fraction.

Stage II occurs as the particles first come into irreversible contact. In this stage the areas of the film that are still at low volume concentrations still exhibit a constant rate of evaporation. However, the overall the rate of evaporation decreases greatly throughout this stage. During this stage if the rate of evaporation occurs slow enough, colloidal crystallisation can occur.[31] Further, if particles are soft enough, then particle deformation will occur. In some extreme cases this can occur before contact between particles.[32,33] As the volume fraction rises particle packing leads to particle deformation and, in turn, particle coalescence. Vanderhoff *et al.* states that this coalescence marks the end of stage II of the drying profile.

Stage III of the film formation process involves the initial formation of a continuous film. Water leaves the systems though any remaining interparticle channels followed by diffusion through a continuous polymer skin. This leads to a diminishing rate of evaporation, followed by a rate that approaches that of diffusion alone.

Contrary to the work by Vanderhoff *et al.* Croll observed a two stage drying profile.[24,25] Where a constant rate period is followed by a falling rate of evaporation, it was reported that an evaporation front moved across the film leaving a porous region containing no continuous water. At this stage as long as there remains wet latex below the porous region then the rate of evaporation will remain at a constant rate. There have been various studies that have shown similar drying behaviour to Croll's two stage process. Eckersley and Rudin used a gravimetric study combined with ESEM to prove that their system followed a Croll like mechanism.[34] Through the use of ESEM Keddie *et al.* have further proved a Croll like mechanism can exist by confirming the presence of voids in a film in which evaporation has seized.[26,35] From the above discussion, it is clear that the vertical distribution of particles in a drying film will dictate how evaporation from the film occurs. Below Figure 1:10 shows three schematics giving the three possible scenarios as presented by both Croll and Vanderhoff *et al.*
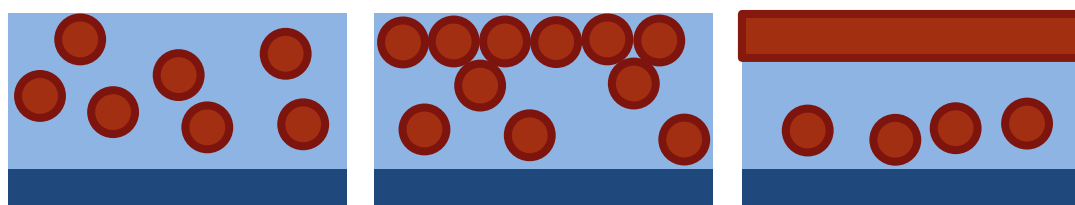
| **Scenario 1** – Uniform rate of evaporation from dilute latex as reported by Croll | **Scenario 2** – consolidation of particles at surface of latex. Porous structure results in minimal change in rate of evaporation as reported by Croll | **Scenario 3** – Wet sintering of particles at the surface results in evaporation that is diffusion limited as reported by Vanderhoff *et al.* |

Figure 1:10 – Shows three possible scenarios as described by the work of Croll and Vanderhoff et al.[36] Croll observed a constant rate of evaporation due to the lack of wet sintering during film formation. Vanderhoff et al. observed a much slower rate of evaporation as a result of a polymer film forming at the film's surface.

1.5.3.1.   Vertical Particle Distribution

As was mentioned in the previous section the distribution of particles vertically is responsible for the mechanism by which water evaporates from the system. As water evaporates from a drying film, particles near the surface tend to occupy a close packed structure. A schematic is shown below in Figure 1:11. This structure at the surface has been studied by both Ma *et al* and Roberts *et al.*[37,38] In these studies cryoSEM was used to study the formation of the aforementioned close packed structure at the surface of the film. Both Ma *et al.* and Roberts *et al.* studied the evolution of the structure over time, from the dilute stage through to the fully dried film. Roberts *et al.* subsidised the cryoSEM study with contact angle measurements in order to help explain the distribution of water through the packed particles at various stages of the film formation process. Producing films with a defined vertical structure has become an area of some interest in recent years due to their potential use in numerous applications, including: controlled drug release, photovoltaic devices and to improve the properties of pressure sensitive adhesives.[39–42] Recently, it has been shown that producing a stratified film with a defined structure can be achieved using a system containing multiple different particles of different sizes and composition in a process called auto-stratification. Discussing this further is beyond the scope of this thesis, however, Schulz and Keddie provide a useful review.[43]
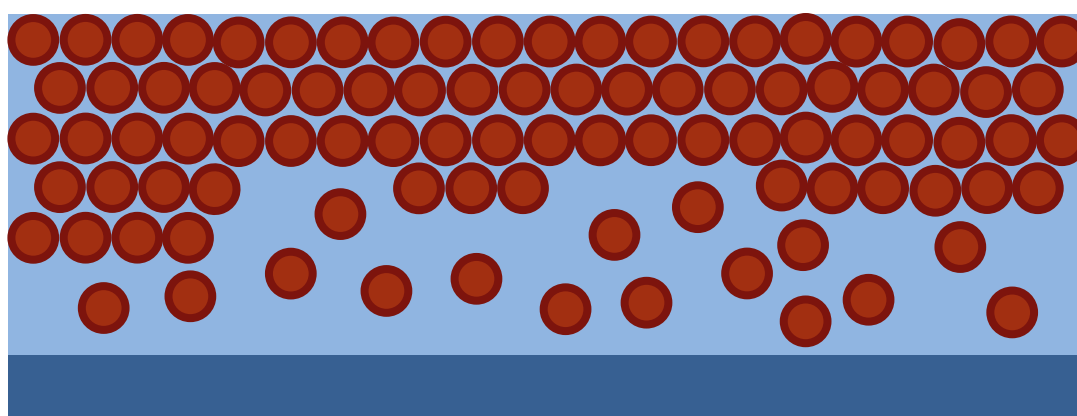
Figure 1:11 – Shows a schematic diagram of the close packed structure that latex particles occupy at the surface of a drying latex film. As the film begins to consolidate particles that come in close proximity to the surface are drawn into the surface structure.

As mentioned as the film dries particles begin to pack at the top service. As Croll stated this porous structure doesn't provide much resistance to the evaporation of water. However, if the particles are particularly soft then coalescence can occur at this top surface. This coalescence at the top surface causes a skin to form. This skin acts as a barrier to evaporation of water and hence drastically increases the drying time. The reason for this slower rate of evaporation is as the diffusion of water through the polymer skin becomes the rate-limiting step. Skin formation is much more prevalent in thicker films, as one may know if you have left a pallet of paint uncovered for any length of time. This skin formation becomes particularly undesirable when latex is used as a binder for water-borne paints as it provides a surface on which brush-marks will be left if attempt is made to correct the applied film. The time at which a correction can be made to a paint's surface is defined as open time and will be discussed later in section 1.5.3.3. However, it is not just skin formation that can hinder the evaporation of water from the surface of a drying latex film. Both a molecular monolayer or an additive that saturates the surface of a drying latex film could provide a physical barrier to the evaporation of water and act, as a skin does, to slow down the evaporation of water. The use of molecular monolayers as a method to slow down the evaporation of water will be discussed in greater detail in section 3.2.1. This inhomogeneity is not confined to the vertical geometry, it can occur on the horizontal axis as well. In fact when drying a latex sample on a small scale such as a microscope slide drying fronts within the film are observable by eye. In the next section horizontal drying fronts will be briefly discussed.

1.5.3.2.   Horizontal Drying Fronts

It can easily be observed that latex films do not dry homogeneously along the horizontal axis. Below Figure 1:12 shows an example of the movement of a drying front across a latex film throughout film formation.
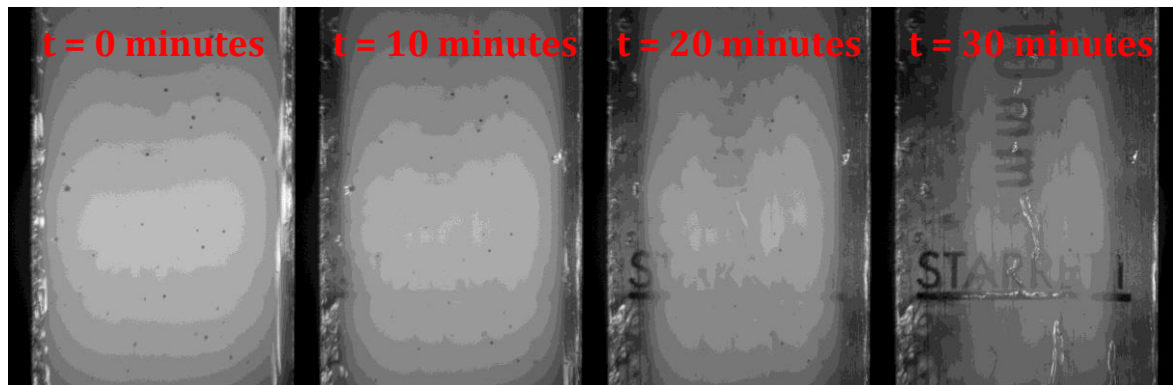
Figure 1:12 – Shows a film of latex 223-2 cast on a steel shim at various points along its drying time, note the inhomogeneity across the film, this is called the drying front.

Horizontal drying fronts have been an area of interest since the work of Hwa in 1964.[44] It is still a relevant area of research today with recent studies by Nassar *et al.* and Divry *et al.* exploring this effect in great detail.[45,46] Nassar *et al.* compared a 1D mathematical model of a drying front to experimental data for a silica colloid particle. Divry *et al.* explored the drying mechanisms in plasticised latex films. In this study they compared the speed of the drying front as predicted using the Routh and Russel model, to experimental data. [47,48] The speed of the drying front was measured using a camera with the overall rate of water loss being followed gravimetrically. As the horizontal drying front moves across the drying film the mobility of the particle is reduced. This causes a problem when corrections need to be made to the already applied film. After a certain time corrections made to the film are no longer possible without leaving permanent marks to the applied film, the time at which this occurs is called the film's open time. In the next section open time will be briefly discussed and how it is measured.

1.5.3.3. Open Time

Measuring the rate of water loss in a film gravimetrically provides a good way to monitor changes in the drying process. However, this method does not translate to how paint is used in a real-world situation. The downfall with modern water-borne paints compared to their solvent-born predecessor is the drying time. This becomes important when corrections to the film need to be made. If the film dries too quickly if any corrections need to be made to the film then doing so without leaving brushstrokes is not possible. The time at which corrections to the film

without leaving brushstrokes can no longer be made is called the open time. This property can be measured experimentally, the method for doing so has been outlined by the American Society for Testing and Materials test number *(ASTM)* D7488-11.[49] In this test a film is drawn down and then "X" marks are made in the applied film. An attempt is then made to cover these marks using a brush at set time intervals, usually around every 1 minute. The time at which correction cannot be made without leaving permanent marks is defined as the open time. The issue with this process is that it is open to experiment error due to the method that is used, alongside this it also has a poor time resolution due to time taken for the correction to be made. Despite this, there have been a number of studies that have used open time as a characterisation technique to study the film formation of latex films. Zong *et al.* have used the ASTM standard technique to study the open time of a low VOC system containing a new commercially available open time extender.[50] In this study Zong *et al.* found that the newly developed open time extender OTE-500 provided a way to increase the open time from around 4 minutes to 8 minutes. When looking at the literature in this area it becomes obvious that this is an area of great commercial interest with numerous patents protecting proprietary work around this area.[51,52] Despite this focus, when looking for smaller changes to the film formation process or when exploring the fundamentals of latex film formation the ASTM open time experiment is rarely used. However, its industrial relevance will always mean that it has a place in this area of the literature. Open time falls at the very end of the drying stage of latex film formation. In the next section the final stage of the film formation process will be discussed: Particle Coalescence, Deformation and Cracking.

1.6. Particle Coalescence, Deformation and Cracking

At its most basic, a paint can be thought of as a number of soft spheres that are dispersed in water. As the water evaporates by the mechanisms discussed in the previous chapter the particles consolidate; it is when the particles begin to pack that particle deformation begins. In order to produce a film that is well suited for use as a water-borne paint the deformation should be great enough to form a film with minimal voids. The amount that the particles need to deform obviously depends on the type of packing that the particles occupy. There have been a number of studies that have studied the packing in drying latex films. It has been found that the rate of evaporation is crucial in the type of packing present. Most of the time the packing that occurs is some form of close packing. This has been studied in a number of ways from SEM to SAXS.[53,54] The work of Kooij *et al.* used SEM to study the packing of a latex film. They followed the amount of coalescence from this initial structure depending on the T_g of the particle used. In the study conducted by Chen *et al.* SAXS was used to study the effect that temperature and humidity have on the packing structure on a drying latex droplet. They observed clear changes in the density of packing at different temperatures, especially when the droplet was dried below its MFFT. In the next section the MFFT of a film is discussed.

1.6.1. MFFT

In order for a paint film to have good mechanical properties and resist abrasion at room temperature, the T_g of the film needs to be above room temperature. This allows the film to be resilient to general wear and tear. However, if one dries a latex dispersion of colloidal particles below its T_g then as the particles begin to pack the particles will not coalesce. Therefore, there is a need to create colloidal particles that have T_g that is initially below room temperature, so that they coalesce, but after coalescence the T_g rises and a tough hard coating is created. Another effect would be that a low T_g film is soft and tacky, hence dust and dirt would be more likely to adhere to the finished film. This problem is one that needs to be overcome in order for water-based paints to match the properties of traditional solvent-based paints. Traditional solvent-based paints undergo a crosslinking reaction after the film formation has occurred. This reaction can

either be caused by oxidation in alkyd systems or through the addition of crosslinking agents in two pot systems such as epoxies or urethanes. In order to match these properties, the latex film needs to behave as if it has a T_g below room temperature to encourage a homogeneous polymer film to form upon application, then the system needs to develop to have a T_g above room temperature in order to provide mechanical resistance to damage. One way to achieve this is to plasticize high T_g particles with a solvent in order to promote the particles' coalescence; once the film has been formed the solvent is then free to evaporate and the T_g of the system returns to that of the native particle. These additives are called coalescence solvents and are used in low concentrations in nearly all water-based paints.

Legislative change has forced paint manufacturers to reduce the amount of VOCs in paint formulations and has therefore limited the amount and type of coalescence solvents that can be used. As has been discussed in section 1.1.1, a VOC is defined as an organic compound that has a boiling point below 250 °C, this limits the type of molecule that can be used. It also means that the film will take longer to reach a point at which the T_g is above that of room temperature. One of the most common coalescence solvents, and the one that is used in this thesis, is produced by Eastman and is known by the trade name Texanol™. The chemical name for Texanol™ is 2,2,4-Trimethyl-1,3-pentanediol monoisobutyrate. It is a liquid organic compound in the ester alcohol family. Due to the aforementioned VOC definition, with a boiling point of 254 °C, Texanol™ does not constitute a VOC.[55] As mentioned, the primary reason for the use of coalescence aids such as Texanol™ is to lower the T_g of the latex and hence lower the MFFT. In the next section the factors that cause cracking within latex films, and hence affect the MFFT, will be discussed.

1.6.2.　　Film Cracking

One of the main purposes of a paint is to act as a barrier, protecting the substrate from various external factors. If there is cracking in the surface of the paint, some of these factors such as moisture can freely enter the substrate below. Cracking in a paint film is therefore, in large part, highly undesirable. Typically cracking in paint films is most prevalent in older paints that have degraded over time, however, cracking can also occur in paint films that are incorrectly applied or not suited for the application. In some cases cracking can be a desirable thing that is seen as adding character to an item. This is however often confined to artwork where cracking is referred to as craquelure. Cracking patterns in an oil-based painting can act as a fingerprint to its origin, with variation between the cracking patterns stemming from differences in the materials used and the climate the painting was produced in.[56–58]

Cracking in colloidal films has been an area of research interest since Chiu *et al.* began to study the cracking in the early 1990s.[59,60] These studies focused on cracking in binder-free granular ceramic films. In their studies both optical microscopy and ESEM was used to characterise crack morphology in these systems. They also found that there was a critical thickness at which cracking in these films stopped. Despite these studies being fundamentally relevant, in this thesis the focus is on latex films and hence the main point of discussion from now on. In recent times there has been interest in providing a universal model that explains how cracking in drying colloidal films varies with not only film thickness but also particle rigidity. Singh and Tirumkudulu have described a regime for producing crack-free films with both hard and soft colloidal dispersions. In this study there was strong agreement shown between experimental results and the theory presented.[61] There are a number of factors that can affect the cracking in drying latex films, some of which we have already mentioned, such as coalescence solvents and some that we have not. In the following sections some of these will briefly be mentioned.

1.6.2.1.   Film Thickness

As previously mentioned, there is a critical thickness at below which cracking within a film stops. However, the work of Lazarus and Pauchard has also shown that the morphology of the cracking can be altered through variation in film thickness.[56] In this study they found that changing the film thickness from around 3 microns to 15 microns changed the cracking in a film of 30 nm latex particles from isolated cracking junctions to a completely connected cracking network. They also found that in films that are even thicker ($\approx$ 150 microns) circular and spiral cracks could form. This is consistent with work that has been carried out by Néda *et al.* in which they observed similar cracking during the drying of the sediments of various Iron and Nickel compounds.[62]

1.6.2.2.   Temperature and Coalescence Solvents

As previously mentioned coalescence solvents such as Texanol™ are added to latex dispersions in order to plasticise the particles and facilitate the film formation. Another way that this effect can be simulated is through changing the temperature at which the film is dried. Now it must be noted that, for obvious reasons, it would not be practical to increase the interior temperature of a house so as to allow the film formation of a high T_g latex. But for other applications, such as in the automotive industry where parts are often dried in ovens, this is an area of research that is highly relevant.[63–65] In the next section the effect of temperature on the cracking of latex films will be discussed.

In theory, coalescent solvents are used to lower the T_g of latex particles. This allows the film to form at a lower temperature before the final property of the film is restored overtime as the coalescence solvent evaporates. In decorative paints this has to be done, as unlike the aforementioned automotive industry it is not possible to have control over the temperature that the film is applied at. However, there have been a number of studies that have shown how altering temperature can alter the film formation process.[54,66,67] Initially it may seem as if this has not industrial relevance but when thinking of the different conditions in different parts of the world it becomes apparent why this might be of industrial relevance. For this reason a paint that is used under conditions that are too cold may crack.

Typically as a latex film is dried at ever increasing temperatures the crack spacing will increase until a point that cracking does not occur at all, this point is called the minimum film formation temperature.[58,68] Drying a film above the T_g of its constituent latex may seem like the way to solve all problems relating to film formation and cracking yet just as many problems arise in such cases. If a low T_g latex is used then the final film will be susceptible to damage and prone to dirt pickup. For this reason temporarily plasticising the latex with a coalescence solvent is bar far the most used method for producing a crack free film with good long-term properties. But the aforementioned legislation with the aim to reduce VOCs has led to other routes of reducing cracking being studied. One of these involves using a system with a mixture of hard and soft particles. This will be briefly discussed in the next section.

1.6.2.3.   Particle Mixtures

As mentioned in the last section particles dried above their T_g readily film form, with the downfall that their final film properties is less than desirable. Recently particles mixtures have shown considerable promise with soft particles added to the formulation to promote film formation and hard particles used to give the film the desirable mechanical properties. Tzitzinou *et al.* showed that when a significant amount of a small low T_g latex was added to a larger higher T_g latex significant improvements to the property of the film could be seen.[69] However, particle mixtures are not limited to hard and soft particles in the work of Qiao *et al.* it was found that through the addition of Halloysite Nanotubes *(HNTs)* a significant reduction in cracking could be observed along with a significant increase in film hardness. It was stated that altering porosity of the films played a role in the observed reduction, although a definitive mechanism by which the HNTs where reducing cracking was not stated.

1.6.2.4.   Driving force for Crack Formation

At its most basic cracks form within a drying latex film due to the development of internal stresses. These stresses arise through the development of capillary pressure as the particles begin to consolidate during film formation, this was shown to be the main driving force by Dufresne *et al* who noted that a film remained wet at the point of fracture.[70] It is worth noting that crack formation occurs more in systems in which the particles do not deform viscously, with increasing viscous deformation resulting in increased capillary pressure required for crack formation.[61] Through the measurement of capillary pressure at the onset of crack propagation Man *et al.* have shown that the capillary pressure required for crack formation, increases with decreasing film thickness.[71] They also saw that additional crack would form from pre-existing ones, suggesting the importance that defects and flaws have on the formation of cracking with drying latex films. However, this should not really come as a surprise as the presence of flaws and defects have been known to play an important role in the crack propagation of brittle solids for many years.[72]

A film that is crack-free most often occurs in a system in which particle deformation and eventually polymer interdiffusion has occurred. In the next section the physics behind this process will be briefly described.

1.6.3.   Particle Deformation

As mentioned previously as a film dries the particles begin to consolidate into a close packed structure. If this structure is going to transform into a film that is suitable for use as a paint, then ideally the voids between the particles need to be removed to form a homogeneous polymer film. In order to achieve this the particles need to deform. In order for particle deformation to occur there needs to be a driving force behind it. There are a number of factors that can drive the particles to deform. In the following sections a number of these driving forces will be briefly discussed. [67]

1.6.3.1.   Dry Sintering

Dry sintering is driven by surface tension between the polymer and the air. This theory was originally proposed by Dillon *et al.* and later supported experimentally by Sperry *et al.*[14,73] In the work of Sperry *et al.* an MFFT bar was used to study the influence of water on film formation. In their experiments they cast films of both hydrophobic and hydrophilic latexes onto an MFFT, both before and after it was energised. In respect of hydrophilic latex, the MFFT bar was then energised to allow film formation to be studied in a completely dry system. They found in the case of the hydrophobic latex that the wet and dry film formation was nearly identical. In comparison, in the hydrophilic latex the wet film formation occurred at significantly lower temperatures than dry film formation, although this was attributed to water plasticising the polymer.

1.6.3.2.   Wet Sintering

Wet sintering occurs in a similar way to dry sintering but the driving force is the polymer-water interface rather than polymer-air surface tension. This driving force is far less common than dry sintering due to the slow nature of the deformation when compared to the relatively fast evaporation of water from such systems.[74] Vanderhoff *et al.* first presented wet sintering as the mechanism than was responsible for forming a skin on the surface of a drying latex film, slowing its evaporation to the rate of diffusion of water through the surface polymer skin.[30]

1.6.3.3.   Capillary Deformation

At the surface of a wet film the water-air interface between particles occupies a curved structure, called a meniscus. This meniscus in turn creates a large negative pressure within the fluid, called the 'capillary pressure'. The atmospheric pressure pushes on the exposed particles at the surface of the film resulting in its compression. This mechanism was first hypothesised by Brown.[15] A cartoon that demonstrates the idea of a meniscus forming during film formation and hence driving particle deformation through capillary pressure is shown below in
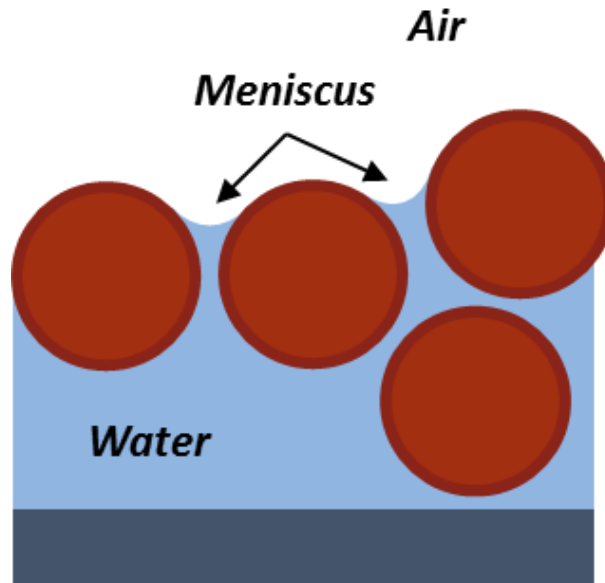
Figure 1:13 – Shows a cartoon representation of a latex film during film formation with the meniscus present at the air-water interface driving particle deformation through capillary pressure. This mechanism was first proposed by brown in the late 1950s.

The maximum pressure that can be applied to the particles can be estimated from the following expression: $12.9 \ \gamma_{wa}/R_0$, where R_0 is the particle radius and γ_{wa} is the water-air surface tension. This estimation by Brown can be developed to introduce various different material responses but the idea of balancing the mechanical response of a particle with the driving force of deformation forms the basis of most film formation models.

1.6.3.4. Mixed Driving Forces for Particle Deformation

As mentioned previously, it is unlikely that a film dries completely homogeneously, either in the vertical or the horizontal plane. For this reason it is likely that during film formation multiple mechanisms are driving particle deformation. Keddie *et al.* described a system in which initially capillary deformation occurred within a drying film. However, before particle deformation was complete most of the water had evaporated, leaving the system to complete particle deformation through dry sintering.[26]

If a film forms with high levels of vertical inhomogeneity a skin can form at the surface hindering further evaporation. Sheetz argued that this slow diffusion of water through the polymer skin creates a large osmotic pressure below. He then proposed that this drives the compaction of particles in the bulk of the film.[16] However, the added time of film formation caused by the diffusion which limits the evaporation of water could in fact allow wet sintering to be the main form of particle deformation. Based on several key parameters such as evaporation rate, film thickness and particles size it becomes possible to predict the mechanism of particle deformation occurring. In the next section the use of deformation maps to predict the mechanism of deformation occurring within a drying latex film will be briefly discussed.

1.6.3.5. Deformation Maps

In 1999 Routh and Russel laid the foundation to the work in this area.[48] In this work they created a deformation map that could predict the mechanism of deformation occurring within a drying latex film based off two dimensionless parameters: $\bar{G}$ and $\bar{\lambda}$. The physical meaning of $\bar{G}$ was the evaporation time divided by the relaxation time of the polymer, whilst $\bar{\lambda}$. represents the time for film to compaction divided by the evaporation time. Based on these parameters a prediction of 4 mechanisms of particle deformation can be established: dry sintering (1.6.3.1), receding water front, capillary deformation (1.6.3.3) and wet

sintering (1.6.3.2). When designing a new film forming system, these values may be used and in turn adjusted to control the mechanism of deformation occurring in the system. This is important in certain applications such as in the paint and coatings sector as the mechanism of particle deformation will control the morphology of the final film, which will control the final film properties. In order to study how the morphology of the latex film is changing and in turn deduce the mechanism of particle deformation there are a number of standard techniques that can be used.

The following chapters will cover a wide range of topics that will increase our understanding of the area surrounding "The Structure-Property Relationships in Drying Polystyrene/Acrylic Latex Films". Chapter 2 will discuss the experimental methods that have been used to characterise the film formation process in this investigation along with the methods that outline sample preparation. Chapter 3 will look at the rate of evaporation of water from latex films using a novel gravimetric technique. Chapter 4 will look at the effect of hydrophilic additives on the observed level of cracking within the dried latex films. Chapter 5 will use SAXS to examine the particle spacing within dried latex films and how the inclusion of various additives can affect this. Chapter 6 and 7 will provide a conclusion to the work carried out in this thesis, and present a summary of the future work that could be conducted respectively.

The work carried out in this thesis advances the current literature in a number of ways. The first is through the development of novel piece of equipment used to gravimetrically monitor the evaporation of water from a drying latex film without the influence of Zero Point Drift. The second is the looking at the effect of the selected hydrophilic additives on not only the rate of evaporation of water from the latex but also as a method of reducing cracking, and hence providing a more environmentally sustainable replacement for conventional solvent based additives. Finally, through the use of SAXS to examine the particle spacing on the same system.

Chapter 2:   Experimental Methods

In order to study how latex film formation is changing various points throughout the film formation need to be studied. Depending on the stage of film formation dictates the characterisation technique that can be used. This chapter will discuss the characterisation techniques that have been used in this thesis along with how the samples used in the studies have been prepared.

2.1.   Sample Preparation and Synthesis

2.1.1.   Latex Synthesis

The most common route for latex synthesis is through an oil-in-water emulsion polymerisation. Emulsion polymerisation is a type of free-radical-initiated chain polymerisation. At its most basic polymerisation involves linking together a number of small molecules of monomer to form a long-chain of molecules known as a polymer. In free-radical polymerisation the polymerisation process is broken into three stages:

1. **Initiation –** This involves the creation of the free-radical active centre. Initially the free-radical is formed by an initiator and then the free-radical is transferred to a molecule or monomer.
2. **Propagation –** This stage involves the growth of the polymer chain by through the addition of monomer to the active centre. This process occurs very quickly, typically in the order of a millisecond.
3. **Termination –** During this stage of the reaction chain growth is terminated. The most common mechanisms by which this occurs are: (i) Combination, this involves the coupling together of two growing chains and (ii) Disproportionation – this involves the abstraction of a hydrogen atom from one growing chain by another.

In emulsion polymerisation this process occurs in a monomer or mixture of monomers in the presence of an aqueous solution of an additive. There are typically three types of emulsion polymerisation processes: Batch, Semi-batch and continuous. In this investigation the small size of latex particles required lead itself to the use of a semi-batch process. To be specific this process was a seeded-emulsion polymerisation. This involves the addition of a small of amount of monomer to the reaction vessel at the start. This was then left to allow complete conversion of the monomer in what is called the seed stage. The rest of the monomer can then be added in batches to allow the growth of the latex particle from this seed.[75]

2.1.1.1. Latex Synthesis

The Latexes used in this investigation were produced in collaboration with AkzoNobel. Through the investigation two latexes were used with their synthesis being outlined in this section. As previously mentioned the synthesis of the latexes was a semi-batch seeded emulsion polymerisation. The masses of the monomers used in the investigation are shown below in Table 2:1 In this study two batches of each latex were produced, the batch number is indicated after the name e.g. latex 223-1 *vs.* latex 223-2.

Table 2:1 - Shows monomer mass Used in both Latex 223 and 225

	223 (g)	*225 (g)*
Acrylic Acid	*28.45*	*28.46*
Methyl Methacrylate	*414.58*	*515.64*
Styrene	*201.12*	*201.13*
Butyl Acrylate	*468.63*	*367.73*
n-Octyl mercaptan	*0.11*	*0.11*

In these reactions the initiator used was Ammonium Persulphate and the additive used was Sodium Alpha Olefin Sulphonate under the trade name Kemsurf OS38. The synthesis of each latex 223 and 225 is outlined below with the only difference between the two reactions being the monomer composition of the pre-emulsified monomer feed.

- 430.9 g of water was added to a 3 litre reactor along with 8.8 g of Kemsurf OS38, this was then heated to 85 °C.
- The monomers mixture outlined in Table 2:1 was then pre-emulsified with 353.5 g of water and 22.0 g of Kemsurf OS38.
- 43.1 g of the emulsified monomer mix was then added into the reactor along with 2.1 g of Ammonium Persulphate dissolved in 17.1 g of water. This process is the seed formation stage and was left to reach completion for 15 minutes.
- The remaining emulsified monomer mixture was then added to the reaction vessel over 180 minutes with the Initiator feed of 0.5 g of Ammonium Persulphate in 19.7 g of water being added over 210 minutes.
- The temperature of the reaction was constantly monitored and kept between 83 and 85 °C.
- The reaction was then be cooled to 70 °C before 0.5 g of Trigonox AW 70 dissolved in 7.8 g of water was added as an oxidiser.
- The reaction was then cooled further to 60 °C before 0.6 g of Bruggolite FF6 dissolved in 7.8 g of water was added over 20 minutes as a reducing agent.
- The reaction was then cooled to room temperature before being passed through a fine grit screen.

Before further use the latex was dialyzed using cellulose dialysis tubing with a 14,000 Da molecular weight cut-off, purchased from Sigma Aldrich. Samples were left to dialyse for a week with a water change every day. This reduced the wt% solids content of the latex. Volume concentration of the dialysed latex was increased by removing water through the use of a rotary evaporator below the T_g of the latex.

2.1.2.   Additive Solutions

Both high (viscosity: 4000 cP) and low (viscosity: 25 cP) viscosity Methylcellulose (MC), was obtained from Sigma Aldrich Co. LLC. The high viscosity MC has an approximate molecular weight of ~88 kDa with the low viscosity MC having a molecular weight of ~17 kDa. The degree of substitution of the cellulose molecule is between 1.5-1.9 if substituent groups attached to the ring hydroxyls.
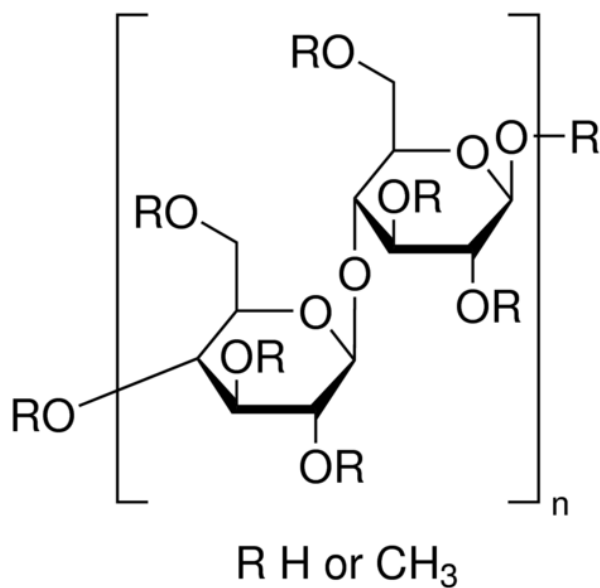
Figure 2:1 – Shows the basic repeat unit for Methyl cellulose. (Image Available from: <https://www.sigmaaldrich.com/catalog/product/sigma/m0512?lang=en&region=GB> [viewed 7th of May 2020])

Both high (viscosity: 2600 - 5600 cP) and low (viscosity: 40 - 60 cP) viscosity weight Hydroxypropyl Methylcellulose (HPMC), was obtained from Sigma Aldrich Co. LLC. The high viscosity HPMC has an approximate molecular weight of ~86 kDa with the low viscosity MC having a molecular weight of ~22 kDa. The HPMC molecules have a methoyxl content of ~28 - 30% and a hydroxypropxyl content of ~7 - 12%.
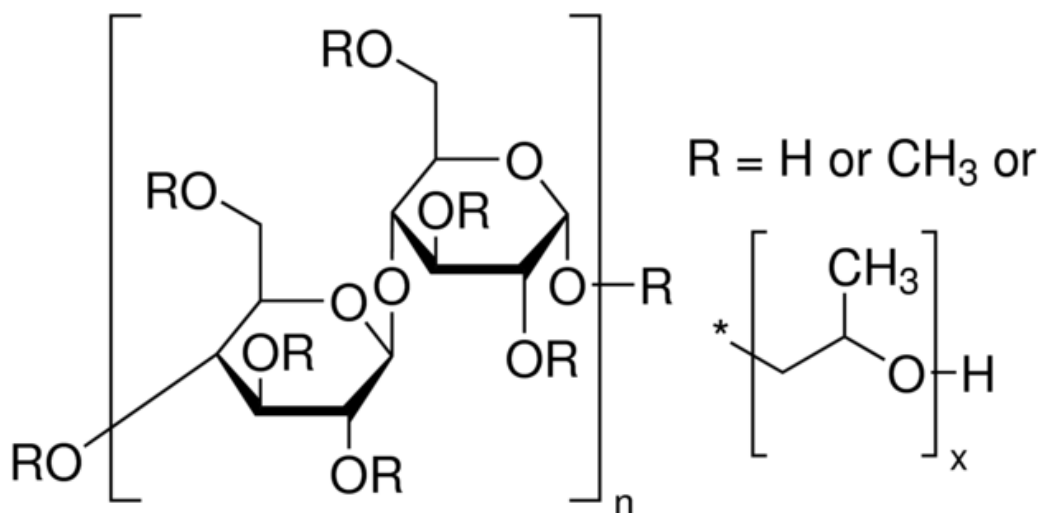
Figure 2:2 – Shows the basic repeat unit for HPMC. . (Image Available from: <https://www.sigmaaldrich.com/catalog/product/sigma/h7509?lang=en&region=GB> [viewed 7th of May 2020])

Pluronic PE9200 and Pluronic PE10500 was obtained from Sigma Aldrich Co. LLC. They have a molecular weight of ~2750 Da and ~3250 Da respectively. The molecules contain 20% and 50% of PEG respectively.
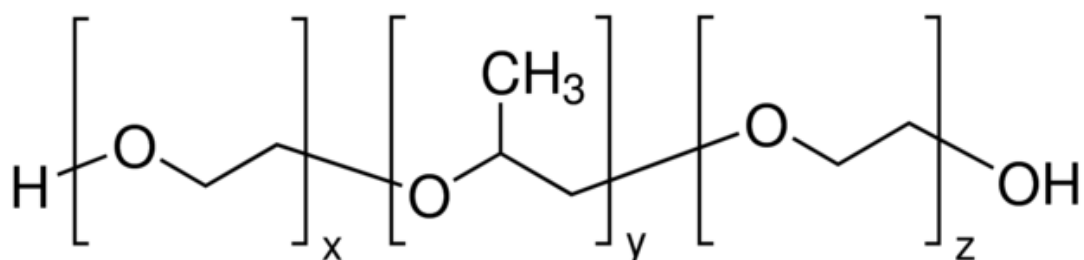
Figure 2:3 – Shows the basic repeat unit for the pluronic additives used in this thesis. <https://www.sigmaaldrich.com/catalog/product/aldrich/435430?lang=en&region=GB> [viewed 7th of May 2020])

All additives were then mixed into standard 2 wt% solutions with distilled water. Samples were left to mix on a Cole-Parmer tube Roller for minimum of 48 hours.

2.1.3.   Latex Formulations

In this investigation the dialysed latexes containing 5 wt% Texanol™ was mixed with varying concentrations of additive. The wt% solid concentration of the latex formulations was controlled at 30 wt% solid concentration. Once the formulation was roughly mixed, it was left on a Cole-Parmer tube Roller for minimum of 48 hours.

2.2.   Microscopy

Microscopy can prove to be a powerful tool in the analysis of drying colloidal films. In this study a number of microscopy techniques have been used to study the latex particles at various points through film formation.

2.2.1.   Optical Microscopy

Optical microscopy is used in many fields. However, due to he small size of colloidal latex particles (<1 μm) its use is limited. In 1873 the Ernest Abbe realised that the use of optical instruments such as telescopes and microscopes were fundamentally limited by the wavelength of light. This limit is called the diffraction limit, this can be approximated as: $d = \lambda/2$. Since the wavelength of light falls around 500 nm, most latexes can not be studied with great resolution using standard optical systems. There has been some work on producing techniques that can break through the optical limit.[76] However, these techniques are very much in the early experimental stage but could provide a way to study film formation in the future. In this investigation microscopy was used at minimal magnification to study the level of cracking in the films.

2.2.1.1.   Equipment Used

In this investigation microscopy on dried latex films was conducted using a Motic SMZ-168 stereomicroscope. The Magnification used was dependant on the sample under investigation.

2.2.2. Electron Microscopy

As previously mentioned optical microscopy has a resolution limit. This limit is problematic in the area of colloid research due to the inherently small size of the particles under investigation. However, electron microscopy can be used to study artefacts below the diffraction limit of light. This is as it uses the wave characteristics of particles. Louis de Broglie first noted this relationship in 1924. He said that any particle travelling with a linear momentum should have a wavelength, with the wavelength being given by:

$$\lambda = \frac{h}{p}$$

(10)

Where λ is the wavelength, h is Planck's constant and p is linear momentum. In electron microscopy a beam of electrons of a well-defined de Broglie wavelength replaces the light source. Instead of a lens, a magnetic field is used to focus the electrons onto the sample. There are two main category of electron microscopy: (i) Scanning electron microscopy *(SEM)* and (ii) Transmission electron microscopy *(TEM)*, in this study the latter was used. In TEM the electrons pass through a sample, like in standard transmission optical microscopy, and are collected on a screen. The resolution of electron microscopy techniques is typically 2 nm for TEM and 50 nm for SEM.[77]

In this investigation TEM was used to study the size of the latex particle. As the particles under investigation were soft then the particles need to be studied whilst still in their aqueous environment. In order to do this Transmission electron cryomicroscopy *(cryoTEM)* was used. In cryoTEM the samples are frozen down to cryogenic temperatures before being examined using TEM. Other cryogenic techniques have been used extensively in the literature to study latex film formation, such as: Enviromental Scanning Electron Microscopy *(ESEM)* and Cryogenic Scanning Electron Microscopy.[37,78]

2.2.2.1.   Equipment Used

Latex samples were diluted from 40 wt% solid to approximately 0.1 wt% solid concentration. The solutions were then cast onto holy carbon grids before being cryogenically frozen. Samples were run on a Phillips CM100 100 kV electron microscope equipped with a LaB6 gun and Gatan 1Kx1K digital camera.

2.2.3.   Atomic Force Microscopy

In order to overcome the aforementioned diffraction limit Atomic Force Microscopy *(AFM)* uses a physical approach to image a samples surface. AFM uses a sharpened stylus attached to a cantilever to scan the surface of a sample. As the sample is moved across the surface the topography of the samples causes the cantilever to deflect. This deflection can then be monitored using either interferometry or a laser beam. A schematic diagram of an AFM is shown below in Figure 2:4.
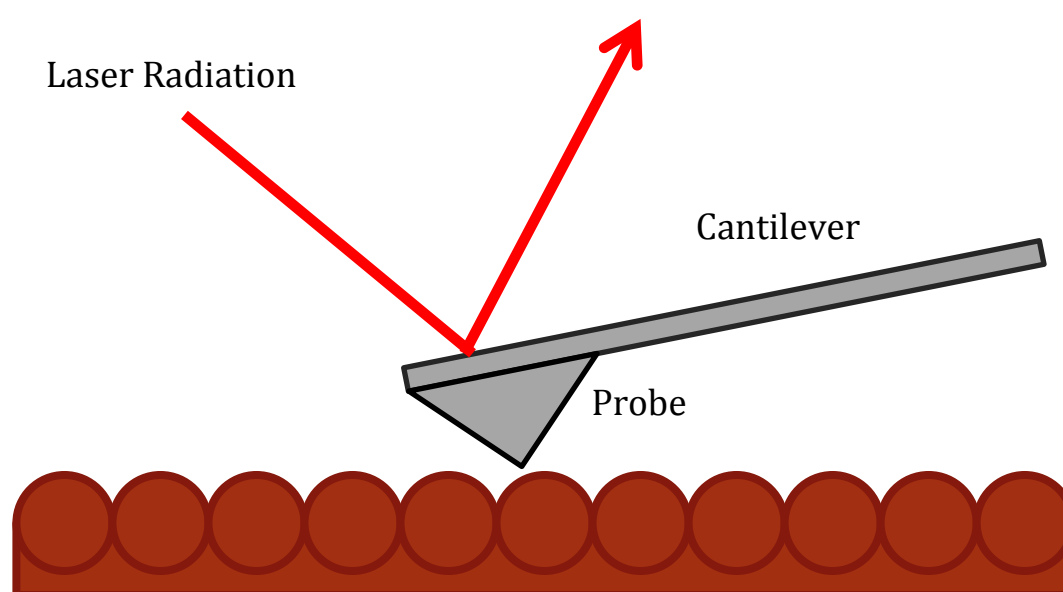
Figure 2:4 – Shows a schematic diagram of an AFM tip in contact with a sample surface. As the tip is moved across the surface of the sample deflection caused by the topography of the sample is detected by either a laser beam or through interferometry.

When the AFM tip is scanned over the sample in constant contact with the surface, the technique is called *Contact Mode.* Contact mode is used to gather height information at the surface of the sample. Using a feedback loop the height of the sample is adjusted to maintain a constant force on the cantilever.

In soft samples the use of contact mode AFM can prove difficult. This is as the AFM tip can get caught on the surface of soft sample, either damaging the sample or leading to incorrect measurements. To overcome this an alternative technique was developed, *Tapping Mode.* In tapping mode the cantilever is driven at a set frequency by a piezoelectric oscillator. In tapping mode it is possible to gain information on more than just the topography of the sample. Looking at the oscillation of the output signal in comparison to the frequency inputed by the piezoelectric oscillator a phase lag can be calculated. Looking at the phase lag as a function of the spatial position of the AFM tip can give information on the properties of the sample. Using this method it is possible to contrast in a phase image of an AFM micrograph with respect to sample modulus. For the reason outlined above it was chosen that in this investigation the AFM was to be run in tapping mode.

2.2.3.1.　Equipment Used

Dried latex films were run on a Dimension 3100 AFM with a Nanoscope 4 controller. The AFM was run in Tapping mode and Height, Phase and Amplitude images were collected.

2.3.   Scattering Techniques

2.3.1.   Dynamic Light Scattering

Perhaps one of the most common methods of characterisation of particle size in latex systems is Dynamic Light Scattering *(DLS)* also called Photon Correlation spectroscopy *(PCS)*. DLS works by looking at the Brownian motion of the particles in a dilute system. This random motion of the particles is caused through collisions with the molecules in the solvent. The equation that governs this movement is as follows:

$$D_0 = \frac{kT}{6\pi\mu R}$$

(11)

Where D_0 is the self-diffusion coefficient, k is the Boltzman constant, T is temperature, μ is viscosity of the continuous phase and R is particle radius. It can be seen that if the temperature and viscosity of the system is known it becomes possible to measure the particle size by looking at the rate of particles diffusion. In a DLS with a detector at a fixed position the rate of diffusion is calculated *via* an autocorrelation function. It is used to measure the difference in scattered intensity with respect to time. In this investigation DLS was used as a method to characterise particle size before a SAXS investigation was conducted.

2.3.1.1.   Equipment Used

DLS was run on a Malvern Zetasizer Nano S, samples were made to approximately 0.001wt% and were left to equilibrate at 25 °C for 2 minutes before 3 sets of 13 measurements were taken.

2.3.2.   Small Angle X-Ray Scattering

In order to understand how Small Angle X-ray Scattering *(SAXS)* can be used to monitor structural changes in drying latex films first a general overview of the technique needs to be given. At its most basic SAXS involves the illumination of a sample with an X-ray source, the X-rays are then scattered by the electrons within the sample and the scattered light is captured by a detector. Scattering contrast within a sample is provided by the variations in electron density between regions,

in the case of a latex between the polymer and water. The final observed scattering pattern *(I(q))* is influenced by a number of different factors. These factors can be split into three different contributors all of which are represented in equation (12).

$$I(q) = \langle \eta^2 \rangle . S(q) . P(q)$$

Where I(q) is the scattering vector, S(q) is the structure factor of the system, P(q) is the form factor and $\langle \eta^2 \rangle$ is the contrast. S(q) is influenced by interactions between scatterers, in the case of a latex between the particles. With dilute systems having a lower contribution from S(q) and more concentrated systems having higher contributions. P(q) represents the scattering contribution caused by the shape of the scatterer, in the case of a latex, a sphere. However P(q) can provide an insight into more than just the shape of the scatterer. Scattering is caused by the variation in electron density of the observed system therefore, the contrast, if the observed scatterer has internal structure and hence internal variation in electron density it will show in P(q).

Due to I(q) being affected by such a vast amount of variables, sample preparation and experimental design is important when trying to isolate factors affecting I(q). Probably the most common problem with SAXS is when trying to separate the effects of S(q) from P(q). This is most commonly done to provide an insight into the size, shape and structure of the scatterer under investigation. In order to achieve this, a sample would typically be run under a very dilute concentration in order to minimize the inter-scatterer interaction and hence the contribution of S(q).

The simplest system that could be imagined, and as the samples in this investigation are typically spherical a suitable example, would be the scattering caused by a single homogeneous sphere. In this system it could be imagined that the entire contribution towards I(q) would come from P(q). The scattering from a sphere can be given as:

$$I_{Sphere}(Q, R) = K^2(Q, R, \Delta\eta)$$

Where:

$$K(Q, R, \Delta\eta) = \frac{4}{3}\pi R^3 \Delta\eta\, 3\,\frac{Sin(QR) - QRCos(QR)}{(QR)^3}$$

$$(13)$$

Using this expression the scattering patterns of spheres of two sizes where plotted, one had a radius of 25 nm and one a 50 nm radius. This is shown in Figure 2:5. In this example there is no contribution from the structure factor.
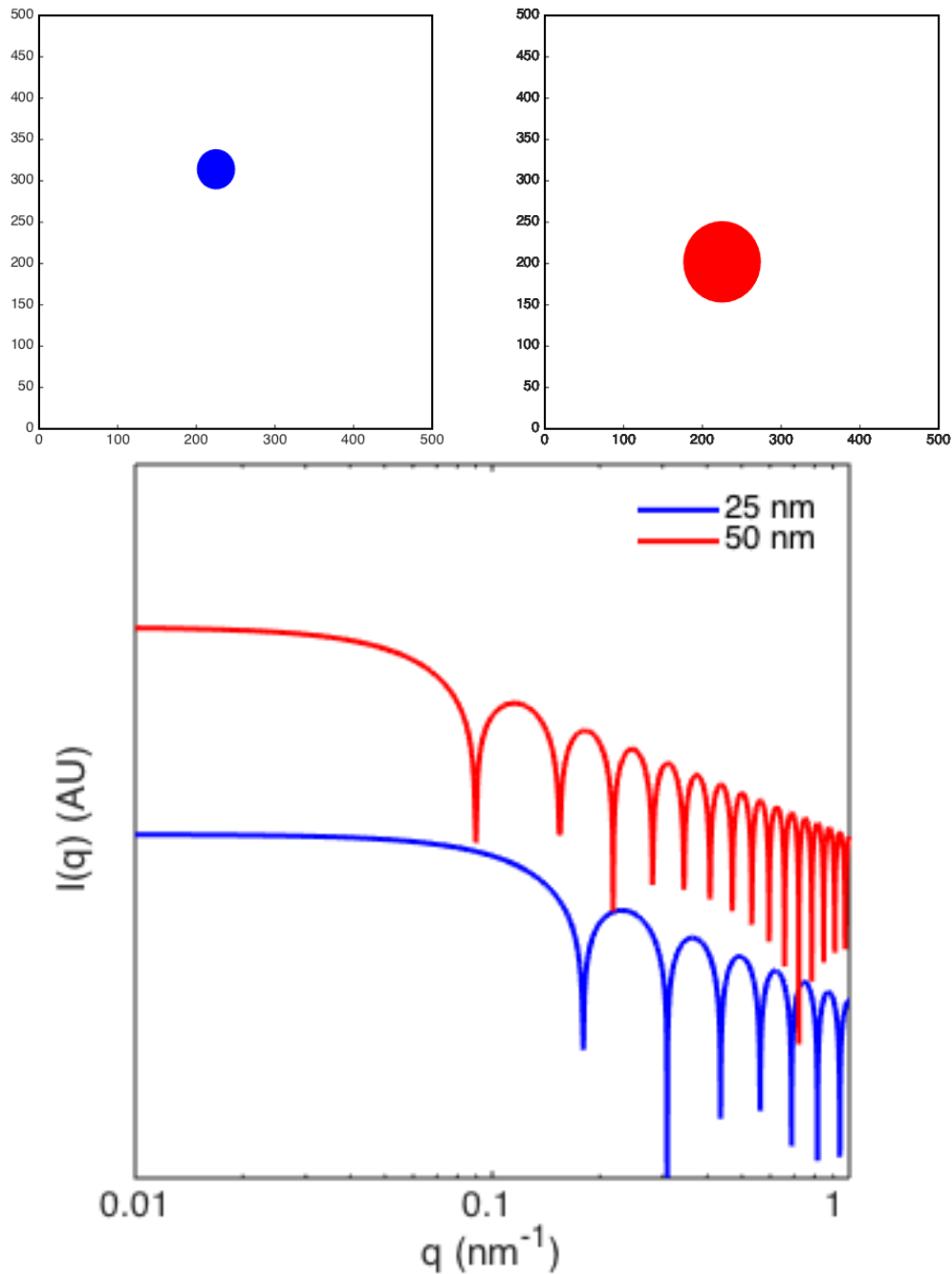
Figure 2:5 – Shows the simulated scattering patterns of two particles of different sizes. It can be seen that as you increase the size of the scatterer the scattering pattern is shifted towards lower q. This shift means that it was chosen to use smaller samples in this investigation to leave to option open for such scattering experiments.

Once the form factor of a system has been fitted it is then possible to continue to study the structure factor of the system. In this study the samples used are spherical and hence the aforementioned spherical model can be used, assuming the lack of internal structure. However, due to particle deformation upon film formation the form factor measured in the dilute state may change. This makes studying the film formation through SAXS a tricky prospect.

2.3.2.1. Equipment Used

All samples were run on the Xenocs Xeuss 2.0 laboratory beamline equipped with a Dectris Pilatus 1M detector and an Excillum liquid gallium MetalJet X-ray source ($\lambda = 1.34$ Å)

2.4.   Physical Testing

The use of physical testing to measure the properties of a film at various points throughout film formation can prove invaluable. The two methods of testing used in this thesis have been discussed below: Minimum Film Formation Temperature Bar *(MFFT Bar)* and Dynamic Mechanical Analysis *(DMA).*

2.4.1.   Minimum Film Formation Temperature Bar

The MFFT bar is perhaps one of the most widespread techniques for characterising the film formation of latex films. This is most likely due to is inherent simplicity. The use of an MFFT bar was first proposed in 1960 Protzman and Brown.[79] Since then its use has been standardised with ASTM D2354-98 outlining proper use.[80] The MFFT of a latex film is defined as the lowest temperature at which a film forms. This property is discussed in greater detail in section 1.6.1. At its most basic an MFFT bar is a metal surface with a temperature gradient across it. A film can be drawn down across it with some of the film being exposed to temperatures above the MFFT and some under. When using MFFT apparatus there are a number of transition points that can be observed, although none of which are actually defined in the test standard. These are shown below:

- ***Cloudy-Clear Transition*** - As the name may make clear this is the point at which a film transitions from a slightly cloudy to a clear film, this transition is usually the point at which MFFT is determined. Below this point the particles do not deform enough to produce a void-free film hence the cloudy appearance, above this point the particles deform, removing voids and hence forming a transparent film.

- ***Crack Point –*** Again another transition in which the name gives away its position along the film. This transition is caused by a critical point of particle interdiffusion.

- ***Knife Point –*** This point was defined by Lee and Routh and is described as the point at which the film resists mechanical shearing.[68]

It must be noted that the use of an MFFT bar must be done with caution. Keddie and Routh describe a number of points that need to be considered during an MFFT measurement.[21] One of the most important to note is the subjective nature of the measurement. The user is relied on to identify the point at which the film transitions from cloudy to clear. This in itself relies on user consistency, for this reason it is advised that one user carries out all measurements and that multiple runs of each sample are required for a confidant measurement to be collected. Despite this MFFT is a commonly used technique in the literature, with numerous studies using it as method of film characterisation.[34,38,81]

2.4.1.1.   Equipment Used

MFFT experiments were run at the AkzoNobel Laboratory in Slough. The experimental was run according to ASTM D2354-98.

2.4.2.   Dynamic Mechanical Analysis

Dynamic mechanical analysis *(DMA)* can be used to measure a wide range of material properties such as Glass Transition Point *(T_g)* Modulus. DMA works by applying a cyclic deformation to a sample of known geometry. The sample can either be studied with a controlled stress or a controlled strain. For a known stress, the sample will deform a certain amount. Both the amount of stress and the amount of strain are measured and the differences between them are used to calculate a number of material properties. A schematic of the Force Displacement curves are shown below in figure 2.4.2.
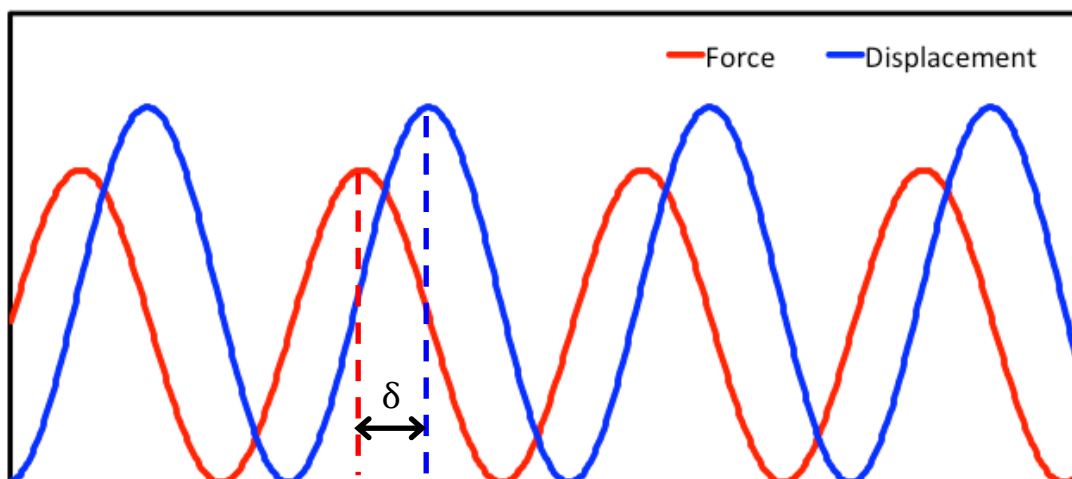
Figure 2:6 - Shows the relationship between applied stress to strain. The Sinusoidal shape of the curves are generated by the force motor. The phase angle (δ) is the difference in phase between the stress and strain curves and gives information about the properties of the material.

The information that can be calculated using DMA is as follows:

- Storage Modulus (E') – This gives information on the sample's stiffness
- Loss Modulus (E'') – This gives information on the sample's ability to dissipate energy through molecular motion.
- Tan δ – Is the Loss modulus divided by the Storage Modulus, the peak in tan δ when plotted *vs* temperature gives the T_g of the polymer.

In this study DMA was only used as a way to measure the T_g of the polymer. The experimental parameters for this are outlined below.

2.4.2.1.   Equipment Used

DMA was performed on a Perkin Elmer DMA 8000. The sample was run in a tensile geometry with an applied frequency of 1 s^{-1}. Samples were drawn down onto glass slides before carefully being removed to produce a freestanding film. The films were then carefully cut into geometry of around 10 mm by 15 mm.

Chapter 3:   Rate of Evaporation from Latex Films

This section will investigate whether a number of additives have the potential to be used as humidifying agents for the purpose of modifying the drying properties of water-borne paints. An additive's affinity for water is characterised by measuring its water activity. The rate of evaporation of water from films with varying concentration of additive will then be studied at varying levels of humidity.

Arguably the most important property of paint is its drying behaviour. Unlike solvent-borne systems, the drying behaviour of water-borne latex paints is more difficult to track as they are more susceptible to changing environmental conditions such as humidity and temperature. This has caused a demand for the development of a water-based paint with improved drying properties, making it comparable to a more traditional solvent-based system. One way that this could be achieved is through the use of hydrophilic additives by using these as a means of controlling the rate of water loss from these systems. However, controlling the loss of water to the atmosphere is only one piece of the jigsaw. The time at which corrections can be made to a paint without leaving brushstrokes is called the open time. As discussed previously in section 1.5.3.3, in a real-world scenario open time is crucial. The problem with this is that it requires the latex particles to remain mobile and free to move past one another. This leaves one fundamental problem with the use of hydrophilic additives, the fact that the water they hold back in the film is not free but rather hydrating the hydrophilic additive. This inherent problem is discussed below in the next section.

3.1.   Statement of the Problem

At its most basic, the problem that needs to be overcome is one of particle mobility. The longer that the particles can move freely within the system, the longer the open time of the film and the better the surface finish. There are a number of ways that this problem can be approached. The first way would to be completely re-design the system to move away from a particle based one and instead utilise an alternative system. In this alternative system the rate of reaction could be tuned so that, at its fastest, the system dries slow enough that the gel point of the system allows for correction to the film application to be made, producing a smooth uniform film. After this point the reaction would continue until the film has a high enough T_g that it has good barrier properties and is resilient to dirt pick-up and damage. However, the health concerns with a system containing a reactive monomer means this is ruled out.

The approach that we were therefore tasked with required an extension on the current approach. Currently the systems contain a coalescence solvent that eventually evaporates after the film has formed. This allows the use of particles with a higher than room temperature T_g to be used as the film will have better barrier properties than a film that has formed at RT without a co-solvent. In order to then slow the drying of the system and hence produce a film with a better open time, an additive or opentime extender is added with the aim to hold-back water. However, the problem with this approach lies with the way that an additive interacts with water in the system. In order for the particles to remain mobile, water in the system needs to be "free". This means that the water is not bound to anything and the particles can move freely through it. However, an additive binds to the water and stops particles from moving as freely. Despite this fundamental problem, we were tasked with focusing on the effect that hydrophilic additives have on the properties of drying latex films.

3.2. Existing Methods for Slowing Evaporation Water

Before going on to look at the work that was done to characterise the effect of the hydrophilic additives used within this investigation. It is worth briefly mentioning some technologies that have been used to slow the evaporation from both latex films and open water reservoirs.

3.2.1. Molecular Monolayers

As early as 1917 Irving Langmuir noted the presence of a molecular monolayer upon the surface of water, a discovery that later earned him the Nobel Prize in Chemistry in 1932. However, it was not until the 1920s that their effect on the rate of evaporation was noted by Rideal.[82] Following Rideal's work, La Mer *et al.* continued to study the effects that monolayers had on the evaporation of water on a laboratory scale. More recently La Mer and Healy, reviewed this along with other early work on this research topic.[83] In this review they discussed the potential for molecular monolayers as a cost effective way to reduce evaporation from large bodies of open water intended for use as drinking water. In this work, they concluded that despite the exact rate of evaporation from such bodies of water being difficult to monitor due to water being lost through other means, such as ground seepage, that the use of molecular monolayers should be considered as a "thrifty" way to control water loss through evaporation. In recent years, the use of such monolayers to reduce the rate of evaporation has been a keen area of interest from both the view of application and use in real-world environments as well as from a perspective of new and novel molecules. Recent work from Wandel *et al.* studied the spread of such monolayers across a 6 m water tank to simulate the spread across a large open reservoir under both ideal conditions without wind stress and under varying degrees of wind stress.[84,85] Due to the limitation of work been conducted in a 6 m tank, large degrees of extrapolation are needed to simulate the spread across an open reservoir. Despite this, this work increases the understanding in the field and highlights the need for further work in the area before a practical solution can be found. Looking towards the work being carried out on a more fundamental level, Tsuji *et al.* studied the small differences in evaporation rates between fluorocarbon and hydrocarbon monolayers using thermogravimetric tracing.[86] It is on this more fundamental level that could be

harnessed to limit the evaporation rate in latex films. It could be imagined that a molecular monolayer could be formed at the water-air interface of a drying latex film, in turn retarding the evaporation rate of water. However, in this study this was not the chosen route. A class of compounds that are more similar to the hydrophilic additives used in this investigation are humectants, these are briefly discussed below in the next section.

3.2.2. Humectants

Humectants are a class of compound that are used to keep moisture within a system. A humectant is designed to draw moisture from its surroundings to stop a product from drying out. Humectants are used in a wide variety sectors from the Food industry to the cosmetic industry. There are a wide range of chemical compounds that are used as humectants, including: Glycerol, Sodium hexametaphosphate and Lithium Chloride to name a few.[87,88] There have been a several pieces of work that have looked into humectants as a way to slow down the drying of water borne latexes films however, typically the humectants used have a low boiling point and are hence considered a VOC.[89] Due to the high commercial value of such additives there are also a large number of patents protecting at the use of humectants within the paints and coating sector.[90–92] Due to the nature of the hydrophilic additives used in this thesis, they could be considered to act as humectants. However, as the desired effect is to not only withhold water within the system but to also retain particle mobility into the later stages of film formation, we shall refrain from this use of terminology when referring to the hydrophilic additives.

3.3.   Water Activity of Additives

In order to measure the chosen additives' affinity for water enabling the creation of a system with the best possible chance of controlling the rate of water evaporation from the film, the Water Activity *(Aw)* of the additives was measured. Water activity is defined as the ratio of the partial pressure of water in the atmosphere at equilibrium with the system under investigation, to that of the atmosphere in equilibrium with pure water at the same temperature. It is expressed on a scale of 0 to 1 where 1 is for pure water.[93] A_w is related to the chemical potential of water, μ_w, at equilibrium when the chemical potential for the water and vapour phase are identical. This can be expressed using the following equation:

$$A_w = e^{\frac{\mu_w - \mu_w^0}{RT}}$$

(14)

Where μ_w^0 is the standard chemical potential of water.[94]Water Activity measurements were carried out using a Rotronic - Hygropalm – HP23-AW-A - Portable Water Activity Meter. As per the manufacturers guidelines the water activity meter was used in a temperature stable environment, an aluminium sample cell was also used to provide extra thermal mass to ensure that any short-term fluctuations in temperature did not affect the measurements. The water activity meter was used with the standard dwell time of 4 minutes for each measurement, each sample was run in total 5 times. The sample cell was filled up to the manufacturers recommended fill line before being run. Before measuring the water activity of the additives the reproducibility of equipment was measured using saturated salt solutions. The water activities for these salt solutions are shown below in Figure 3:1.
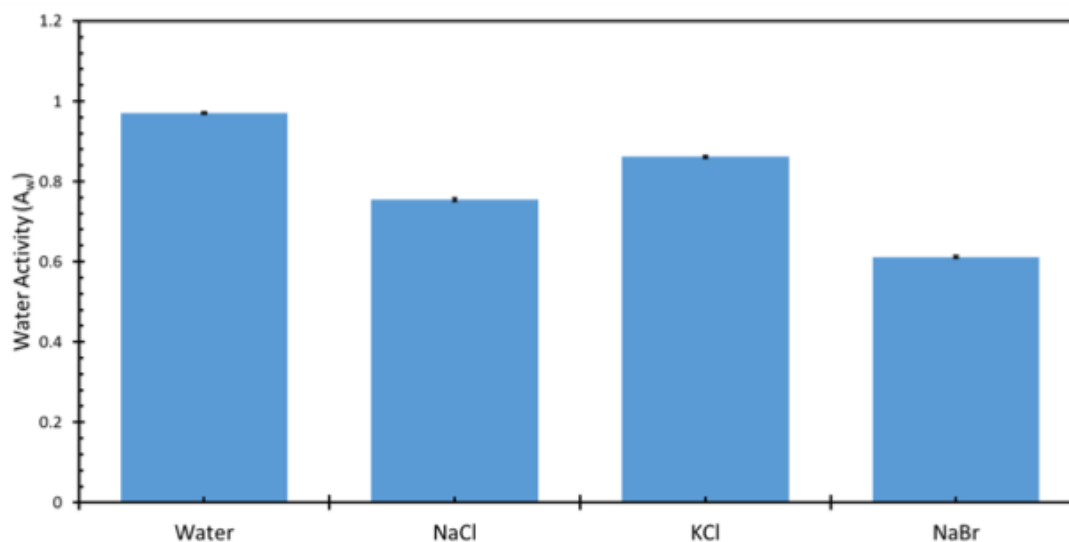
Figure 3:1 – Shows the water activities of a number of saturated salt solutions as well as pure deionized water. It can be seen that the water activity for water is not 1 as it should be, but the values for the salt solutions are close enough to the literature values to be confident in the technique as a comparative tool.

Figure 3:1 shows the measured water activities for several standard saturated salt solutions as well as deionized (*DI*) water. It must be noted that the purpose of this experiment is to compare the change on water activity that the different additives are having. For this reason, the fact that the water activity of the deionized water sample is less than 1 does not change how the data from this experiment will be used. It does however show that the DI water sample contains a level of impurity that is shifting the value of water activity, or that the probe may need a recalibration to normalise the data for DI water having a water activity of 1. However, if we compare the measured values for the saturated salt solutions with literature values, the measured values are consistently slightly lower than the literature values, the literature equilibrium humidity values for the concentrated salt solutions are presented in Table 3:1.[95] This deviation from the literature values would only matter if the data was being used to quantitatively compare the values to the literature. But as the consistency of the measurements are good, as can be seen from the small error bars in the above figure, this method for acquiring the water activity is more than good enough to use to compare the changes to water activity that the different additives are having.

Table 3:1 – Shows the literature equilibrium %RH values at 20℃ for the saturated salt solutions used in this study

	NaCl	KCl	NaBr
Equilibrium Humidity	75.5 %RH	84.3 %RH	59.1 %RH

As an initial trial, several hygroscopic materials available in the laboratory were investigated. These ranged from additives to known drying agents. Each of the samples were measured in their pure state and not in solution which had been the case with the previous measurements. The aim of this experiment was to see how the water activities of known drying agents compared to possible additives that could be used in water-based paints. The chosen additives that are going to be investigated include a Pluronic block copolymer as well as two cellulose-derived additives: Methylcellulose *(MC)* and Hydroxypropyl Methylcellulose *(HPMC)*. MC and HPMC are common additives used in cement and concrete. In these applications they are known to slow down the hydration of the cement phase during the first 24-hour period.[96–98] For these reasons it is possible that such additives would act in a similar fashion when used in a water-based paint. To test the effectiveness of the additives chosen in this investigation dilute samples of the chosen additives where made with both water and a latex 223-2 as the solvent, the results are displayed in Figure 3:2.
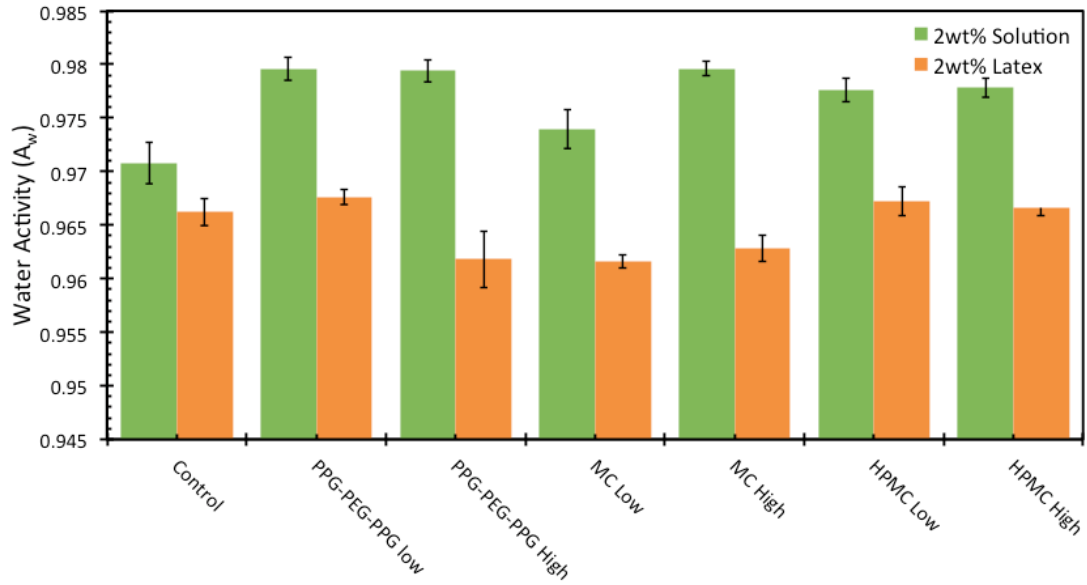
Figure 3:2 – Shows the water activity of a number of solutions containing latex and additive and water and additive. The control for the latex samples is latex 223-2 without added additive and for the additive solutions it is pure water. Note the small range in the y-axis. It can be seen that adding additive at these concentrations does have some effect to the water activity, albeit minimal. The reason that a higher concentration of additive was not studied, is as a sample with more additive will have a viscosity that is too high for use as a waterborne paint.

Figure 3:2 shows the water activity for each of the additives under investigation. The green bars show the additives in a 2wt% solution whereas the oranges bars show the additives at 2wt% in latex 223-2. The first thing to note is that the effect that the additives have at this concentration is negligible. The additive solutions at 2wt% seem to raise the water activity above that of the control, pure water; it can be assumed that they are not significantly affecting the rate of evaporation at this concentration. Turning to the latex solutions containing 2wt% additive, we can see that the water activity for all solutions, even those containing no additive, is lower than that of the control. One point of interest that can be noted with this experiment is the effect of molecular weight *(MW)* on the water activity of the additives. It can be seen that the water activity of the lower MW additives are lower than those of the higher MW. This is likely to be caused by the number of end groups in a sample of the same mass concentration with the lower molecular weight samples have more end groups present to interact with water molecules, thus lowering the water activity. The concentration of additive used in this investigation was used to represent a typical amount of additive that could be used in such latex systems. As one begins to increase the concentration of additives in latex formulations, the mixture begins to become increasingly viscous, especially when dealing with high MW additives and polymers. This effectively creates an upper limit on the amount of additive, as a highly viscous paint would be difficult to apply by a brush or roller.

Despite the negligible effect that the additive appears to be having on the water activity of the latex, along with the aforementioned statement of the problem in section 3.1, chosen decision was made to see if the additives had any effect on the rate of evaporation from the latex films. It was decided that going forward the additives that were going to be studied were the low MW ones. This is due to the aforementioned lower water activity along with their lower viscosity. The upcoming sections will discuss the development of the experimental procedure used to measure the rate of evaporation from these systems along with a discussion on the results observed when using a number of different additive concentrations.

3.4. Initial Mass Loss Studies

Previously it was mentioned that both the rate of water loss and the open time of a latex systems gives an insight into its suitability for use as a water based paint. The standard test for measuring the open time of a latex paint is the American Society for Testing and Materials test number *(ASTM)* D7488-11.[49] This test involves drawing down an area of the paint under investigation and applying "X-marks" in the paint at regular intervals. At predetermined time intervals a brush is then used to cover-up these previously made marks. The point that the marks are still visible after the second paint film is applied is defined as its open time. This test is a good real word test for measuring the properties of water-based latex paints. However, from the initial water activity studies it was seen that the additives have little effect on the systems' affinity for water. For this reason a different approach was chosen to measure the effect that the additives were having on the film formation of the latex films. A mass balance was used to study the rate of evaporation of water from these systems, meaning it is possible to study changes on a much smaller scale due to the high sensitivity of the balance used. This is one area in which the ASTM for open time falls down as it typically has a time resolution of about 1 minute limited by the time taken for the user to apply a second coat of paint.

Since the drying of latex films has become an area of research interest the rate of evaporation has been studied gravimetrically.[24,25,99,100] At first glance using a precision balance to measure the rate of water loss may appear a simple task. It is possible that a film could be applied to a substrate and then placed on a balance that is attached to a data-logger. If particular care was being taken, the humidity and temperature would also be controlled so as to limit the effect on the rate of evaporation from environmental factors. However, as the films under investigation are usually thin (<100 μm), and therefore the total mass of the film is fairly low, measurements can be affected by an experimental error, Zero-Point Drift *(ZPD)*. In the next section a method used to eliminate incorrect readings caused by ZPD will be presented.

3.5. Zero-Point Drift Correction

Precision analytical balances are highly complex and sensitive pieces of equipment. Whilst most laboratories have at least one analytical balance, the correct operating procedure is rarely enforced. Care needs to be taken to ensure that the balance is in area free from draughts and that the balance is placed on an anti-vibration table for example. If these measures (along with a few others) are applied then one-off measurements will most of the time be fine. It is when a balance is used to take a continuous reading that problems may be encountered. All balances rely on measuring the difference between the zero-point and the measured value. Over time the zero-point of the balance drifts, the amount by which this value drifts is dependent on environmental conditions. This drift is often not a problem when a one-off measurement is taken, for example weighing the reagents for a synthesis. However, when a continuous measurement is taken, such as measuring the water loss from drying latex films, problems can occur. In equipment that is designed for continuous gravimetric analysis such as Thermal Gravimetric Analysis *(TGA)* or Dynamic Vapour Sorption, the balance head tends to be positioned as far from the measurement chamber as possible. In some cases the balance head is even coupled to the sample by a magnet, thus allowing the sample to be run in extreme conditions, such as high temperature or corrosive atmosphere.[101] This separation allows the balance head to be kept in a stable environment; when this is combined with the fact that some TGAs can correct for ZPD during a run by decoupling from the sample, this means that a measurement can be taken with little to no effect from ZPD. This outlines the level of consideration that should be used when attempting a continuous measurement, especially when using small sample masses. It must be pointed out that ZPD is a very small effect and hence when the change in mass is large enough ZPD will not cause any issue. However, in the case of a thin latex film the mass is small enough for the ZPD to affect the shape of the drying profile. The next section discusses a method by which ZPD can be corrected.

3.5.1.   A-B-A Weighing Equipment

As previously mentioned most precision balances exhibit ZPD. Most manufacturers will quote a value for this drift at a set humidity and temperature value. It could be imagined that at a constant humidity and temperature ZPD could be corrected by subtracting a known drift value form a mass loss run. However, in this study changing the humidity is of interest. The issue with this is that ZPD varies with changing temperature and humidity. For this reason a method needs to be developed that works across all values. Figure 3:3 shows how changing the humidity changes the rate of ZPD and hence rules out subtracting a known ZPD after an experimental run.
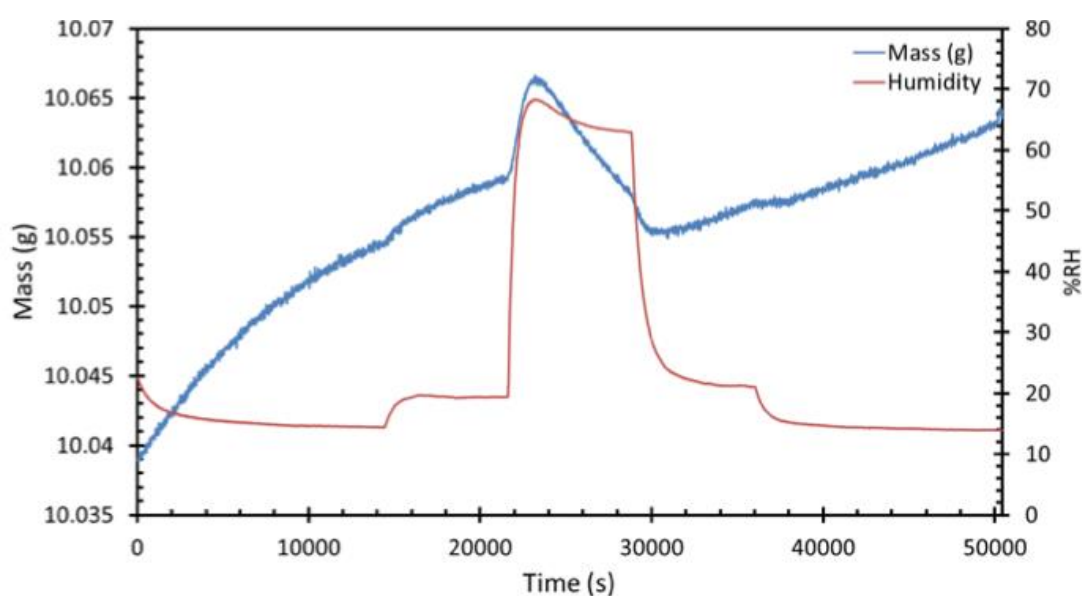
Figure 3:3 - Shows how recorded mass of a 10 g standard changes with respect to fluctuations in humidity. Looking at the data it can be seen that depending on the humidity the ZPD can either have a positive or a negative gradient. This fluctuation in the ZPD means that a background drift correction cannot easily be applied to the data. When measuring small mass changes continuously it could be imagined that these fluctuations could cause misinterpretation of the data.

Looking at Figure 3:3 it can be seen that the effect of ZPD is strongly influenced by changing environmental conditions. It can also be seen that over approximately a 12 hour period the ZPD accounts for a mass change of around 0.02 g. This means that in a thin drying film of around 0.1 g this could account for around 20% of the drying profile. However, it must be noted that this is an extreme case, as the system has not been left to equilibrate at each humidity step. If the system was left to equilibrate at each humidity step then the ZPD would account for much less than 20% of the total mass change over the time taken for a latex film to dry. All this being said, in thin films ZPD may cause errors in the drying profile that could be removed through correct experimentation.

It is possible to correct ZPD by using a fairly simple modification to a standard laboratory precision balance. At the heart of the equipment lies an A&DHR-250AZ 4.d.p balance. On the balance lies a 10g mass standard, the sample can then be lowered onto and off the balance using a linear stage. The balance is connected to a data-logger and the mass of both the mass standard and the mass standard + the sample can be monitored.
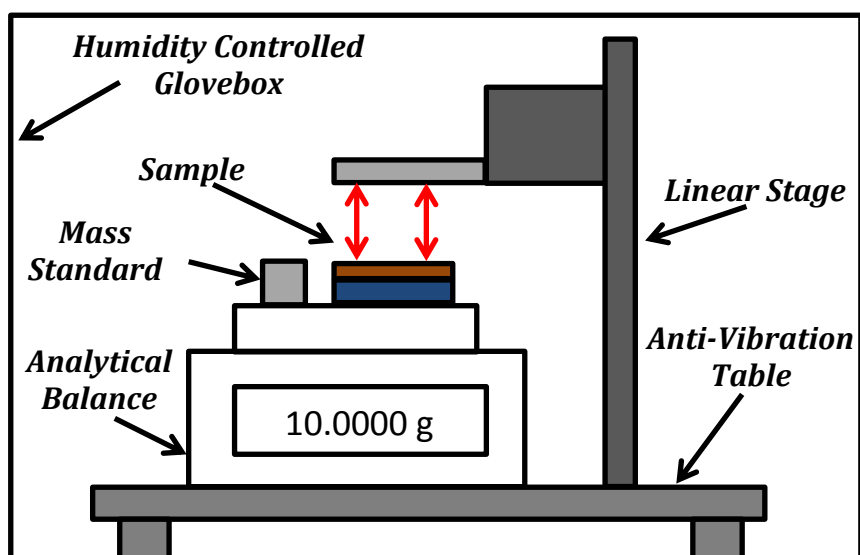
Figure 3:4 – Shows a schematic diagram of the modified balance that allows for the ZPD correction. The sample can be moved on an off the balance to allow for correction of ZPD before a reading is taken. The stage is controlled using an Arduino and MATLAB, with mass data collected via A&Ds data logging software.

Using the above equipment the mass of a 5 g mass standard was monitored over a change in humidity. The aim of the experiment was to see if the equipment could be used to account for ZPD, even in the most extreme of cases. The raw data for this experiment is shown below in Figure 3:5 and Figure 3:6.
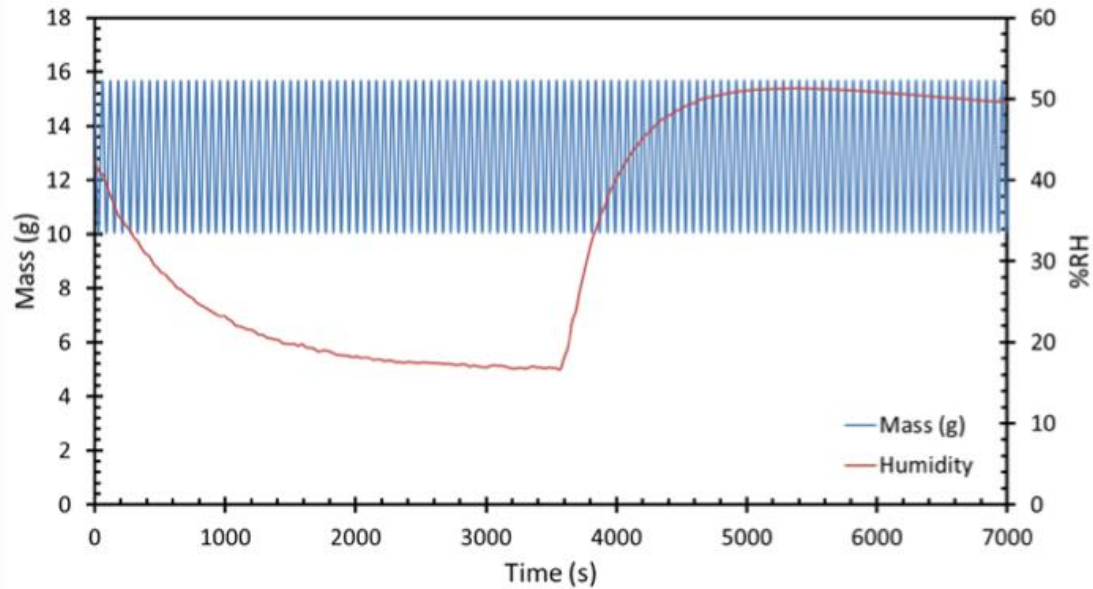
Figure 3:5 – Shows that raw data that the balance measures though the sample being removed and replaced cyclically. At this scale the ZPD is not visible in the data.
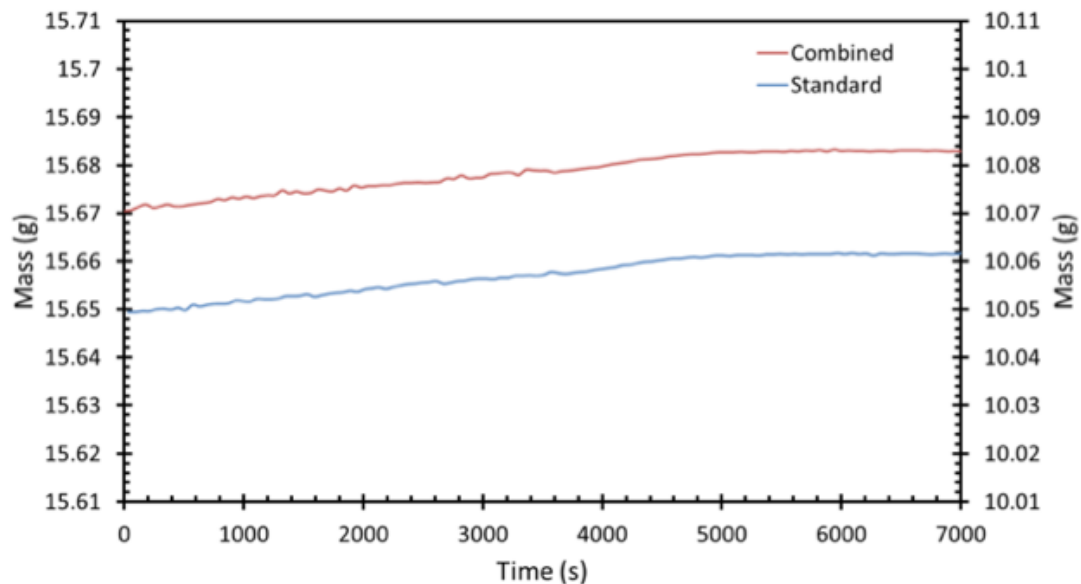
Figure 3:6 – Shows the two separated mass values. In this case the two vales are both standard vales. When in use the idea will be to allow a changing mass to be measured without the effect of balance drift skewing the data.

Looking at the data in Figure 3:5 and Figure 3:6 it can be seen that over the experiment, the change in humidity from around 20 %RH to around 50 %RH causes a ZPD of around 0.01 g. In order to extract the sample mass from the data the experimental standard needs to be subtracted from the combined mass value. This data is shown below in Figure 3:7.
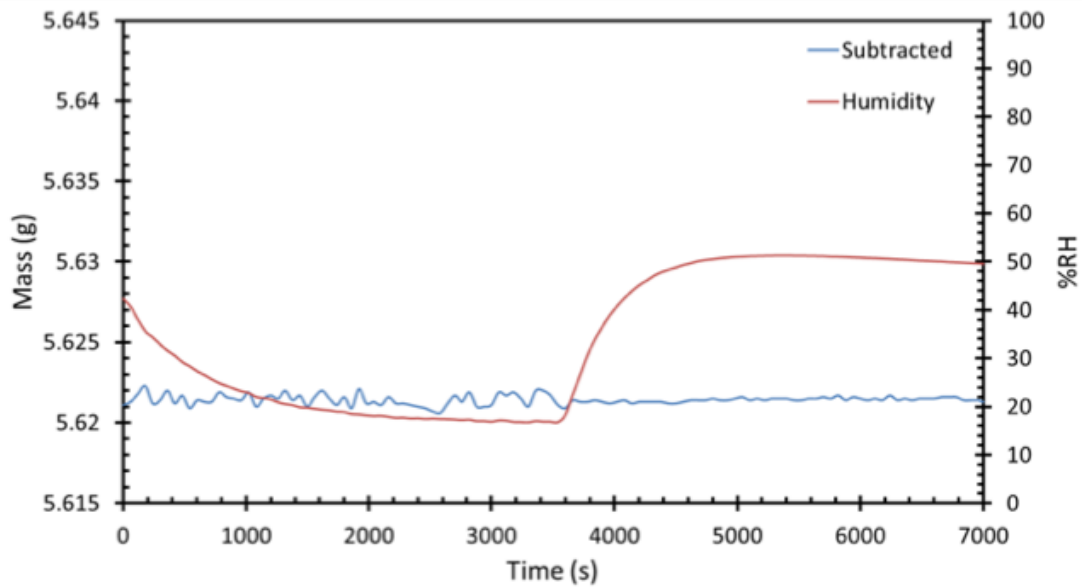
Figure 3:7 - Shows the corrected mass for the 5 g mass that was measured. It can be see that there is some slight noise in the data at the 20 %RH region but as the humidity is increased, the mass reading stabilizes.

Looking at Figure 3:7 it can be seen that when the mass data for the 5 g mass standard has been corrected for ZPD, despite the change in humidity it remains constant with only minor fluctuations observed. This shows that with simple modifications to a standard laboratory balance, constant mass change data can be measured with a high level of accuracy. Now that the equipment has been tested, it can be used to measure the rate of evaporation in a drying latex film.

3.5.2.   ZPD Corrected Drying Profile

As mentioned in section 1.4, as a latex film dries it goes from a dilute solution of latex particles to a consolidated array of particles. In order for this transition to occur water needs to be lost. Although on porous substrates, such as plasterboard or wood, some water is lost into the substrate, in the laboratory a controlled system needs to be created to study the effects of the additives on the rate of evaporation. For this reason the substrate used is glass and hence water is only lost through evaporation. In order to test the ZPD correcting equipment, a system containing latex 223-2 with 5 wt% Texanol™ has been used. The ZPD corrected drying profile has been shown below in Figure 3:8.
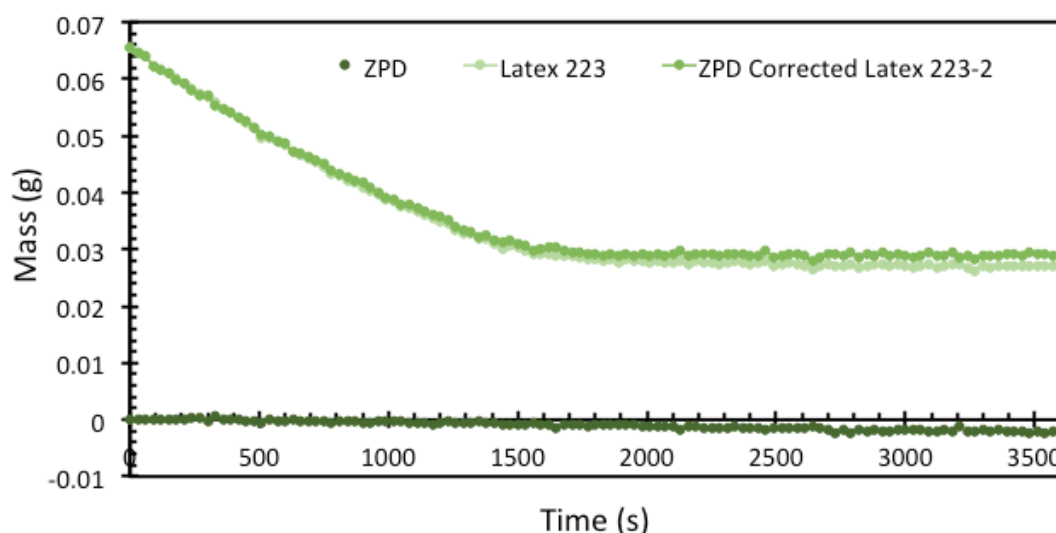
Figure 3:8 – Shows a thin film drying with both the raw, corrected and ZPD mass values displayed. It can immediately be seen that the baseline without the corrected mass value appears to still be changing. This could lead to false conclusions as to the drying behavior of the film being studied.

In the above figure the same experimental procedure was applied as described in section 3.5.1. The ZPD was corrected by subtracting the experimental mass standard from the combined mass. The amount of ZPD has been plotted above in Figure 3:8. It can be seen that the total ZPD accounts for approximately 3% of the total starting mass of the film. Further, when the ZPD-corrected drying curve is compared to the raw data there is a clear difference. If the drying curve is not corrected for ZPD it could appear that the film is still losing mass all the way to

3500 s, whereas in reality the observed residual loss of mass is actually ZPD. This residual mass loss could be wrongly identified as mass loss from another source, such as from the evaporation of a coalescent solvent. It must be noted that if the sample under investigation is significantly heavier then the ZPD would not cause issues due to the small percentage of mass that ZPD would account for. However, there are a number of studies that have used regular laboratory balances without modification to measure the mass loss in small drying films and droplets.[102,103] This study differs from approach.

3.6.   Final Mass loss Measurements

As mentioned previously, it is necessary to discuss the effect of both additive concentration as well as relative humidity on the rate of evaporation. As stated in section 1.5.1.1 the humidity variation in the UK varies from around 60 %RH to around 100 %RH. In order to reproduce the humidity range that is observed in both the average UK home as well as the climate of the UK, a humidity-controlled glovebox was used for all experiments. Due to limitations of the glovebox, the humidity range that was used ranged from 20 %RH to 60 %RH. Although this does not exactly mirror the humidity of the UK, it does provide the same humidity range. The climate control in the laboratory was set to 20 °C. The ASTM for "Standard Environment for Conditioning and Testing Paint, Varnish, Lacquer, and Related Materials" states that the temperature at which a paint can be applied should vary by no more than ± 2 °C and, when closer tolerances are required, ± 1 °C.[104] After monitoring the temperature in the glovebox, its temperature falls within these test standards.

Usually the way that a latex film is applied is through the use of a film applicator such as a drawdown cube or a K-bar. Initially in this study a drawdown cube was used, however, due to the changing viscosity of the latex with respect to additive concentration it was not possible to create a film of constant surface area. The films that contained little additive had such a low viscosity that after application the films spread out and therefore had a larger surface area than the films of high viscosity. In order to combat this a 20 mm diameter PTFE O-ring was glued to the glass substrate. In order to produce the sample, a known starting mass of latex was applied into the O-ring which flowed out to fill the well produced by the PTFE O-ring. This system will produce a sample of both consistent surface area and thickness irrespective of sample viscosity, so long as the starting mass is well controlled.

In this study the latex used is latex 223-2, it is used with 5 wt% Texanol™ with varying concentrations of additives. In this study the samples were formulated to have a solid concentration of 30 wt% the concentrations of both the Texanol™ and the additives used in this study are listed below in **Error! Reference source not found.**, the wt% of both Texanol™ and the additives are calculated off the mass of solid polymer within the dispersion. The mass loss data for this study is then presented in Figure 3:9 - Figure 3:11.

Table 3:2 – wt% Concentration of solids of Texanol™ and Additive

Sample Name	223-2	MC1	MC2	HPMC1	HPMC2	Pl1	Pl2
Texanol™	5	5	5	5	5	5	5
Additive	0	1.2	0.6	1.2	0.6	1.2	0.6
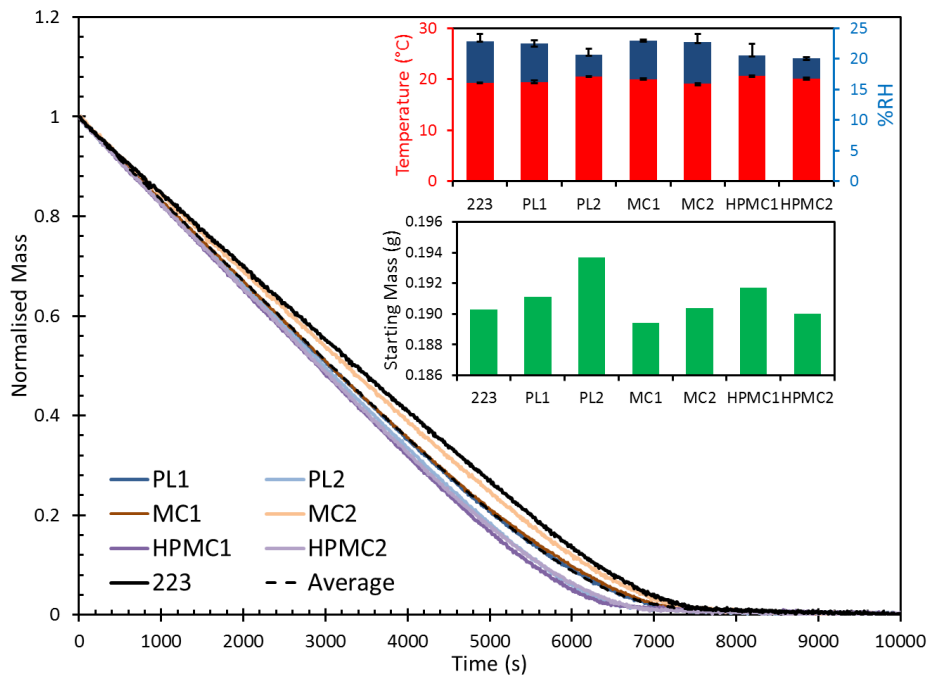
Figure 3:9 – Shows the mass loss curves of various formulations of latex 223-2 dried at approximately 20 %RH and 20 °C with the concentrations of additive in each system being shown in Table 3:2. The humidity and temperature for each run is shown along with the starting mass of each film.

97
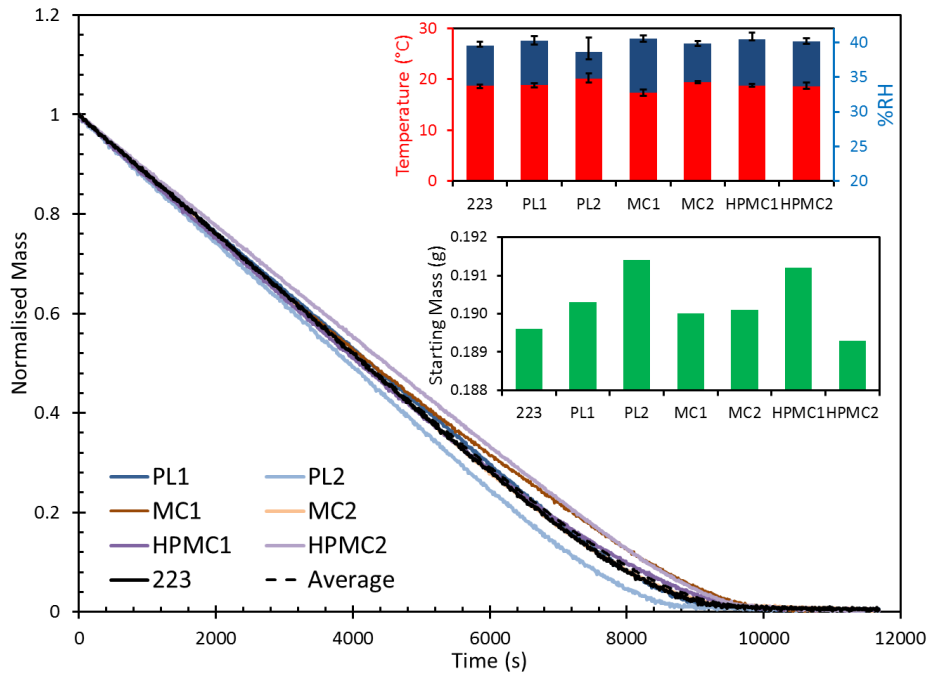
*Figure 3:10 - Shows the mass loss curves of various formulations of latex 223-2 dried at approximately 40 %RH and 20 °C with the concentrations of additive in each system being shown in **Error! Reference source not found.**. The humidity and temperature for each run is shown along with the starting mass of each film.*
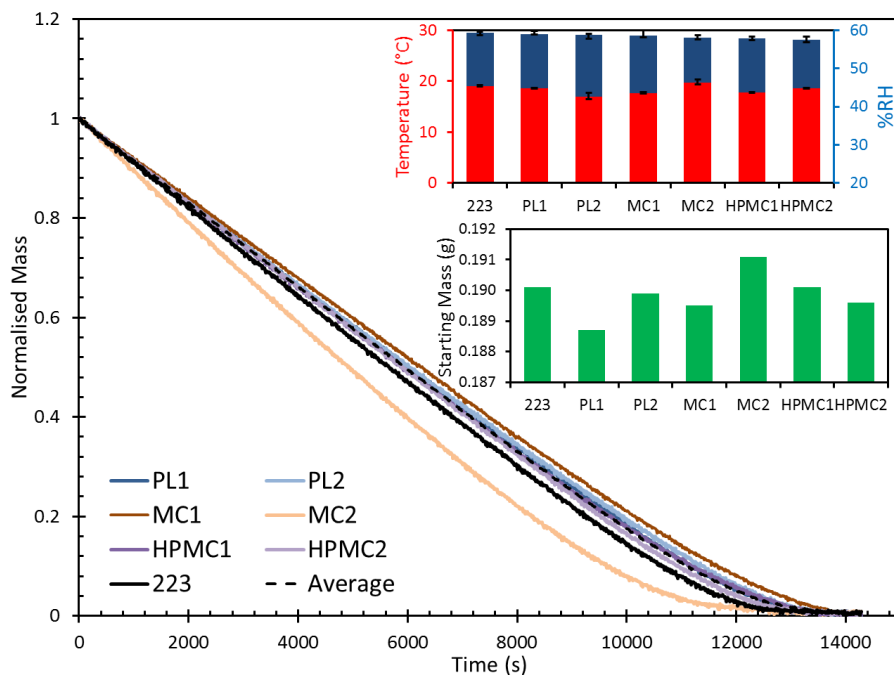
Figure 3:11 - Shows the mass loss curves of various formulations of latex 223-2 dried at approximately 60 %RH and 20 °C with the concentrations of additive in each system being shown in Table 3:2. The humidity and temperature for each run is shown along with the starting mass of each film.

Looking above at Figure 3:9 - Figure 3:11 it can be seen that there is no obvious considerable effect on the rate of evaporation as a result of the inclusion of an additive. However, it may be possible to extract some meaning from the data with further analysis. What can be seen is that as the humidity is increased between experimental runs, the drying time significantly increases. If we compare Figure 3:9 with Figure 3:10 and Figure 3:11 it can be seen that through increasing the humidity by 20 %RH the drying time is increases by approximately 2000 seconds. One thing to note is the anomalous run of MC2 in Figure 3:11 , in particular it can be seen that its rate of evaporation is considerably faster that it should be, especially since the starting mass of the film is the highest in the set of experiments. If we look at the trend of the data sets as a whole, the minimal change in the mass loss caused by the inclusion of the additives highlights that if an additive is going to be able to compete with daily and seasonal fluctuations in humidity, they need to have a considerably greater effect on the rate of evaporation than what is observed in Figure 3:9 - Figure 3:11.

It was hypothesised that through the addition of the additives the rate of evaporation would be decreased. However, when the water activities of the additives were studied, a similar, lack of trend, was observed. The problem with using these additives as a way to slow down the evaporation of water from these systems, is that with increasing concentration also comes with an increase in viscosity. If the viscosity becomes too high, then the systems' use as a paint becomes limited. Although it has been said that the additives appear to have a negligible effect on the rate of evaporation, it can clearly be seen that humidity does have a drastic effect. This shows just how susceptible water-borne latex paints are to external environmental factors. In order to show how much of an effect humidity has on the rate of evaporation, a surface plot has been fitted to all of the mass loss data. This is shown below in Figure 3:12.
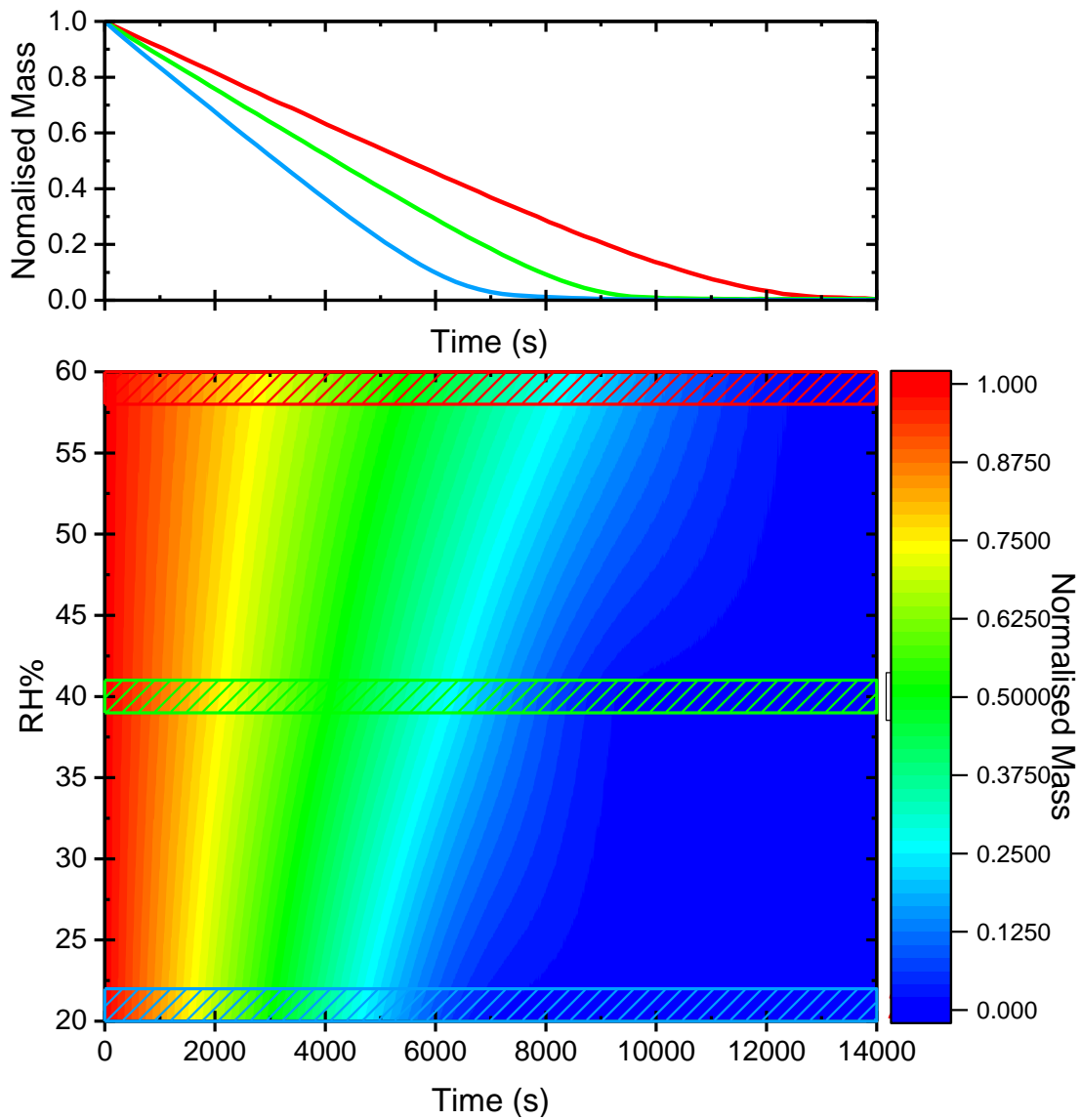
Figure 3:12 – Shows a surface plot of Humidity vs Time vs Mass. The plot was fitted to all the mass loss runs using OriginPro. From this plot the effect of humidity can clearly be seen. Looking at the normalised mass loss data it can be observed that as humidity is increased the rate of evaporation is decreased. The boxes drawn onto the surface plot show an area that has been used to calculate theoretical mass loss curves. Looking at the top of the figure it can be seen that these curves show a strong resemblance to the average moss loss curves in Figure 3:9 - Figure 3:11.

Figure 3:12 shows how changing humidity has an effect on the rate of evaporation of the latex system. It can be seen that an increase in 20 %RH yields an increase in drying time of around 2000 seconds. This means that over the observed humidity range of the UK, a change in drying of around 50% could be expected. This brings up the question of just how much of an effect a film additive could have on the drying time of a film. In order for an additive to produce a reasonable effect on the rate of evaporation it would have to compete against the variable climate of the UK. The one question that this experiment raises is the importance of controlling the environmental conditions when examining the drying of latex paints. Looking at the aforementioned ASTM D3924-16 states that the standard conditions for drying a latex film should be followed in an environment in which the humidity varies by no more that ± 10 %RH and, in cases where tight tolerances are required, by no more than ± 5 %RH. Comparing this to Figure 3:12 it can be seen that even in a best case scenario and where the tighter tolerances are used, an alteration in drying time of around 1000 seconds could be expected. This becomes an issue when trying to develop a system containing an additive designed to alter the drying time. Due to the drastic changes that can occur through altering the humidity, tightening the humidity range of the ASTM could be a good idea. This would result in minimal fluctuations in drying time through environmental factors and would allow the effects of additives to be studied with greater confidence. However, it must be said that despite the extra care taken over the standard ASTM, no effect could be observed through increasing additive concentration. In an attempt to extract more information on the rate of drying in these formulations, the mass loss data has been fitted. In the next section this will be discussed.

3.6.1.   Fitting mass loss data

In the previous section no clear trends were seen between the use of additives and the rate of drying. In order to try and gain a better understanding of the way that additives are affecting the rate of drying of the films, if any effect is in fact present, it was decided to fit the initial rate of evaporation. Since the work of Vanderhoff *et al.* in 1973, in which a three stage drying model was presented, and later the work by Croll, in which a two stage drying model was presented, there has been interest in modelling the mass of data of a drying latex film.[24,25,30] Due to the complex nature of the drying films, modelling the mass loss requires the development of a complex multi-stage mathematical model. As the additives are most likely to reduce the rate of evaporation of water, the initial linear region will be fitted in an attempt to see if the additives are producing a small effect that is not immediately noticeable. The initial slope of the mass loss curves has been fitted using OriginPro, an example of the fitted curves are shown in Figure 3:13, with the full complement of fits corresponding to the data shown in Figure 3:9 - Figure 3:11 being shown in section V. a in the appendix.
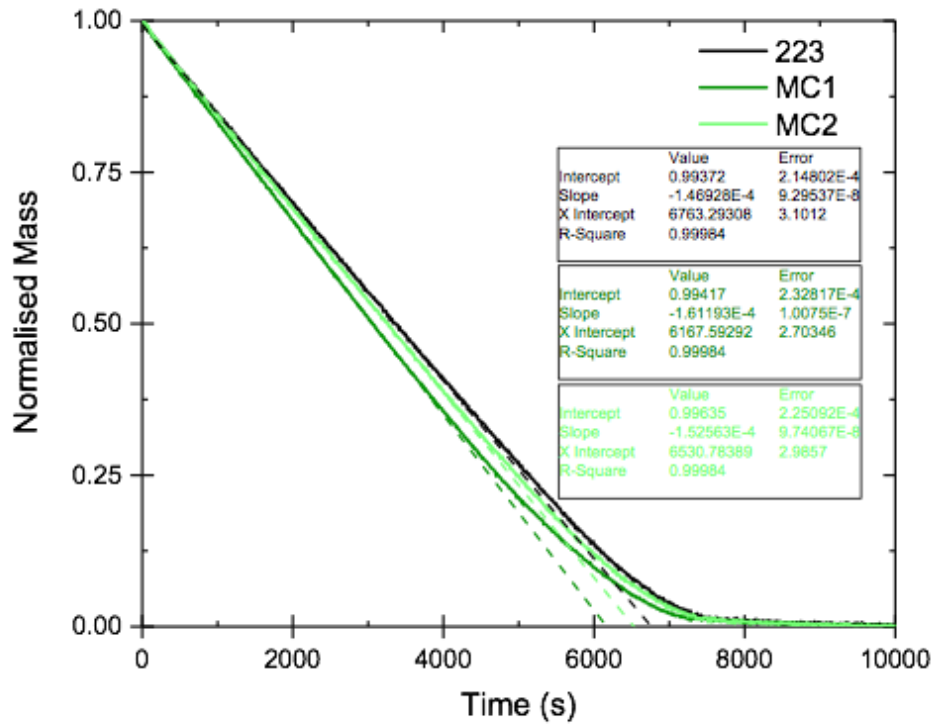
Figure 3:13 – Shows the drying profiles for three samples containing Methylcellulose dried at 20 %RH and 20 °C. The initial linear regions have been fitted using OrginPro. Upon initial inspection it can be seen that the data appears to be showing an opposite trend to what would be expected with the sample containing no methylcellulose taking the longest to dry.

In both the Vanderhoff and the Croll model the initial mass loss proposed is linear. In these linear regions water loss is said to be close to the evaporation rate of pure water as the particles are only hindering the evaporation minimally. If the additives are reducing the rate of evaporation, this region is a good place to start as it allows the effect to be isolated from other factors such as particle packing and skin formation. The initial evaporation rates normalised for surface area of all the runs with different additives and additive concentrations, along with varying humidity levels are shown below in Figure 3:14 - Figure 3:16.
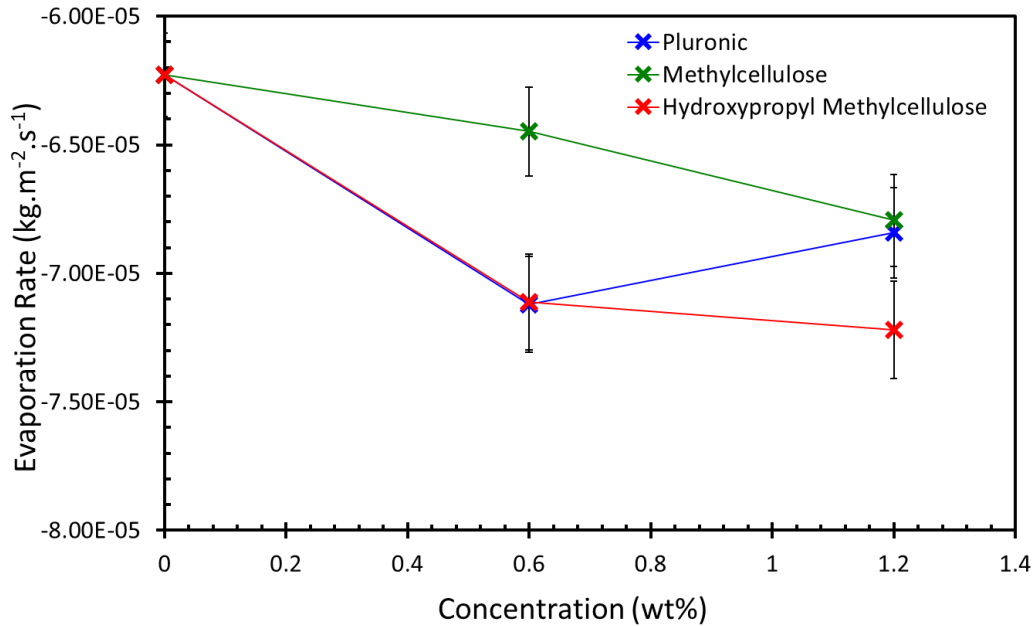
Figure 3:14 – Shows the initial rate of evaporation of water from a film of latex 223-2 and 5 wt% Texanol™ with the addition of three different additives dried at 20 %RH. It can be seen that with an increase in additive concentration the rate of evaporation is actually increased, which goes against the hypothesis. However, the amount that the additive is increasing the rate of evaporation is very small.
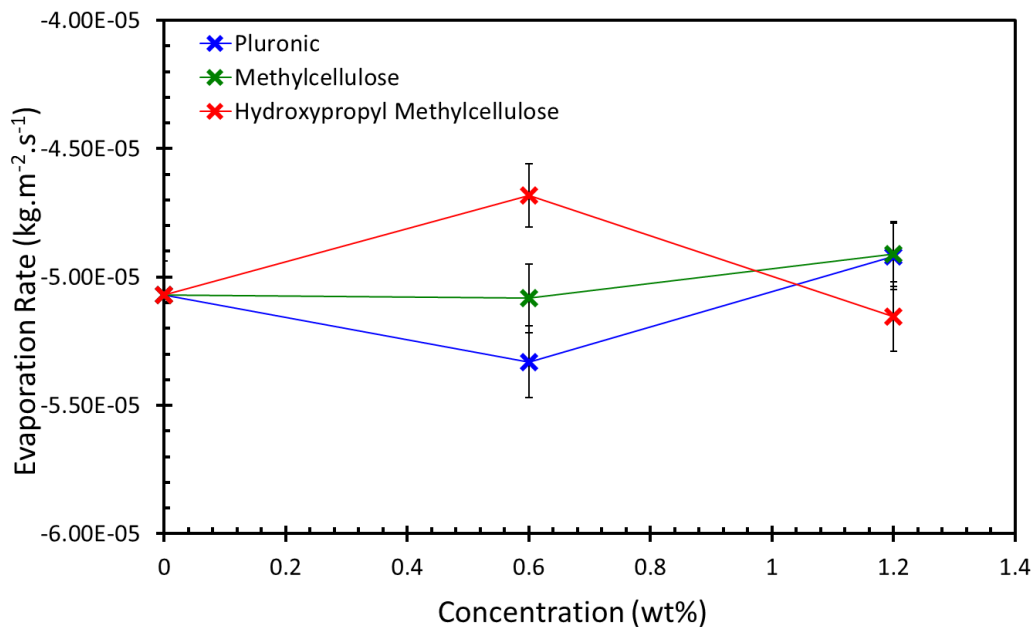
Figure 3:15 - Shows the initial rate of evaporation of water from a film of latex 223-2 and 5 wt% Texanol™ with the addition of three different additives dried at 40 %RH. It can be seen that increasing the concentration of additive appears to have no effect on the rate of evaporation, this is in contrast to the films dried at 20 %RH in which increasing the concentration of the additive appeared to increase the rate of evaporation.

104
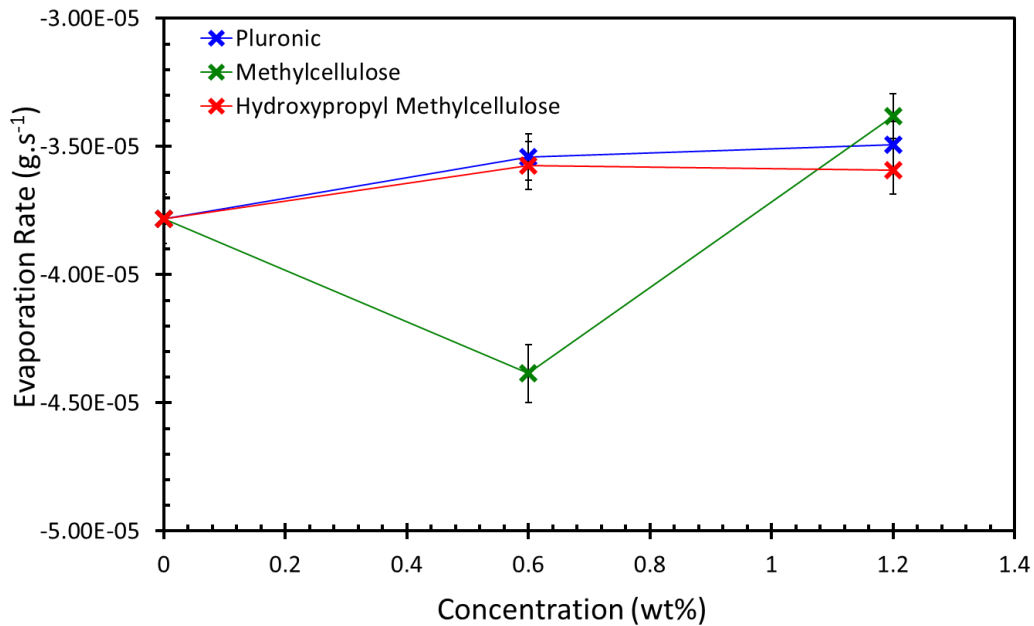
Figure 3:16 – Shows the initial rate of evaporation of water from a film of latex 223-2 and 5 wt% Texanol™ with the addition of three different additives dried at 40 %RH. It was mentioned that in Figure 3:11 there was an anomalous data set for sample MC2. If this is removed from the above figure, then it can be seen that with increasing concentrations of additive the evaporation rate is slightly decreased. However, comparing this small decrease at one of the three measured humidity levels, to the change in rate caused by altering the humidity it can be seen the effect is negligible.

Looking above at Figure 3:14 - Figure 3:16 the first thing to note is that the values observed in this experiment are comparable to the values that Croll reported in some of his early work in this area.[24,25] Croll reported that for a latex of 19% and 47% volume fraction dried at 50 %RH he observed an evaporation rate of 3.2 – 7.1 x10^{-5} kg.m^{-2}.s^{-1} and 3.1 – 6.8 x10^{-5} kg.m^{-2}.s^{-1} respectively, this was dependant on the airflow over the drying sample. Therefore, the range of rates that were observed in this experiment of 3.4 – 7.2 x10^{-5} kg.m^{-2}.s^{-1} fall well within a range of values that could be expected with the variation of humidities studied. Beyond this it can be seen that changing the concentration of additive has a minimal impact on the rate of evaporation. At each of the three measured humidity levels the concentration of additive affected the rate of evaporation differently. At 20 %RH (Figure 3:16) with an increase in concentration came gave rise to an acceleration of evaporation. This sits at odds with what was expected to happen, with the

105

hypothesis being that increasing the concentration of hydrophilic molecule would decrease the rate of evaporation. When the humidity was increased to 40 %RH (Figure 3:15) on average across the three additives no change in rate of evaporation was seen. In contrast at 60 %RH (Figure 3:16) increasing the concentration of additive appeared to reduce the rate of evaporation, which is in agreement with the hypothesis. However, when comparing the observed changes in the rate of evaporation where the concentration of additive is varied, either positive or negative, with the changes in the rate of evaporation caused by humidity, it becomes apparent that the former are almost negligible. Looking at the system experiment conducted at 60 %RH, which exhibits the best improvement to the drying property of the latex, it can be seen that the sample containing the most additive has a rate of evaporation that is ~0.2 x10^{-5} kg.m^{-2}.s^{-1} less than the sample with no additive. Using the sample containing no additive it can be seen that changing the humidity from 20 %RH to 60 %RH changes the rate of evaporation by ~2.5 x10^{-5} kg.m^{-2}.s^{-1}. Comparing the two values it can be seen that the effect of humidity is far greater and that only at higher humidity levels does the additive have the desired effect, albeit minimal.

It is clear that, taking in to account the concentration limit imposed by viscosity, varying the additives does not have enough of a desirable effect on the rate of evaporation at the concentrations used to have a practical significance. At higher concentrations evaporation may be retarded but at the price of a system with a viscosity too high for use as a paint.

3.7. Conclusions

In order to improve the properties of water-borne paints fundamentally the rate of evaporation needs to be decreased. A decrease in the rate of evaporation correlates with an improved opentime. In this section an attempt was made to use an additive, specifically an additive, to slowdown evaporation. However, adding such an additive has limitations. The additives were chosen as they have a high affinity for water in their concentrated state, as characterised by their water activity. In their concentrated state their water activity is low and therefore one could theorise that they would be a good additive in order to slow down evaporation. However, with increased concentration also comes increased viscosity. If a paint's viscosity is too high upon application, any surface defects introduced through the application process will not self-correct through the natural flow of the paint. This will result in a poor finish and, due to a high viscosity, the inability to correct these defects formed upon the initial application.

As these additives have such an effect on the system's viscosity, only low concentrations of additive can be used. Unfortunately, at these low concentrations the effectiveness of the additives at slowing the rate of evaporation is reduced. In order for an additive to function at reducing evaporation, as well as allowing a paint to flow and have a good opentime, the water needs to remain mobile. At its most fundamental, in order for the properties of a water-borne paint to be drastically improved the vapour pressure of water needs to be changed dramatically. Vapour pressure can be altered through the addition of salt and other additives but not by enough without leading to other problems with the film formation, such as viscosity.

By looking at how humidity changes the rate of evaporation from these latex systems, it can be seen how altering the vapour pressure of water results in paint with improved properties. Across the observed humidity range of the UK a change a in drying time of around 50 % was seen. Even if the vapour pressure of water in a water-borne paint could be drastically changed, due to fluctuations in humidity the drying time will always be heavily dependent on external factors. The section discusses future work that could be undertaken to advance this study.

All this being said, during this chapter the additives used seemed to alter the properties of the dried films in a different way. Upon initial inspection although the additives have not altered the drying time as desired, they seem to have had an influence on the observed cracking within the film. Usually coalescent solvents such as Texanol™ are used to facilitate good film formation. However, regulation still states that it is defined as a VOC. Not only are the additives used in this study not defined as a VOC, some of them are derived from cellulose and hence a renewable resource. In the next chapter this phenomenon will be studied in greater detail.

3.8.   Future Work

In this chapter mass loss was used as way to quantify the drying characteristics of a drying latex film. As mentioned earlier this is not the only property that can be used to quantify how additives are altering the drying properties of a latex film. Open time provides information on how the mobility of the particles are evolving throughout the drying time of the film. However, as mentioned earlier the ASTM for measuring open time leaves room for a lot of experimental error and offers poor time resolution. If future work was to be carried out in this area the focus needs to be on looking at additives that would allow particle mobility to be increased further at higher particle volume fractions. Two methods that could be used to quantify this would be: (i) the use of a linear drying time recorder and (ii) a study of particle mobility.

3.8.1.   Drying Time Recorder

ASTM D5895-13 outlines the method of using a drying time recorder.[105] A linear drying time recorder consists of multiple styli that have 2 mm rounded tips. They are typically drawn over a sample that is applied to a 25 by 300 mm glass panel. Pressure is controlled with the use of a 5 g weight mounted on the tip of the stylus. The speed at which the recorder moves is controlled precisely so that its position on the panel relates to a known time. Points throughout the drying profile of a latex film correspond to characteristic marks left by the stylus. A schematic of the different stage of film formation are outlined in Figure 3:17.
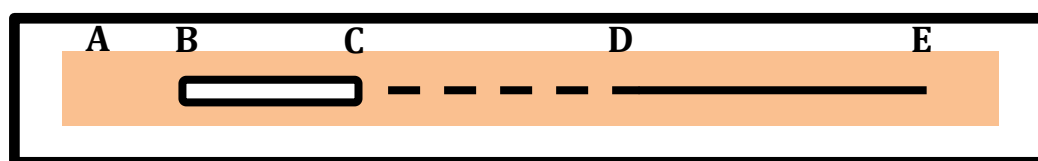
Figure 3:17 – Shows a schematic of the characteristic stages that can be measured with a linear drying recorder. A – Start Point, B – Set-to-touch time, C – Tack-free time, D – Dry-hard time and E – Dry-through time.

As it can be seen using a linear drying time recorder information on all stages of film formation can be gathered. One preliminary investigation was carried out with a system containing Latex 223-2 dried at three different humidity levels, for each run the set-to-touch time was used as it is the time that would represent open time closest. The data for this is shown below in Figure 3:18.
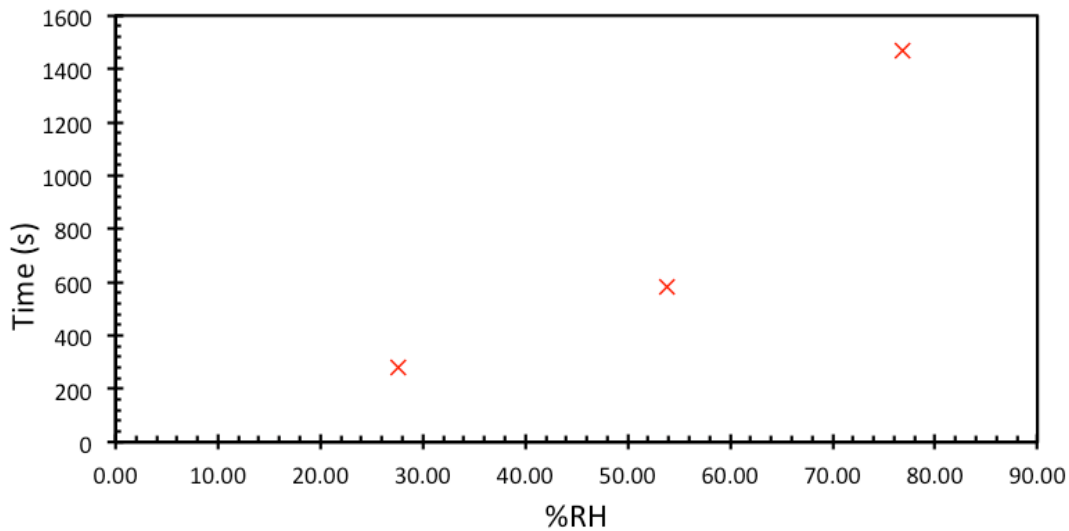
Figure 3:18 – Shows the set-to-touch time of latex 223-2 with 5 wt% Texanol™ at three different humidity levels. It can be seen that as expected the time increases with respect to increasing humidity level.

It has been shown that with increasing humidity the set-to-touch time behaves as expected and increases which is in agreement with the mass loss data. However, with the addition of additives, the later stages of film formation could be affected, something that was not investigated using gravimetric analysis. However, adding an increased concentration of additive still increases viscosity and makes controlling film thickness using standard equipment difficult. In order for a linear drying time record to be used to study the effects of additives on the drying behaviour of latex films a custom way to control film thickness, regardless of viscosity, would need to be developed. Once this had been achieved, using a linear drying time recorder would be a good way to further investigate the effects of additive concentration on all stages of film formation.

3.8.2. Particle Mobility

As mentioned, particle mobility is directly related to the open time of paint. Recently there has been a drive to characterise the mobility of particles throughout a drying latex film. This makes the analysis of particle mobility an ideal direction to take this work alongside the use of a linear drying time recorder. Perhaps the most researched area is around adaptive speckle imaging, also called diffuse wave spectroscopy.[28,106–109] This technique is in essence an extension of DLS that can be used in opaque systems. The experimental set-up involves shining a laser at a drying latex film, a camera can then be used to study the backscattered light. From this the correlation function, and in turn the speckle time, can be calculated. This method allows the examination of very small latex samples, such as latex 223-2 that is used in this study. A study that used adaptive speckle imaging in conjunction with a linear drying time record would provide a good way to investigate how the various stages of film formation relate to the mobility of the particles in the system. The effect that additives have on particle mobility could then be investigated and compared to changes in the physical properties of the paint.

Chapter 4:   Cracking in Latex Films

This chapter explores how increasing the concentration of additive reduces cracking. The relationship between the two parameters has been studied using a number of techniques including Dynamic Mechanical Analysis *(DMA)* and Atomic Force Microscopy *(AFM).* The aim of the chapter is to further understand how the additive affects the film formation process.

In order for a paint film to have the correct barrier properties the film needs to be homogeneous, without any cracks or deformities. One only has to observe an incorrectly applied paint or old paintings to see that cracking can be a real problem for the paint industry. This has been the case long before the use of water-borne paints. In fact it can be seen in some of the most famous paintings around the world, including the Mona Lisa, Figure 4:1.
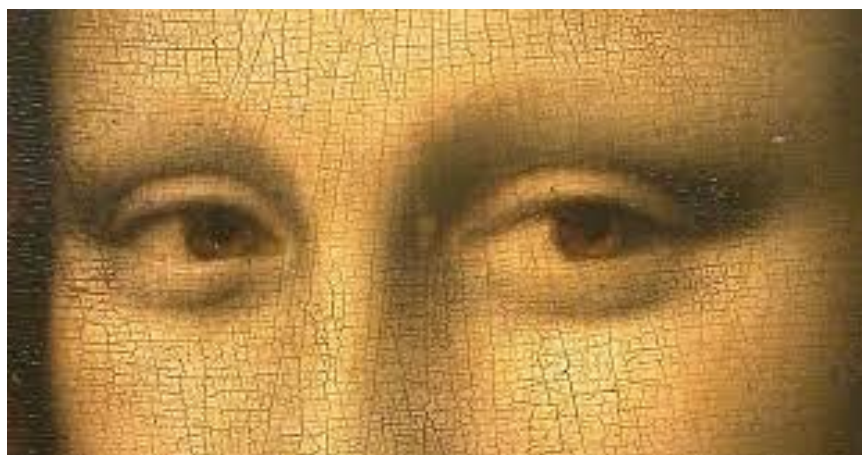
Figure 4:1 – Shows a section of the Mona Lisa painted by Leonardo Da Vinci c. 1506. Looking closely it is possible to see the regular cracking structure know as craquelure in the art industry. (Image Available from: <https://www.pexels.com/photo/woman-art-painting-mona-lisa-40997/> [viewed 17th of September 2019]) As mentioned in greater detail in section 1.6.2 the cracking pattern is specific to the region that the painting was produced and is as a result of the materials and conditions used in its production.[56,57,110]

The cracking patterns in the oil based paintings of this era act as a fingerprint to the origin of the painting. In particular the variation between the cracking patterns stems from differences in the materials used and the climate the painting was produced in. Interior decorative paints can also exhibit cracking, a topic that is covered more extensively in section 1.6.2.

When a thin film of latex is applied to a substrate, such as paint being applied to a wall, evaporation concentrates particles into a close packed array. As the latex particles typically bind to the substrate, it essentially "pins" the film to the geometry to which it was applied. This results in a film that resists deformation in the transverse plane, combining this with further evaporation to the film can result in tensile stresses that can cause a film to crack. If the particles in the latex are dried above their T_g then the voids that result from the particle packing will be lost, as the particles deform under the stress of the film formation leading to a transparent film. When it comes to studying the cracking in paint films, at first glance it would appear to be a simple process due to the relatively large size of the cracks. However, in order to investigate the reason for the cracks alternative microscopy techniques had to be used.

4.1.　　　Effect of Coalescence Solvent on MFFT

In order to reduce the cracking during film formation and allow a homogeneous film to form, coalescent solvents are often added to latex formulation. In brief, these solvents are added to a formulation to lower the T_g of the system to a point whereby the film forms at room temperature. The solvent then evaporates over time to leave a film that has a T_g higher than that of the ambient temperature. The amount of coalescent solvent that is added to the latex dispersion depends on the T_g of the latex particle and the desired level of plasticization. In order to keep the VOC level to a minimum, the T_g of the system is required to be at a temperature such that the system will form a homogeneous film at ambient temperature. The use of coalescent solvents has been discussed in greater detail in section 1.6.2.2. The temperature at which a latex film forms a continuous film is termed the minimum film formation temperature or *MFFT.* The MFFT of a system needs to be below the temperature that the film is being applied otherwise the film will be subject to cracking resulting in a poor finish. The latex used in this investigation, latex 223-2, has an MFFT of around 20 °C. The MFFT of this latex with varying concentrations of Texanol™ has been studied with the results being shown below in Figure 4:2.
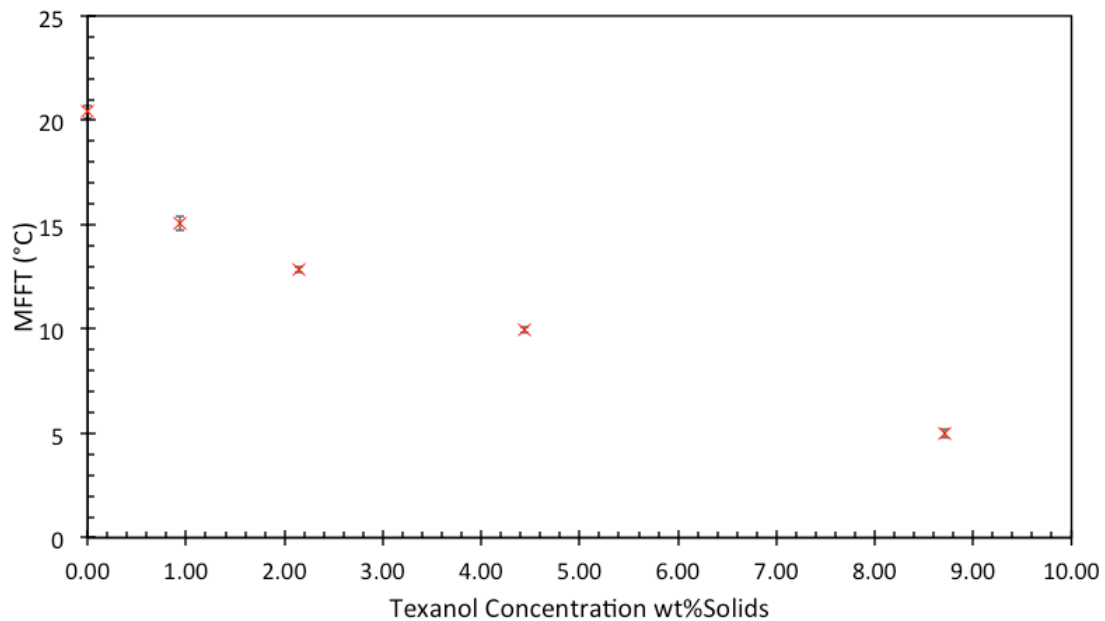
Figure 4:2 - Shows the relationship between the concentration of Texanol™ and MFFT in a film of latex 223-2. It can be seen that through increasing the concentration of Texanol™ the MFFT is significantly decreased from around 20 °C to around 5 °C.

Figure 4:2 shows the relationship between the concentration of coalescent solvent and the MFFT in a film of latex 223-2. The MFFT decreases with an increase in the concentration of Texanol™. This is consistent with what is generally observed in the literature.[111] As mentioned in section 1.6 this is as a result of increasing the polymer interdiffusion between the latex particles. However, using coalescent solvents such as Texanol™ still adds to the VOC level of the system. With the drive towards reducing and eventually eliminating all VOCs, alternative methods for lowering MFFT are required. At the end of Chapter 3: it was mentioned that a number of the additives studied had some effect on the level of cracking in the films studied. These additives are not classified as VOCs and hence this property could be of great interest when trying to produce films with lower levels of VOCs. In the following sections this reduction in cracking has been investigated further.

4.2.　　　Optical Microscopy

As mentioned in the previous section, traditionally coalescent solvents are used to minimise cracking and to maintain the required structural and barrier properties of the paint film. However, during the drying time investigation in Chapter:3.6 it became apparent that through the addition of certain additives, the cracking in the latex films could be reduced. In order to investigate this further a study into the cracking of latex films was conducted in order to deduce the reason behind the reduction in observed cracking.

Although not in the original scope of the project, a reduction in cracking using non-crude oil derived additives should be of interest to AkzoNobel from both an environmental and economic standpoint. Initially the latex films were dried at 20 %RH with the wet film thickness of ≈0.5 mm controlled with PTFE O-Rings. Latex 223-2 has a Fox T_g of approximately 15 °C and a MFFT at 250 µm thickness of 20 °C. The latex without additive is mixed with 5 wt% Texanol™ and a number of additives at different concentrations were added. The concentrations used in the investigation are shown in Table 4:1, it has been reproduced below for ease of comparison. The dried films were then imaged using a Motic SMZ-168 stereomicroscope; the images are shown in Figure 4:3.

Table 4:1– wt% Concentration of solids of Texanol™ and Additive

	223-2	*MC1*	*MC2*	*HPMC1*	*HPMC2*	*Pl1*	*Pl2*
Texanol™	5	5	5	5	5	5	5
Additive	0	0.6	1.2	0.6	1.2	0.6	1.2
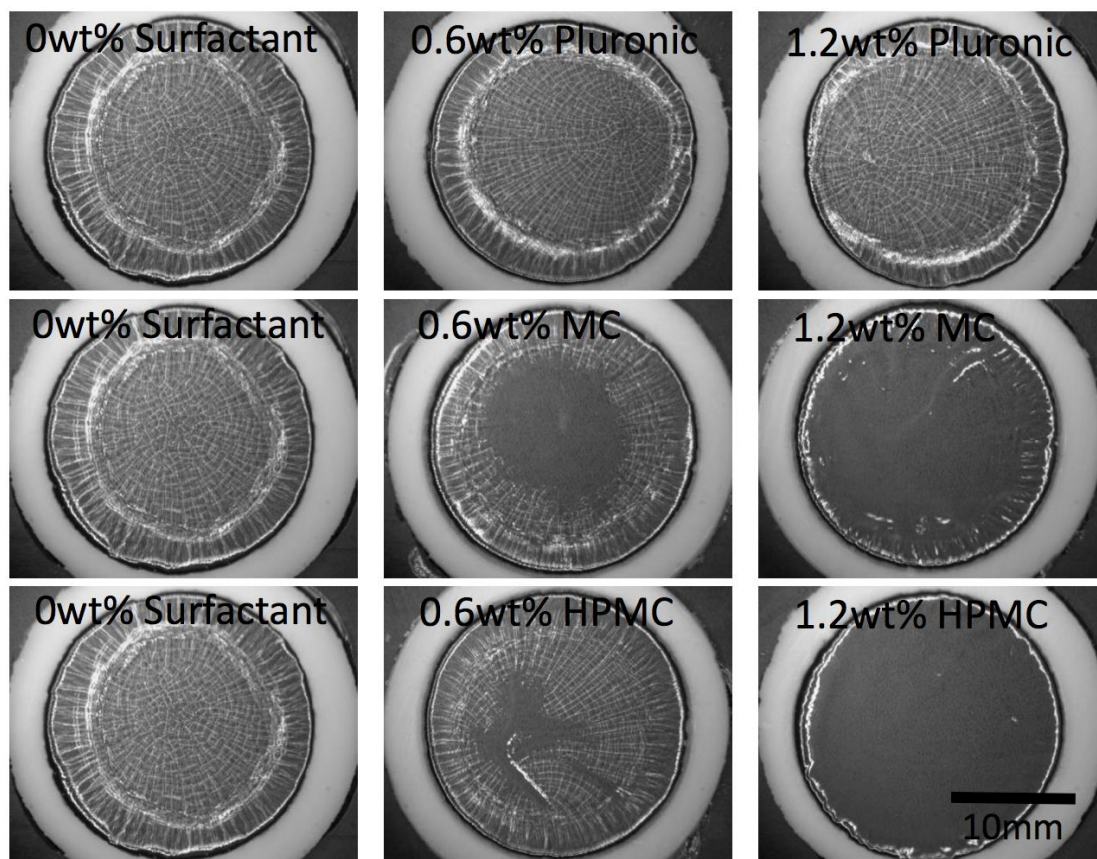
Figure 4:3 – Shows films of Latex 223-2 containing 5 wt% of Texanol™ and varying additive concentrations dried at a controlled humidity of 20 %RH at 20 °C. It can be seen that through the addition of the Pluronic additive no change in cracking is observed. However, it can be seen that with increasing concentrations of the cellulose-derived additives, cracking is drastically reduced.

With reference to Figure 4:3 above, there is a clear difference between the different film formulations. The first thing to note is that at this temperature and film thickness, and without any added additive, the film containing just latex 223-2 and Texanol™ has a high degree of cracking. Looking back at Figure 4:2 it can be seen that without any added coalescent solvent the MFFT of latex 223-2 is approximately 20 °C and with the concentration of Texanol™ *(5 wt%)* used in this sample the MFFT should be around 10 °C. This observation alone illustrates one of the biggest problems when it comes to quantifying the MFFT of a system, the fact that the cracking characteristics of a film are dependent on the thickness of the film as well as the composition of the latex particle and the concentration of the coalescence solvent. This problem translates to the application of these latex films as water-borne paints. If the films are applied with discrepancy in thickness,

either due to poor substrate preparation or due to incorrect application, then the film could show areas of cracking that the user could interpret as a "bad paint". In this study looking at the effects of added additives to the latex systems it is crucial to control the thickness of the film under investigation. This is particularly important with the additives used due to the changes in viscosity that they cause. These viscosity changes could cause issues when using standard film application techniques such as a "draw down cube" or a "K Bar" that rely on the viscosity of the system to stop the film from flowing and changing thickness once the wet film has been applied. This would make it almost impossible to isolate the effects of the added additives from the effects of the changing thickness. Therefore, it is important to note that the films shown in Figure 4:3 have a well-defined thickness due to the use of PTFE O-rings. For this reason it is possible to study the effects of the additives alone, without any added complications caused by changing viscosity and hence film thickness. It could be imagined that the dried film thickness would increase with increasing additive concentration. Theoretically the dried film without the addition of any hydrophilic additives would be 380 μm thick. At the concentrations used in this investigation the maximum increase in thickness of the films caused by the inclusion of the additives would be about 4 μm. This small increase would be nearly impossible to measure with any confidence with the equipment available if the film was perfectly flat, let alone with a film that has as many cracks and small imperfections that these films show. For these reasons it was decided that physical measurements of the film's thickness would not be conducted in this investigation.

Looking again at Figure 4:3 some initial observations can be made. Firstly comparing the effects of the different additives it can be seen that the cellulose derived additives, Methyl Cellulose (MC) and Hydroxypropyl Methyl Cellulose (HPMC), have a much greater effect on the level of cracking compared to the Pluronic (PEG-PPG-PEG) additive. Looking in greater detail it can be seen that the Pluronic additive does not appear to reduce the cracking in the film at all whereas the level of cracking in the films containing MC and HPMC reduces with increasing Texanol™ concentration. There are a numbers of ways that cracking can be

reduced in a drying colloidal film, some of which could be responsible for the reduction in the studied films.

The first way that cracking can be reduced is by controlling the drying rate of the film. If the rate of evaporation is reduced then the film is less likely to crack under drying.[112–114] One of the reasons for this is that the slow drying allows the network of latex particles to pack more efficiently and in some cases even form a colloidal crystal.[21] In this ordered structure each particle has more neighbours meaning that during the coalescence phase a stronger network can develop.

It has already been shown that the addition of these additives does not have a drastic effect on the drying time of the films under investigation. However, in order to fully exhaust this hypothesis a further 7 films were dried at a higher humidity. Under these conditions it has been shown in the previous section that the drying time will be increased by approximately 25%. Therefore, if the mechanism by which the cracking is being reduced is caused by the aforementioned particle rearrangement due to a longer drying time, then increasing the humidity should reduce the cracking. Images of the films dried at 40 %RH are shown in Figure 4:4.
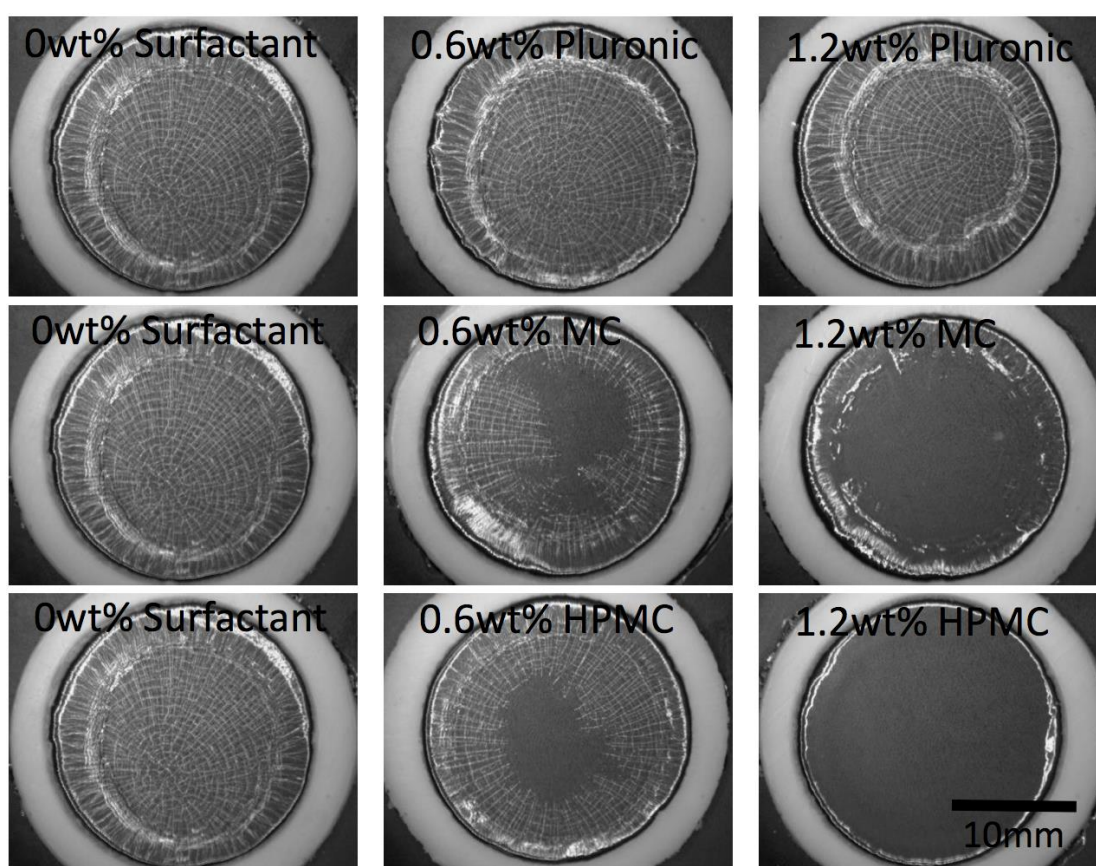
Figure 4:4 – Shows films of Latex 223-2 containing 5 wt% of Texanol™ and varying additive concentrations dried at a controlled humidity of 40 %RH at 20 °C. The same trends can be observed in relation to cracking as in Figure 4:3, with the Pluronic additive having little effect and the cellulose-derived additives reducing cracking drastically. However, no changes in cracking can be observed with an increase in Humidity and hence drying time.

Looking above at Figure 4:4 it can again be seen that the cellulose derived additives have more of an effect on the film formation than the Pluronic additive, with both HPMC and MC reducing the film cracking as their concentration increases. However, when comparing the samples dried at 40 %RH with the samples that were dried at 20 %RH there is minimal difference. For this reason the initial hypothesis, that the rate of drying allows the particles to rearrange to reduce the stress development, hence reducing the film cracking, no longer stands.

Since the differences in the level of cracking are not related to the rate of drying, the additives must be affecting the film formation in an alternative way. When thinking about the ways that the additives could be affecting the film formation the obvious comparison is to investigate the way that coalescent solvents work by plasticising the latex and allowing film formation to occur below the T_g of the particles. If the additives were reducing the cracking by plasticising the latex then the final properties of the dried film could be detrimentally affected, despite the reduction in cracks. The reason for this is as a coalescent solvent, such as Texanol™, evaporates over time, albeit slowly, this means that over a period of a few weeks after the films application the solvent evaporates and the film's T_g approaches that of the particle. This means that the paint film will have the desired properties such as low dust pick up that is required from an interior decorative paint. However, as the additives used tend to be solids or very high viscosity liquids their boiling points are very high. This would mean that if they do plasticise the latex films then they would remain this way resulting in a finished film unsuitable for use as a decorative paint film, despite its good appearance. In order to test this hypothesis the T_gs of the films were studied.

There are a number of techniques that can be used to measure T_g including *Differential Scanning Calorimetry* (DSC) and *Thermo Mechanical Analysis* (TMA). However, perhaps the most sensitive technique for measuring T_g is *Dynamic Mechanical Analysis* (DMA); this technique was used to measure T_g in this study. The following section will briefly reintroduce the technique and look at how it has been used to study the potential plasticisation of the latex and hence a potential change in the film's T_g.

4.3.   DMA

DMA is a powerful tool when exploring the T_g of polymer samples. In brief DMA works by applying cyclic deformation to a sample of known geometry. The sample can either be studied with a controlled stress or a controlled strain. For a known stress, the sample will deform a certain amount. In DMA this is done sinusoidally. How much the sample deforms is related to its stiffness or, to be more precise, its modulus. In order to use this to measure a sample T_g or other thermal transition points the sample can be run over a range of temperatures. It is then possible to look at how the modulus of the sample changes and therefore where the onset of the transition is. A more detailed explanation and discussion into DMA is provided in section 2.4.2.

When conducting a DMA investigation one of the most important things to get right is the correct sample geometry. Depending on how stiff the sample is, the thickness of the sample will depend on the geometry that the sample can be run in. Since the samples under investigation are typically thin with a fairly low modulus the geometries that can be used are fairly limited. One way that this problem can be overcome is to use a materials pocket. As the materials pocket is made of a stiffer material than the sample it allows the T_g of the sample to be investigated but as the modulus is dominated by the aluminium formation on the modulus, the material cannot be gathered. Materials pockets prove particularly useful when studying samples such as powders.[115] However, it was not entirely possible to control the sample preparation using this method which caused discrepancies in the data. If a rough idea of the T_g of a sample is needed then using materials pockets would be more than sufficient and, given the ease of the experiment, it would make a good starting point. Having said that, in this investigation it was necessary to examine small changes in sample T_g , therefore materials pockets were not sufficient. It is also important that the thickness of the sample is comparable to the thickness of the sample when used as water-based paint. For these reasons it was necessary to use the latex films in a tensile geometry. A requirement for this geometry is that the films are freestanding with no substrate. The films were therefore cast onto glass slides and then carefully

removed to produce a freestanding film. A better explanation of the method by which the samples were produced is provide in section 2.4.2.

A decision was made to focus on the sample containing Methyl Cellulose as it showed a full range of cracking levels, from a fully homogeneous film to a film that was fully cracked. It provides the best opportunity to determine whether the additive is plasticising the whole film or if the additive is reducing the MFFT *via* a different mechanism. Before looking at the results from the DMA experiment, it is worth noting that Edelhauser, and later Vijayendran *et al.,* have shown that SDS plasticises P(VAc) latex particles.[116,117] It has also been shown that the T_g and MFFT of an acrylic-acetate latex are lowered through the addition of a nonylphenol ethoxylate additive.[118] With this in mind, if the DMA data on the T_g of the latex film containing MC shows a reduction then it could reasonably be said that cellulose derived additives are indeed plasticising the Styrene-Acrylic latex 223-2. The data from this experiment is shown in Figure 4:5.
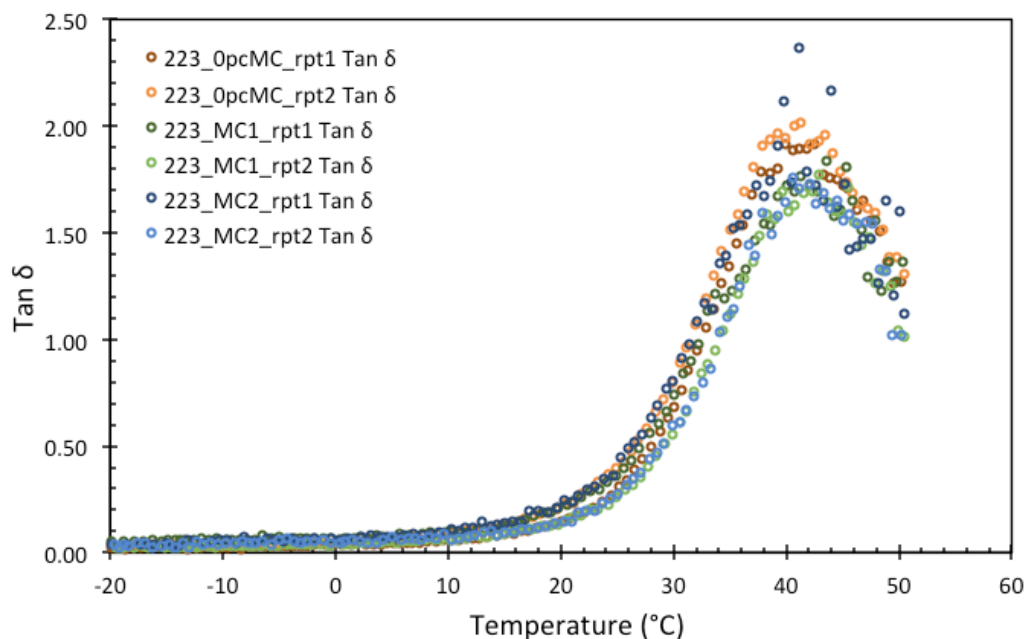
*Figure 4:5 - Shows the Tan δ values for latex 223-2 containing varying concentrations of Methylcellulose. **Error! Reference source not found.** shows the concentration of Texanol™ and MC used in the study.*

Looking at Figure 4:5 it is apparent that there is no real change in the T_g of the film, at least not a change that would account for the disparity in the level of cracking observed . If anything, it may be argued that the films containing more additive seem to have a slightly higher T_g. This disproves the initial hypothesis that the additives are plasticising the latex particles and hence lowering the T_g of the film, allowing coalescence of the particles and crack free film formation. However, this does not mean that the additive cannot partially plasticise the particle. If the additive plasticised just the outer edge of the latex particle it could be imagined that this would allow the particles to coalesce with just the outer edges of the particles deforming due to their plasticised state. Alternatively as DMA is measuring the final property of the film, and does not take into account how the additives are affecting early stages of the film formation, if the additives were altering the properties of the system in the early stages of film formation and not the final property of the film then DMA would not measure a change. Therefore, in order to explore the effect that the additives are having on the film formation as a whole, rather than focusing on the final appearance or T_g of the system, the MFFT of the films have been measured.

In the next section the films' MFFT will be measured for a number of different additive concentrations giving an idea of how varying the additive concentration will affect the MFFT. If the MFFT of the films are consistent with the microscope images then it shows that the additives are affecting the film formation in a way that does not involve the plasticisation of the latex particles, at least not the whole particle.

4.4.   MFFT

As discussed in in section 4.1 measuring MFFT gives a numerical value for how well a film forms by giving the minimum temperature at which the film formation takes place. In section 4.1 the effect of adding varying concentrations of the coalescence solvent Texanol™ was examined. It was shown that adding an increasing concentration of Texanol™ drastically reduced the MFFT. In this section the effect of adding varying concentrations of additive will be studied. It has been shown that adding additives has enabled better film formation for both the cellulose derived additives, with the pluronic additive seemingly not affecting the film formation at the concentration used. However, when the effect of MC was studied using DMA to measure the films' T_g, no effect was observed. If the additives are actually affecting the mechanism by which the film forms and the final properties of the film, then a positive correlation between the microscopy images in section 4.2 should be seen. Below, Figure 4:6 shows the relationship between the additive concentration and the MFFT.
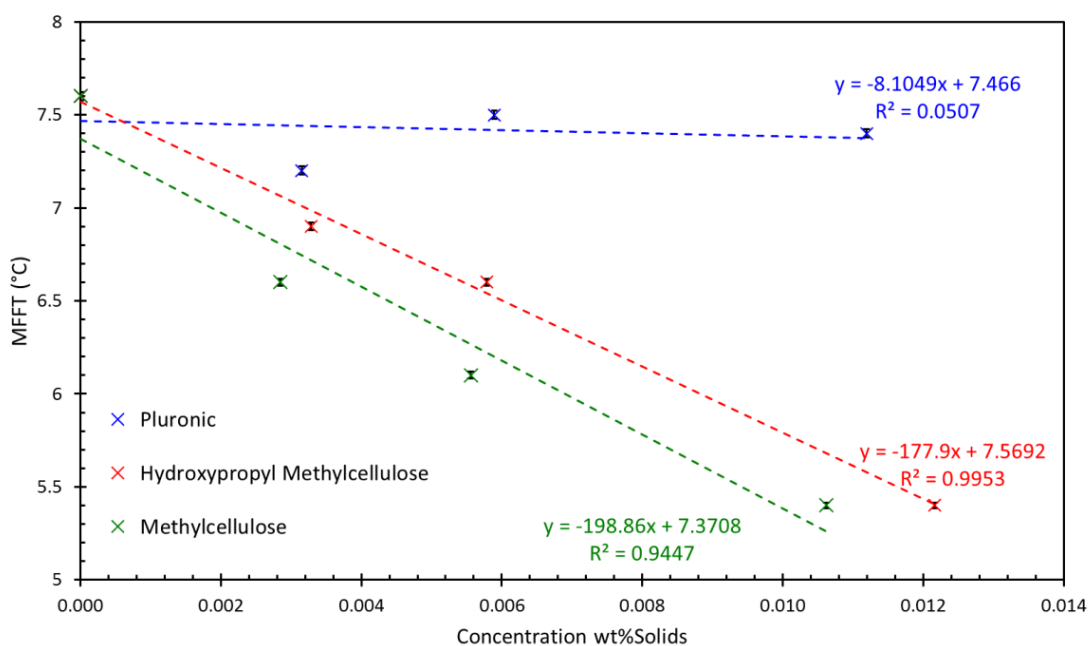
Figure 4:6 – Shows the relationship between MFFT and Concentration of additive in a system containing latex 223-2 and 5 wt% Texanol™. As observed in the films in Figure 4:3 - Figure 4:4 the Pluronic additive has minimal effect on MFFT. In contrast the cellulose-derived additives both reduce the MFFT with respect to increasing concentration. This reduction is minimal, only reducing the MFFT by around 3 °C, but still in agreement with the previously observed films in Figure 4:3 - Figure 4:4.

The first thing that must be discussed in relation to Figure 4:6 is the uncertainty in the measurements. On the graph the error bars represent a ±0.3% error in the measurement based on the manufactures specifications however, when using an MFFT bar it is really the systematic uncertainty that must be considered. One of the main sources of error is down to the way that the MFFT is identified, the measurement relies on the user to identify the cloudy-clear transition point therefore errors between different users can occur. In this experiment, all measurements were conducted on the same day by the same user to minimise any errors. To further the confidence in the experimental data presented in Figure 4:6, in this study it is the general trend in the data presented that is of interest, rather than the exact values of MFFT. Looking at the data in Figure 4:6 and comparing it to the images in section 4.2 we can see that it roughly aligns. One thing to note in particular is that the film produced for MFFT follows the experimental method outlined in section 2.4.1. This means that the films used in the MFFT measurement are thinner than the films used in the drying experiment from section 3.6 and therefore the microscopy images early in this chapter. This is important, as the thickness of a film is proportional to the level of observed cracking. This is as each latex system has a Critical Crack Thickness *(CCT),* meaning that a thicker film requires a higher temperature in order to form a homogeneous crack-free film.[102]

As has been previously discussed, due to the changing viscosity of the latex systems, when different additive concentrations are used using a standard film applicator (such as a drawdown cube) this can produce film with varying thickness due to the flow of the sample after application. This error was controlled in the drying experiments in section 3.6 through the use of a PTFE O-ring, hence removing the effect that film thickness has on the cracking levels within the film. However, in the MFFT experiments the thicknesses of the films has not been controlled in the same way as in the previous section, instead the films have to be applied using a standard 100 μm drawdown cube. This could mean that trends observed in the MFFT experiment could be an artefact of the higher additive concentration/higher viscosity systems retaining their applied thickness and cracking less. However, by conducting a simple thought experiment it can be shown that, although the MFFT shown in Figure 4:6 may not be the case under

different circumstances caused by changes in the application, changes in the viscosity caused by the additives does not cause a false positive result. Reflecting on how additive concentration affects the viscosity of these systems, it is evident that increasing the concentration of additive increases the viscosity of the system. A wet film with a higher viscosity will have less of a tendency to flow after application than a wet film with a lower viscosity. Therefore, a film containing less additive will be less viscous, resulting in a thinner film that would show an artificially low MFFT. In comparison, a film containing more additive will be more viscous, resulting in a thicker film that would show an artificially high MFFT. With this in mind if looking back at Figure 4:6 it can be seen that even if the worst case scenario is true and the films containing less additive are displaying an MFFT that is incorrectly low and *vice versa,* the influence of the cellulose-derived additives on the MFFT of the systems is great enough to display a positive trend with relation to additive concentration.

The trend that is observed between the concentrations of the cellulose-derived additives and the MFFT of the films, provides information on how to further study these systems. Given that the films' T_g is unaffected but the MFFT is, then the previous hypothesis still stands: that the additive could be aiding film formation by plasticising the outer boundary of the particle, but not the system as a whole. In order to further test this hypothesis the system needs to be investigated on the particular level. As previously discussed, the particle size is below the diffraction limit of visible light. This means that an alternative microscopy technique needs to be used. The chosen technique to be used is Atomic Force Microscopy *(AFM).* As discussed in section 2.2.3 AFM can give more than just topographical information. For this reason AFM was the chosen technique for imaging the films on the particular level. In the next section the samples from section 4.2 have been imaged using AFM.

4.5.   AFM

In order to investigate the structure of the films on the particular level (to see if there are any signs of the particles being plasticised around the outer edge and hence proving the hypothesis correct) AFM was chosen to image the films. When it comes to imaging artefacts on the submicron level the options are limited to TEM, SEM and AFM. As TEM and SEM provide information based largely on the shape of the sample, compared to AFM that allows a deeper investigation into the physical properties of the sample, AFM was selected as the technique to go ahead with.

The basic principle of AFM is based upon a cantilever/tip assembly that interacts with the sample. As the cantilever/tip assembly, more commonly called a probe, is moved closer to the surface of the sample the attractive force between the tip and the sample causes the probe to deflect towards the surface. However, as the tip is moved even closer to the surface the close range repulsive forces take over. Using a feedback loop the force that is applied to the cantilever is kept constant, this keeps the probe at a constant distance above the surface. Using a laser and a position-sensitive photo diode (PSPD) the position of the tip can be monitored precisely, giving a vertical resolution as low as 0.1 nm. This method of keeping the tip at a constant distance from the surface of the sample is known as "contact" mode. In order to use AFM to gain a deeper insight into the properties of the materials in the sample the AFM can be run in "tapping" mode. In order to run an AFM in tapping mode the probe is attached to a piezo oscillator, as the probe is run across the sample it is set to oscillate at a certain frequency. If the sample has a peak then the probe will be forced to oscillate at a higher frequency. As with the contact mode, a feedback loop is used to adjust the probe-sample separation to maintain the probe's set frequency. Tapping mode was developed as a way to image fragile and soft samples that would otherwise be damaged from the frictional forces generated with contact mode. Alongside allowing soft samples to be studied with AFM, tapping mode also allows "phase imaging" to be carried out on samples. By looking at the shift in phase of the probe's oscillation it is possible to ascertain an idea of (amongst other things) the relative softness of the sample.

This allows one to differentiate between areas of different material within a sample that would otherwise appear to be homogeneous.

AFM was conducted using the procedure described in section 2.2.3. The AFM was set-up to measure height, amplitude and phase of the material. The system containing no additive and 5 wt% Texanol™ is shown below in Figure 4:7.
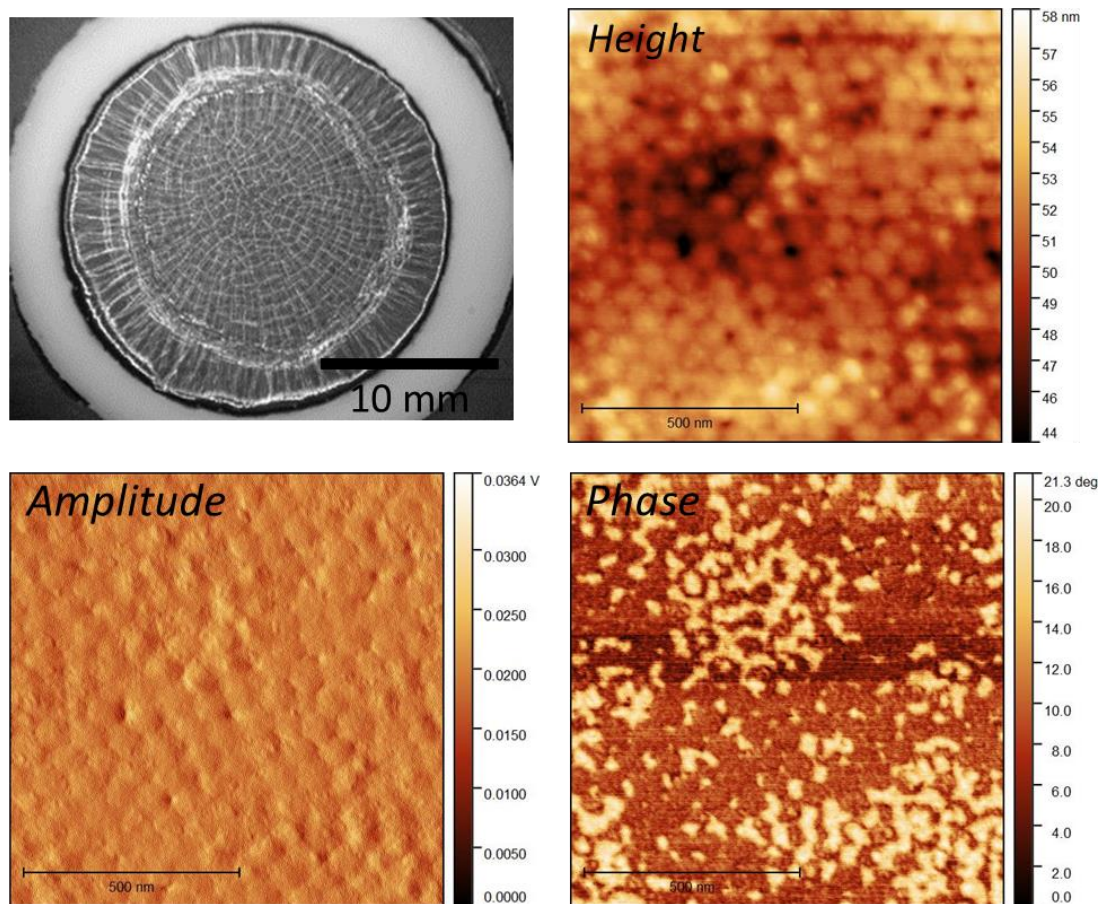
Figure 4:7 – Shows an optical micrograph and Height, Amplitude and Phase AFM micrographs of a film of Latex 223-2 containing 5 wt% of Texanol™ dried at a controlled humidity of 20 %RH at 20 °C. As expected from a film that has a large amount of cracking the particles can clearly be seen in the height image, with only minimal deformation and coalescence observed.

Figure 4:7 shows the AFM micrographs of latex 223-2 containing 5 wt% Texanol™. As can be seen from the image in the top left of the figure, in these conditions the latex is not above its MFFT as it is clearly displaying a high level of cracking. Looking back to section 1.6 it can be expected that the particles making up the film will not have fully coalesced and will have retained their individual structure. Looking at Figure 4:7 we can see that this is in fact the case with clear particles visible in both the height and the amplitude micrographs. However, despite not being above the MFFT, a few points of interest are visible in the micrographs. Upon closer examination it is possible to observe the deformation in the particles into a hexagonal structure. This slight deformation shows that the film is close to its MFFT as the Texanol™ has plasticised the latex enough to deform upon packing, but not enough to allow the formation of a crack-free film. To demonstrate how much of an effect the plasticisation caused by the Texanol™ is having on the particle deformation, an AFM micrograph of Latex 223-2 without Texanol™ has been included below in Figure 4:8.
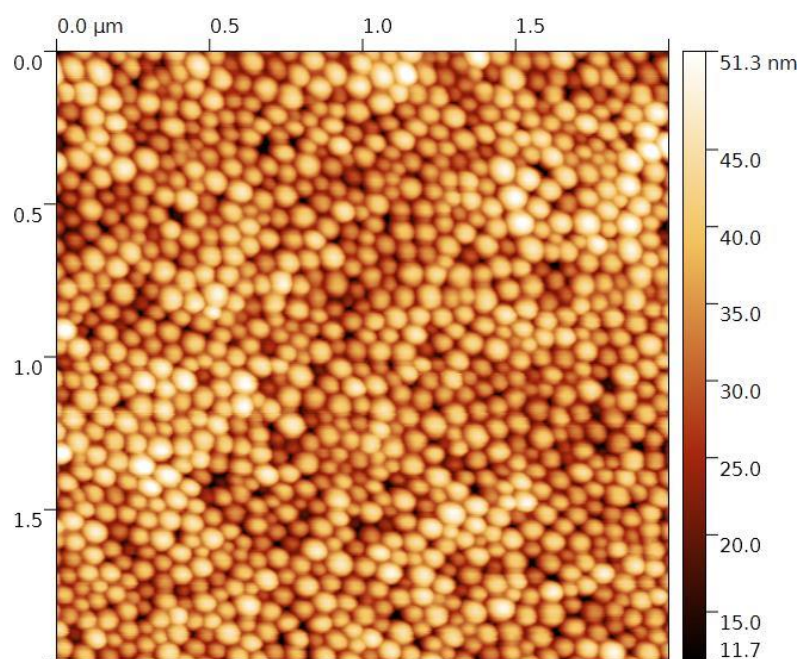
Figure 4:8 – Shows the AFM height Micrograph of Latex 223 without the addition of Texanol™. It is possible to see that without the addition of the Texanol™ the level of particle deformation is less than can be seen in Figure 4:7.

Looking at Figure 4:8 and comparing it to Figure 4:7 it can be seen that through the addition of the Texanol™ the particle deformation is increased from the film without any Texanol™. It can be seen that without Texanol™ the particles appear much moe spherical and the coalescence between particles appears to be less. However, at this concentration of Texanol™, the latex particle is not plasticised enough to allow full polymer interdiffusion across the particle boundaries. The amount of polymer interdiffusion is believed to govern the final mechanical properties of the latex film.[56,119] In this study the fact that the system is not able to form a crack-free film at this concentration of Texanol™ has necessitated the investigation into the effects of adding additives as a way to further promote the formation of a homogeneous film. Despite the particle structure being clearly visible in the height and amplitude, in the phase it is less clear. From the phase micrograph some structure can be observed. However, upon inspection it does not appear to correlate with the structure of the particles observed in the height and amplitude micrographs. Since a phase micrograph gives us information on the mechanical properties of the material and enables us to distinguish between hard and soft regions, we would expect to observe the effect of the coalescent solvent on the particles within the film. Looking at the phase micrograph with this in mind we are able to make more sense of the results. It appears that the film experiences regional plasticisation, with the Texanol™ seeming to be affecting the film in some areas and not others; this can be seen from the phase shift in the AFM micrograph. One thing to note is that the AFM is only focussing on the surface of the film whereas in the bulk of the film the coalescent solvent may be located more homogeneously throughout the structure. The reason that at this point of the investigation a decision was made to image the surface structure alone is that, as has been shown in section 1.4, films that form above their MFFT have drastically different surface structures than films that are formed below their MFFT. Going forward if the additives are acting in a way that promotes film formation *via* a similar mechanism to coalescent solvents, then a similar change in the surface structure could be expected.

Now that an initial understanding of how a sample containing no additive looks under AFM it is possible to theorise how a sample that is less cracked containing

more additive may look. If the additives are acting as a coalescence aid in the traditional sense then the film imaged under the AFM would be expected to show a more uniform structure. Initially the sample containing 1.2 wt% of the total solids of the Pluronic additive was imaged, these AFM micrographs are shown in Figure 4:9.
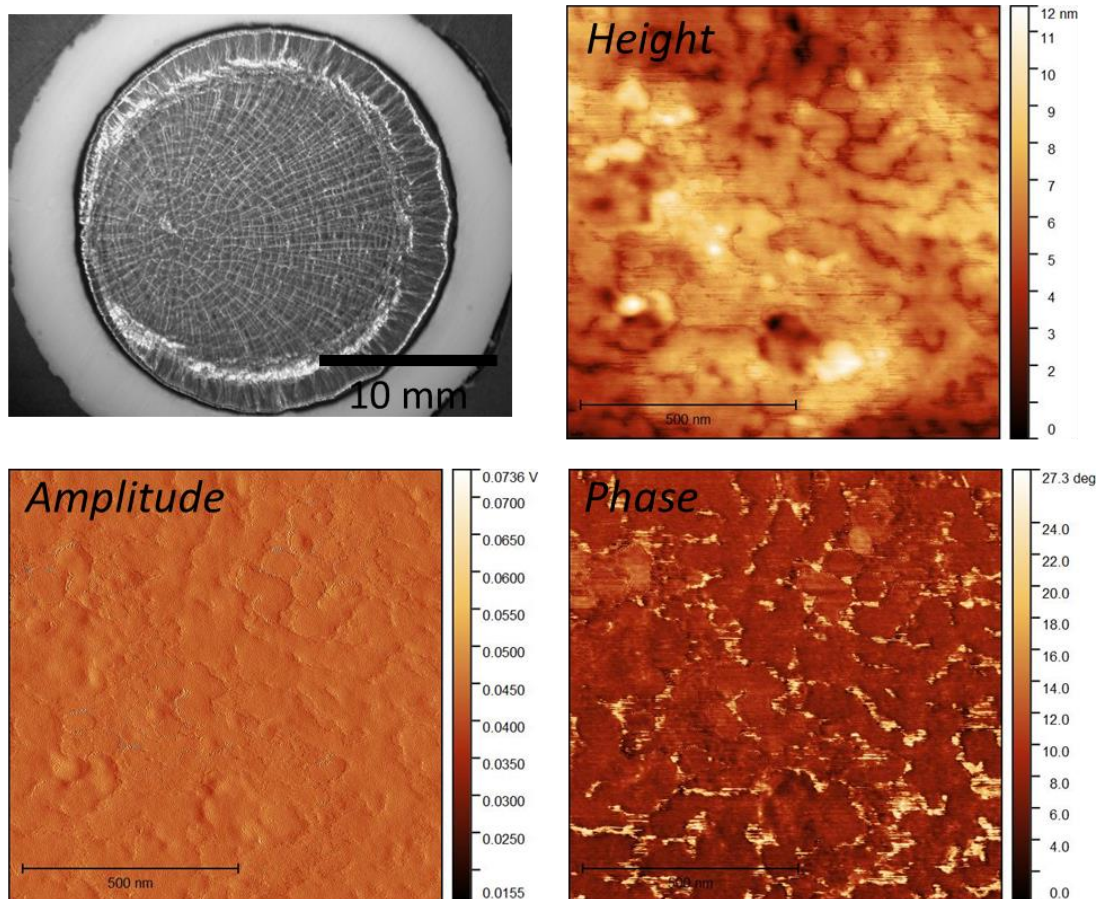
Figure 4:9 – Shows an optical micrograph and Height, Amplitude and Phase AFM micrographs of a film of Latex 223-2 containing 5 wt% of Texanol™ and 1.2wt% Pluronic additive dried at a controlled humidity of 20 %RH at 20 °C. In contrast to the AFM images in Figure 4:7 It appears the Pluronic Additive is having more of an effect on the coalescence of the latex particles. Looking at the height micrograph it can be seen that there are fewer individual particles observable. However, looking at the optical image this level of coalescence is not enough to reduce cracking and push the film below its MFFT.

Figure 4:9 shows an optical micrograph and the height, amplitude and phase AFM micrographs of a dried film containing latex 223-2 with 5% Texanol™ and 1.2wt% Pluronic additive. Comparing the film containing no additive and the film containing 1.2wt% weight Pluronic additive, the appearance of the finished films looks similar. Both films contain a large amount of cracking and both are expected to be below their MFFT. However, upon inspection of the AFM micrographs it can be observed that there is a large difference in the structure of the particles. Firstly, the height micrograph shows some coalescence between the particles; there are

less distinct particles and more of a co-continuous structure present in the height phase. At first this result does not seem to correlate to the level of cracking seen in the optical micrograph, as the level of cracking in each system appears to be similar. However, as reported by J. Lang *et al.* in their work looking at the effects of concentration of a number of different organic solvents on the film formation of latex films, if the additive concentration is not high enough to promote sufficient interdiffusion of polymer chains between particles then the mechanical properties of the film will not be sufficient to stop crack formation. With reference to the phase micrograph, it appears that there are regions of softer material in-between what appears to be coalesced particles. These regions could be additive that have been exuded by the drying film, or areas of plasticised latex.[120] It is again important to note that the images are only showing the surface of the film and hence the structure of the bulk of the film is not known.

With these results in mind, the most recent hypothesis that the additives are acting as a coalescence aid and plasticising the outer edges of the latex particles still stands, albeit the concentration used for the Pluronic additive is not plasticising the latex enough to form a uniform film. In contrast to the systems containing the Pluronic additive, the systems containing both MC and HPMC both seem to have encouraged film formation enough to form a homogenous film. For this reason it is possible that, when studied on a particular level, these films would show a more uniform structure, indicating that the films have undergone sufficient polymer interdiffusion. The AFM micrographs for the systems containing MC and HPMC are shown in Figure 4:10 and Figure 4:11 respectively.
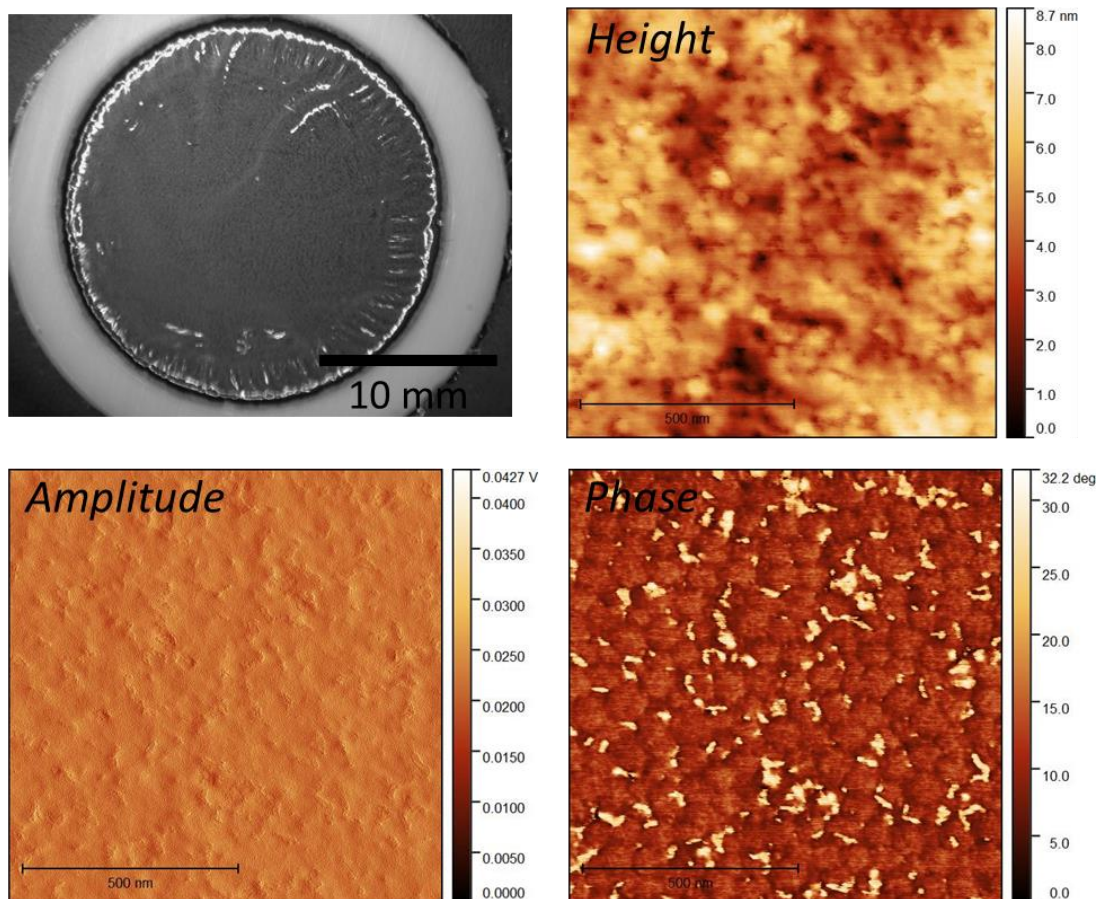
Figure 4:10 – Shows an optical micrograph and Height, Amplitude and Phase AFM micrographs of a film of Latex 223-2 containing 5 wt% of Texanol™ and 1.2 wt% Methylcellulose dried at a controlled humidity of 20 %RH at 20 ℃. Looking the AFM micrographs, only a few distinct particles are again observable in the Height image. It appears that there either a large percentage of the particles coalesced, or additive has been pushed to the surface. The Phase image appears to show more information on the surface structure than the height. These images highlight the fact that more information needs to be gathered as the AFM only provides information on the surface structure.

Figure 4:10 shows the AFM micrographs of latex 223 containing 1.2wt% of MC. The optical micrograph in the top left of Figure 4:10 shows that the film appears to be above its MFFT. The imperfections that can be seen around the perimeter of the film are actually wrinkles in the film rather than cracking. Looking at the height micrographs in Figure 4:10 the film appears to show some level of coalescence between the particles. In this case the coalescence is enough for the film to form a homogeneous structure with enough mechanical integrity to resist

135

cracking upon film formation. When looking at the phase micrograph the structure of the particles becomes clearer; it is possible to distinguish clear particles. It is also possible to see similar regions of soft material between the particles as in Figure 4:9, this again could be plasticised latex or, as mentioned previously, exuded additive. As the bulk of the film has not been imaged the internal structure is an unknown. Despite this, the changes in surface structure of the film has provided a good insight into the mechanism by which the additives are operating. Figure 4:11 shows the AFM micrograph of the film containing 1.2 wt% of HPMC.
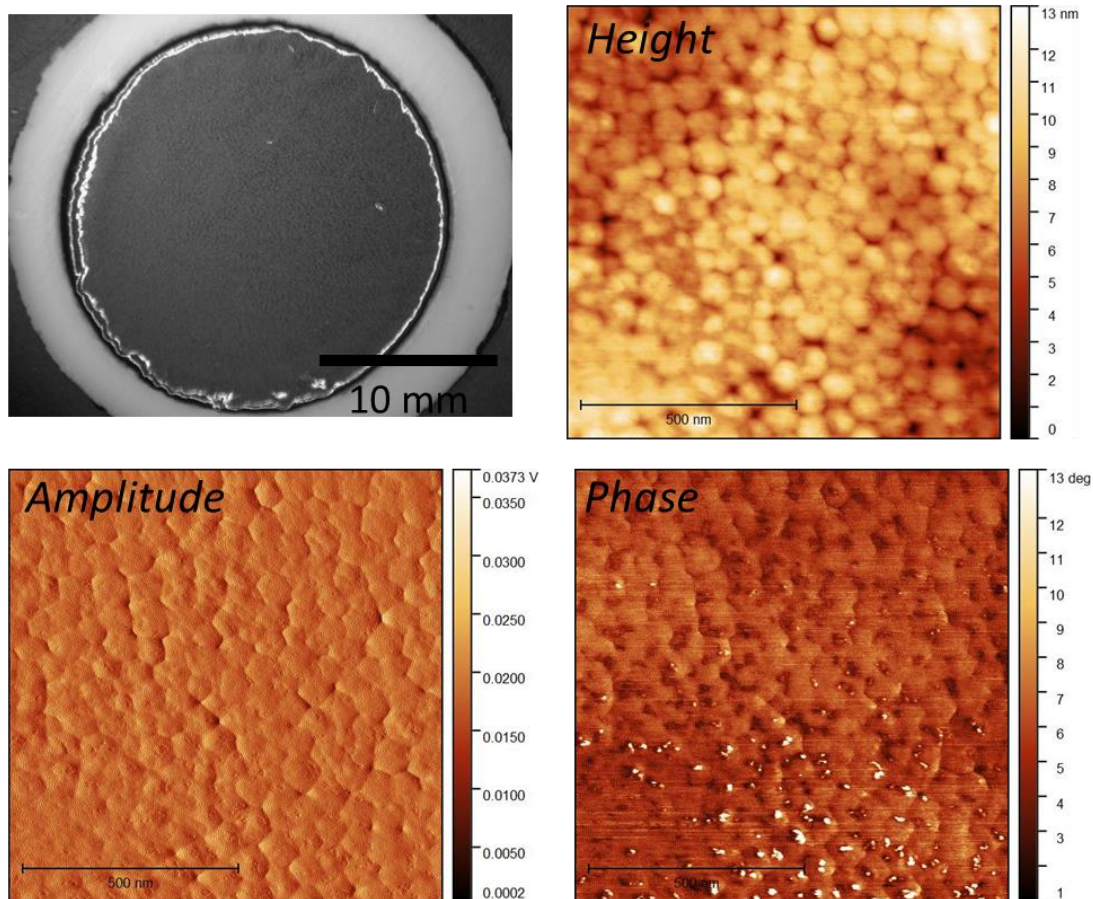
Figure 4:11 - Shows an optical micrograph and Height, Amplitude and Phase AFM micrographs of a film of Latex 223-2 containing 5 wt% of Texanol™ and 1.2 wt% Hydroxypropyl Methylcellulose dried at a controlled humidity of 20 %RH at 20 °C. Looking at the optical micrograph you could expect to see full coalescence in the phase image. However, this is not the case. Looking the phase image a clear array of particles can be seen with minimal coalescence. In order to study how the additive is facilitating the film formation, a study needs to be carried out on the entirety if the films depth and not just the surface.

Figure 4:11 shows that the film containing 1.2 wt% of solids of HPMC has no cracking in the finished film, from this it would be expected that the particles would have completely coalesced and under AFM a homogeneous film would be seen. However, when the height micrograph is examined it can be seen that the particles appear to show no coalescence at all. In fact, when the AFM micrographs of the film containing no additive and the film containing 1.2wt% HPMC are compared there are many similarities. Another point of interest arises when looking at the phase micrograph. Whereas in the previous micrographs the phase

137

images have shown regions of softer material that have been hypothesised to be either plasticised latex or additive, the phase micrograph of the film containing HPMC displays no such regions. These observations disprove the initial hypothesis that the additive is plasticising the outer edges of the latex particle and enabling the film to form without cracking. Work carried out by J. Lang *et al.* has shown that the addition of certain additives can influence the packing structure of a latex film.[121] In their investigation they examined the effects on particles packing by the addition of an anionic additive to an acrylic latex. In their study they found that with the addition of the additive the packing of the latex particle became more efficient. Comparing these results to the results observed in the HPMC system, the HPMC could be behaving in a similar fashion to the additive in the study by Lang *et al.* Lang used AFM as a means of quantifying the change in packing of the latex. However, as has been mentioned a number of times, the AFM images only provide information in relation to the surface of the film and not with respect to its bulk. In order to see how the particle spacing of these films changes with an increase in additive concentration an experimental technique that looks at particle spacing throughout the depth of the film is required. One way of doing so could be to fracture the film and study the fracture surface with a technique such as AFM. The problem with this route would be that the physical process of fracturing or sectioning the film may result in damage to the particle structure producing an incorrect value for the particle spacing. A technique that would be more suited to study these changes would be Small Angle X-ray Scattering *(SAXS)*. In the next chapter SAXS will be used to study the effects of additive concentration on the packing density of these latex films. Once more of an idea of how the latex packing is being affected by the additives is ascertained, a more accurate explanation of the mechanism by which the additives are reducing cracking in the film can be deduced.

4.6.   Conclusions

At the start of this chapter the aim was to investigate the reasons for the reduction in cracking as increasing concentrations of additive were added to the latex films. This chapter has discussed a number of the techniques that have been used to investigate this effect. Starting with optical microscopy the films were imaged and compared. It was observed that in the films containing the cellulose derived additives (MC and HPMC) the films' cracking was drastically reduced as the concentration of additive was increased. In contrast, the Pluronic additive did not seem to have an effect on the overall level of cracking. It is fairly widely understood that by slowing the rate of drying the level of cracking in the film reduces, this has recently been reported by Piroird *et al.* In this work they have shown that as the drying time is increased the level of cracking is reduced. This reduction in cracking usually comes with increased packing order, with the possibility of colloidal crystals forming if evaporation rates are sufficiently slow.[18,19] In relation to the systems under investigation it had been previously shown that the additives do not have a noticeable effect on the rate of evaporation. For this reason altering the rate of evaporation was most likely not the reason for the observed reduction in cracking. To ensure this was in fact the case, films that were dried at a higher humidity were studied. The rate of evaporation in these films was impacted far more by the humidity than by the changing concentrations in additive. When the films that were dried at an increased humidity were studied, no changes in the observed levels of cracking were seen. This shows that the additives must be operating by an alternative mechanism to reduce the cracking in the films.

Edelhauser and later Vijayendran *et al.* have both shown that certain additives can plasticise latex particles. For this reason it is possible that cellulose-derived additives are having a similar effect on latex 223-2. In order to investigate the possibility that additives plasticise latex particles the T_g of a film containing MC was studied using DMA. This experiment showed that the T_g of the film with varying concentrations of MC remained relatively unchanged. This initially disproved the hypothesis that the additive was plasticising the latex particle. However, if the additive was only plasticising the outer edge of the latex particle

and not the bulk, then perhaps a film that had an overall T_g closer to the T_g of the particle could be produced. T_g gives information on the property of the polymer in the final state of the film. In contrast MFFT gives information on the whole system and at what temperature cracking is stopped. A study was carried out to see how the additives affected the MFFT of the films. It was observed that the MFFT data was consistent with the optical micrographs of the films, with the cellulose-derived additives lowering the MFFT, whereas the Pluronic additive had no effect. In order to see if the additive was plasticising the latex it was necessary to use AFM .

When the AFM micrographs were studied it showed mixed results. The Pluronic additive seemed to show some levels of particle coalescence, but perhaps not enough to stop any cracking. Likewise the film containing 1.2 wt% MC also appeared to show some coalescence, this time enough to push the film over its MFFT. In contrast, the film containing 5 wt% Texanol™ seemed to show minimal coalescence between particles as would be expected with the film showing a high level of cracking. In the phase micrographs, it was possible to see contrast around the outer edges of the particles. It could be hypothesised that these are regions of softer material. This could be regions of plasticised polymer or exuded additive. However, when reviewing the AFM micrograph of the film containing 1.2 wt% HPMC the partial plasticisation hypotheses seem to be disproved. In this film it appears that no coalescence had occurred, rather the additive seems to have stopped coalescence from occurring. This is actually consistent with the work by Lang et al. in which it was observed that the addition of an additive actually promoted particle packing to occur more densely and actually stopped the particles from coalescing. In this experiment only the top surface of the film was examined, in order to further explore how the additives are affecting the particle packing an alternative technique needs to be used. This may confirm that a similar process is occurring in the bulk of the film containing MC. In the next chapter SAXS will be used to study how the additives are changing the packing in the bulk of these films. It is possible that if the additives are surrounding the particles they could be creating a soft surrounding that could facilitate film formation without cracking. If the additive is adhered to the latex then upon consolidation of the

particles a system could be created that allows stress relief through deformation of the latex-additive network. This could also allow slight movement of the particles within this network without crack propagation occurring. This would be consistent with the work by Goehring, Clegg and Routh in which it was shown that, if crack propagation is halted by stopping further evaporation, particles could rearrange around the crack. .[122] Therefore if the additive network allowed slight rearrangement of the particles, stress could be relieved before a crack could form. Figure 4:12 shows a schematic of the proposed additive latex network.
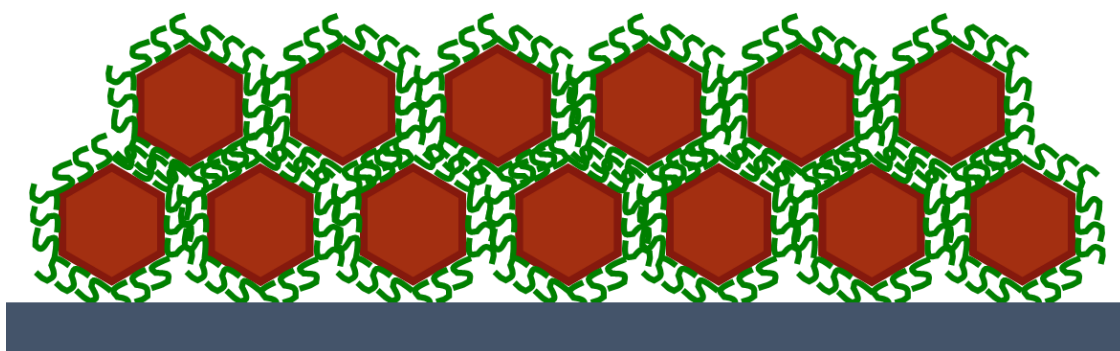
Figure 4:12 – Shows a proposed model for the location of additive in the latex film. The additive is shown as the green lines with the latex particle being shown as the orange hexagons.

In order to study exactly how this proposed additive network alters the stress development in theses latex systems further experimentation would be required. In the next section sets out future work that could be carried out to further investigate this, before in Chapter 5: SAXS is used to investigate the particle packing of the latex films.

4.7.   Future Work

It has been hypothesised that the additives are forming a network that is providing an alternative mechanism of stress relief. This opens up a new avenue of experimentation that could be continued after this study. In order to explore the mechanism by which the additive is reducing the cracking in these films the stress development during drying could be studied.

4.7.1.   Stress Development

As has been previously mentioned, as a latex film dries it undergoes a change from a dilute suspension of latex particles to a packed array of solid particles, through particles coalescence this can become a homogeneous polymer film suitable for use as paint. During film formation the capillary forces that help to drive the drying process and particle consolidation also cause residual stress to build up within the drying film. Since the work of Peterson *et al.* in 1999, measuring stress in drying colloidal films has been an area of reasonable interest.[71,81,123–126] The most common way that stress development tends to be measured utilises the bending of a metal cantilever. In the work by Peterson *et al.* a latex dispersion is applied to a metal cantilever, the deflection caused by stress development is then monitored by a laser beam in a similar way to that of an AFM tip. Peterson *et al.* noted that in their study the deflection caused by the loss of mass was not accounted for. In order to improve this experiment that bending caused by mass loss needs to be accounted for. Below outlines some preliminary work that has been carried out on the development of a cantilever stress analyser.

4.7.2.   Experimental Development

The method needs to be a robust technique that is less susceptible to error caused by external factors, it also needs to be capable of measuring the mass change of the system to allow corrections to stress development by removing the component of deflection caused by the evaporation of water. The method chosen was one that used thin metal shims clamped in a single cantilever geometry. The deflection of the shims were measured with a small USB microscope. Due to the simple design the whole assembly can be placed on an analytical balance allowing the mass of the system to be monitored. The images collected though the

microscope are analysed in real-time using MATLAB. A copy of the script is provided in section V. b. iii of the appendix. Mass loss data measured on a 4.d.p analytical balance is then used to subtract the deflection caused by mass loss from the collected deflection data. Deflection can then be converted into stress development using Corcoran's equation.[127]

In order to test the accuracy of this method a simple test can be conducted. As mentioned previously, when a film dries two components contribute towards the total bending of the substrate: the first is bending caused by stress development of the film and the second is the component of the bending caused by the mass change of the film due to evaporation. It is this second component that can be independently tested to see if this method is suitable for measuring the stress development in dying latex films. In conducting this experiment the deflection of the cantilever was monitored as small weights were added to the tip. A standard beam bending formula was used to convert this observed deflection into the measured Young's Modulus for the cantilever; this could then be compared to a literature value. The measured value for the Young's modulus of the steel cantilevers used is 235 ± 3 GPa. This value is comparable to a literature value of around 200 GPa.[128] It must be noted that Young's Modulus is not strictly the correct value, rather it should be a bending modulus. However, as the experiment is subject to a number of errors, comparing it to this value provides a sufficient idea of how suitable this method is when looking to measure stress development in drying latex films.

As previously mentioned when latex films dry the internal capillary forces result in internal stress development. If the internal stress within the film ever exceeds the mechanical resistance of the film then cracking can occur. However, if the film has a low T_g or the film contains a coalescent solvent that is plasticising the film then the film may resist cracking as the internal stresses can be relieved through alternative mechanisms. As described in the conclusions of this chapter, it was hypothesised that the cellulose-derived additives are surrounding the latex particles and providing a way for film formation to occur without cracking. Figure

4:12 shows a schematic diagram explaining the proposed structure of films containing the cellulose-derived additives.

Through the use of the cantilever stress analyser, information on how the additives are relieving stress could be collected. It is already known that altering the various properties of a polymer affects the stress development in drying latex films.[126] Although information on the additives has not been gathered, a preliminary study looking at how Texanol™ affects stress development is shown below in Figure 4:13.

0 wt% Texanol™   5 wt% Texanol™
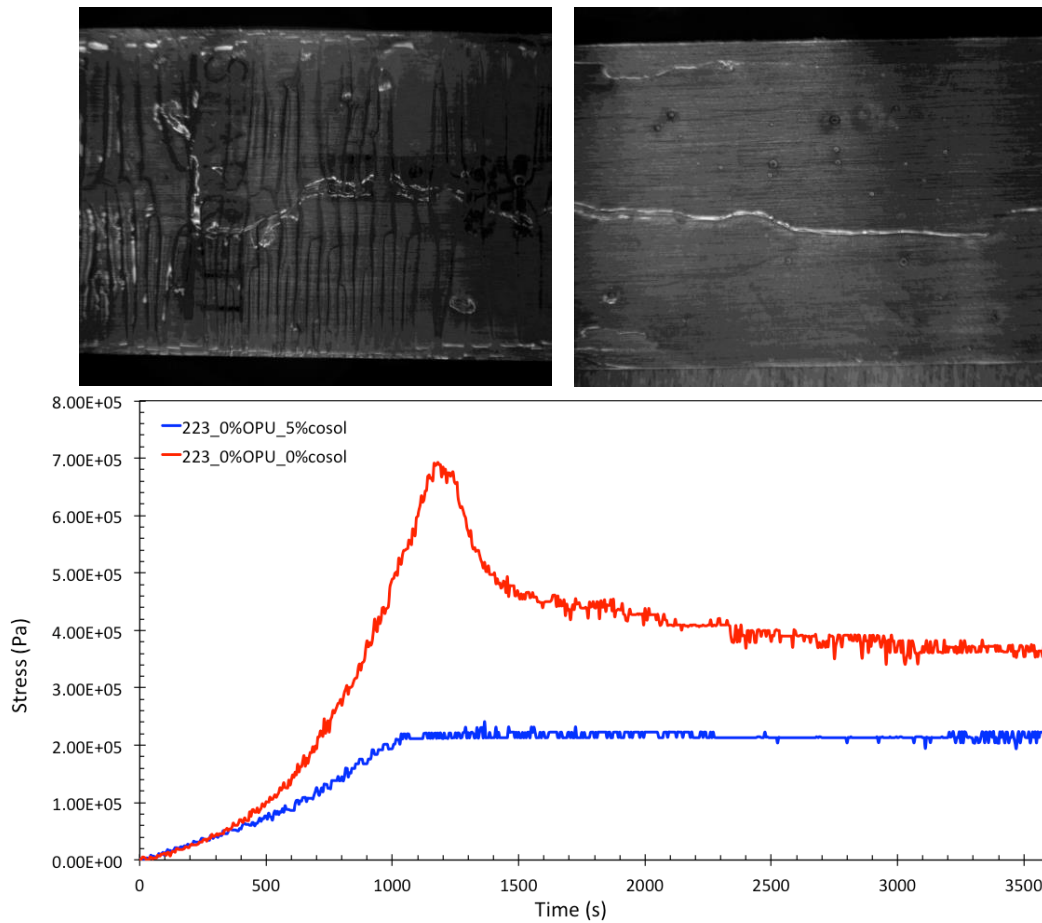
Figure 4:13 – Top left - Latex 223-2 with 0 wt% Texano™. Top right – Latex 223-2 with 5 wt% Texanol™. Bottom - Shows the changes in the stress development of a film of latex 223-2 through the addition of 5 wt% Texanol™. Looking at the shape of the stress development curves, clear difference can be seen. It can be seen that through the addition of Texanol™ there is no longer a peak in the curve, this is as the amount of stress relaxation is increased. In the system containing no Texanol™ stress relaxation occurs through cracking, in the system with 5 wt% Texanol™ stress relaxation occurs through deformation of the softer plasticized latex.

Looking at Figure 4:13 it can be seen that through the addition of 5 wt% Texanol™ there is a drastic impact on the stress development profile. It is worth noting that the comparisons in magnitude of the stress shouldn't be made as the thickness of the films could vary due to the aforementioned difficulty in applying films with low or varying viscosity. However, the shapes of the profiles can provide an

indication of the mechanical properties of the film. When looking at the shapes of the stress development profiles and comparing them to the model developed by Lei *et al.* there seems to be a strong correlation.[129] Firstly, it can be seen that the film containing latex with no Texanol™ can be seen to have elastoviscoplastic properties. Lei *et al.* state that in such a system with increasing stress relaxation there should be a reduction in peak stress development. This accords with the data and with the concept that, with the addition of Texanol™ and a reduction in cracking, there appears to be in increase in stress relaxation.

In future work using this method to study the stress development of systems containing varying concentrations of cellulose-derived additives it would be of interest to see how the stress relief profiles would differ to those systems that are plasticising the latex particles. An extensive study could be carried out in order to investigate the numerous different cellulose derived additives at different concentrations. These stress development profiles could then be compared with systems containing both particles of different T_gs and systems containing known coalescence aids. In order for this study to be carried out there needs to be further development of the experimental process. As mentioned earlier, the viscosity of the latex can cause issues when trying to apply films of consistent thickness. As the current technique uses a metal cantilever, steps taken to control the film thickness using a PTFE o-ring cannot be taken, as has been the case in other areas of this thesis. As the films are also relatively thin, similar problems with fluctuations in the collected mass data could be seen due to the ZPD of the analytical balance. However, if this study was to take place it could reveal valuable information on the mechanism through which alternative additives, such as the cellulose derived additives used in this study, could be acting to reduce cracking in latex films and hence interior decorative paints.

Chapter 5:   Particle Packing

In this chapter the aim is to further investigate the relationship between additive concentration and particle packing. The chosen technique to explore this is Small Angle X-ray Scattering *(SAXS).* By exploring this relationship it will hopefully enable a more detailed investigation into the mechanism by which the chosen additives are affecting the film formation and reducing cracking.

As water within a film begins to evaporate the particles begin to get more and more concentrated until they have no room to move past one another and the film begins to occupy a packed structure. SAXS has been used in an attempt to further the understanding of how the additives affect the packing in these films.

SAXS is very good at providing a deeper understanding of a system as it works on 'average' rather than a select area that other techniques may provide. The problem with SAXS arises when there is not enough information known on the system under investigation. In this scenario an incorrect model can be fitted to the data and still yield a good fit. Fairclough *et al.* have discussed this whilst trying to find a fit for worm-like micelles of a Pluronic additive. Initially in this study a Gaussian radial density profile was used as a simplified fit for a Guinier axial radius. At first it was thought that this was a good fit for the data, however, upon consideration it was shown that the system actually contained mixed structures with some worm-like micelles, elliptical micelles and other mixed structures.[130] For this reason it is important to have a good understanding of the studied system so that a suitable model can be fitted to the data, this may include data from microscopy as well as other scattering techniques such as DLS. As previously described, the system under investigation is latex 223-2 mixed with different additives. Before further investigation can be carried out, the form factor of the latex needs to be established.

5.1.　　The use of SAXS in the study of Latex Film Formation

The field of scattering has long been used to study latex dispersions. Most of the work in the field tends to use small angle neutron scattering (*SANS*) to examine both the latex dispersions in their liquid state as well as to study their film formation behaviour.[131-135] Despite this SAXS has been used to study latex film formation with the work by Dingenouts *et al.* in 1998 marking the first systematic study of latex film formation using SAXS.[136-138] In this work Dingenouts *et al.* dried PMMA and PS latex particles below the T_g of both polymers. The sizes of the latex particle were 69 and 106 nm respectively. As the samples were dried below their T_g minimal particle deformation occurred. This meant that dried films could occupy either a random-packed or crystalline structure. It was deduced that in this investigation there was a lack of true long range order, most likely caused by the dispersity of the latex particles used. However, Dingenouts *et al.* remarked that from their data they were confident that SAXS is a suitable technique to use to study latex packing throughout film formation. Since this early work SAXS has been used fairly consistently within the field of latex film formation, although still with less prevalence than SANS. Due to the nature of SAXS it can be used to study all aspects of film formation however, thin films have the problem of low levels of scattering and hence low scattering intensity. This means that without high intensity synchrotron level radiation, alternative solutions need to be found to ensure adequate scattering. One way that this has been achieved is through the use of latex droplets rather than thin films.[54] The work of Chen *et al.* looked at the 'film' formation of latex droplets at various temperatures and humidity levels. In this work they found that under different conditions the latex particles were found to deform different amounts, with clear intermediate steps found during film formation between the stages of film formation shown in Figure 1:5.

As mentioned previously under specific conditions latex films can form colloidal crystals, particularly when films are dried below their T_g. In such circumstances, the films will exhibit long range order, making it possible to probe the crystal structure through the analysis of Bragg peaks in the SAXS patterns. In 2007 Förster *et al.* published an article in nature materials discussing the use of SAXS to

monitor the evolution of Debye-Scherrer ring to Bragg peaks in a colloidal crystal.[139] In a more recent study Sulyanova et $al.$ has shown how the structure of a PS colloidal crystal changes as it is taken through its T_g through the evolution of its Bragg peaks.[140] Both of these studies show that under the right conditions the structure of a latex film can be studied through the analysis of Bragg peaks, but only where complete long range order exists. Before the structure of the dried film can be analysed and examined for the presence of any Bragg peaks, first an idea of the size and shape of the particle needs to be studied. In the following section serval techniques, including SAXS and DLS, will be used to measure the size and size distribution of the latex particles studied in this thesis.

5.2. Particle Form Factor

As previously mentioned in section 2.3 the form factor is the scattering pattern that is produced by the size and shape of the scatterers. When conducting a SAXS investigation of a system that is comprised of a number of constituent components, such as the films in this investigation being made up of latex particles, it is important to establish a good model of the form factor of the constituent elements. Having a good fit for the form factor of the particles allows one to deduce a number of things about the dried film. In particular, it is possible to measure the type of packing that is present in the films and, if the particle has a T_g that is below RT, you can track the deformation of the particle. Both of these can be done in real time on a dynamic system if the SAXS equipment allows. In order to measure the form factor of the particle a dilute system needs to be used so that any interparticle interactions are reduced to a negligible contribution of the overall scattering. However, before conducting a SAXS investigation of such a system, gathering as much information as possible on the particles using various complementary techniques can help to produce a better model for the system.

The first and often go-to technique is Dynamic Light Scattering (DLS), this is primarily down to its ease of use, with most experiments taking no longer than half an hour. In this time DLS can provide an idea on both the size and size distribution of particles. However, the actual measurement that the DLS takes is the Hydrodynamic Diameter. Hydrodynamic Diameter is defined as the Diameter of a theoretical sphere that would have the same diffusion coefficient as the measured particle. In theory this is all very well, but in practice most particles are not perfect hard spheres. Instead they are solvated, non-spherical dynamic systems. For these reasons it is important to understand that the particle size measured *via* DLS is larger that the actual size of the particle. However, it does provide a useful upper limit on the possible size of the particle and therefore helps to constrain the model.

Despite the aforementioned ease of use, problems can still arise when using DLS. As DLS experiments are so easy to perform, it can lead to a "Black Box" approach

with many researchers, meaning that they get used to putting in samples and getting out answers without much consideration on methodology. Perhaps the biggest stumbling block and often-overlooked variable with DLS is particle concentration. If is often known that a sample needs to dilute in order to be run in a DLS, although the exact concentration is rarely measured and, if it is measured, the same dilution is often used across all samples. In reality it is important to tailor the dilution to the system being investigated. In the following section the results of a DLS study will be presented, including a demonstration as to how much of an effect concentration can have on the measured particle size.

5.2.1. Dynamic Light Scattering

When measuring particle size and size distribution with DLS a dilute solution is required to minimize multiple scattering. The exact concentration is dependent on the system being measured, but typically concentrations of around 0.001 $g \cdot cm^{-3}$ are used. In the case of the latexes under investigation the starting concentration is around 0.4 $g \cdot cm^{-3}$ meaning large dilution is required in order for the particles to be studied with DLS. The general rule of thumb is that the solution should be clear without a blue haze. However, in order to isolate the exact concentration window that yields the correct results, a concentration sweep was conducted with samples ranging from concentrations of $1x10^{-6}$ $g \cdot cm^{-3}$ to 0.1 $g \cdot cm^{-3}$. Two of the latexes under investigation (*Latex 223-1 and Latex 225-1*) were measured alongside one of *AkzoNobel's* proprietary latexes, Latex 1040, as an illustration of how DLS measurements can vary so drastically with particle concentration. The Z average particle size and size distribution were then plotted *vs.* concentration for each latex, this data can be seen in Figure 5:1.
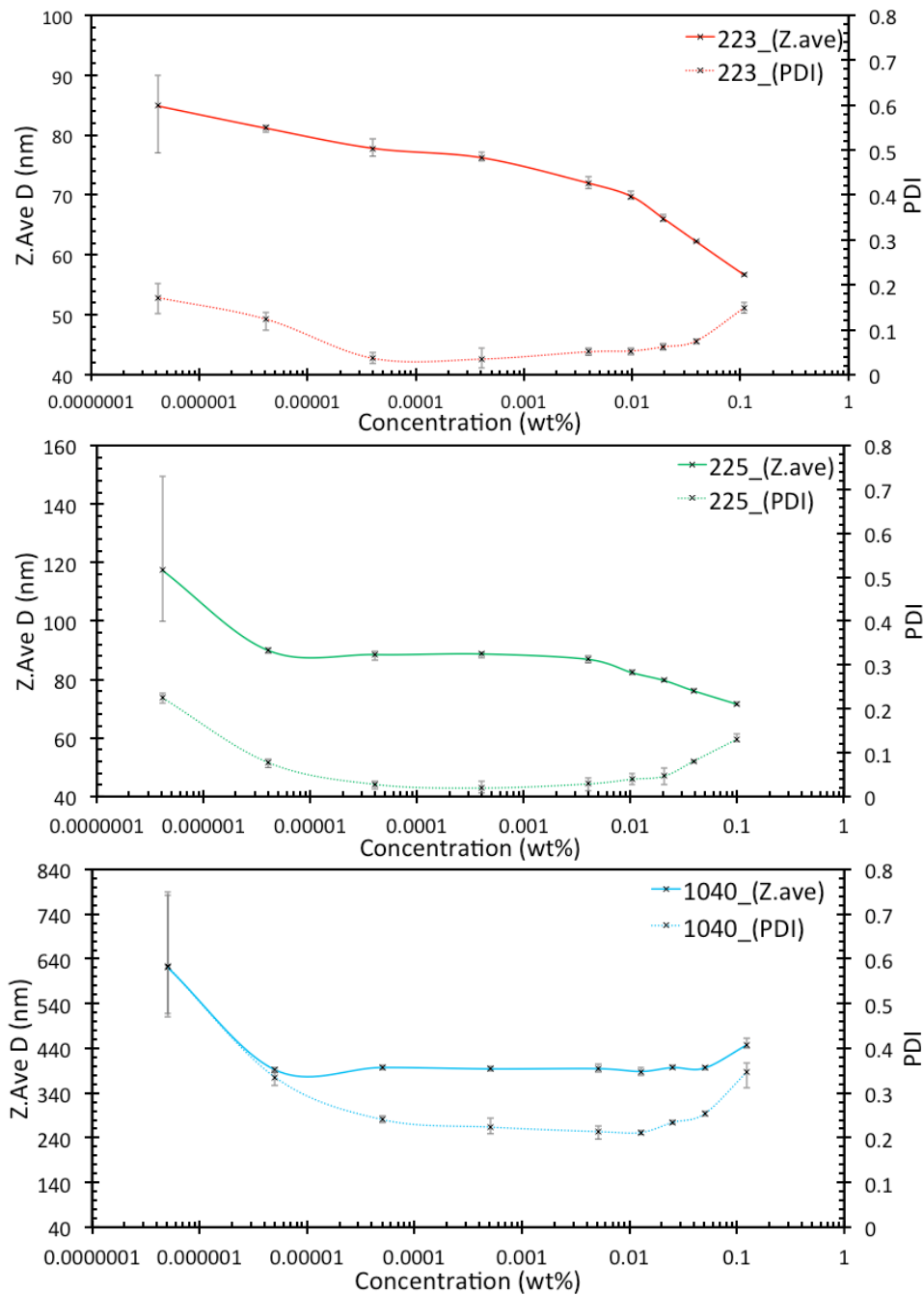
Figure 5:1- Shows how the measured PDI and the Z average particle size varies with varying particle concentration. At low concentrations a large error can be seen in all three latexes; this is caused by high noise to signal ratio at these concentrations. As mixtures approach higher concentrations two different effects can be seen. In latex 223 and 225 an artificial lowering of Hydrodynamic Diameter is observed and in latex 1040 the opposite is seen. This is caused by the effects of multiple scattering in the former and by viscosity effects in the later.

Upon immediate inspection of Figure 5:1 it becomes apparent that altering the concentration of the system has a significant effect on both the measured particle size and the measured particle dispersity. However, the exact effect that the change in concentration has is dependent on the latex. If we first look at how changing the concentration affects the measured dispersity, we can see that in all three cases at both high and low concentration there is an increase in the measured value, with a plateau region falling in between. However, when looking at the change in measured size of the particles it can be seen that for latex 223-1 and 225-1 the same trend is observed, with the measured particle size increasing at low concentration and decreasing at high concentration with a plateau region in the middle. However, when looking at latex 1040 a different trend is observed: at both high and low concentrations, the measured particle size shows an increase. The reasons for these changes, at low and high concentrations are due to either signal to noise (low concentration), viscosity (collisions with other particles), or multiple scattering at high concentrations. Multiple scattering occurs when the sample is sufficiently concentrated to allow light that has been scattered by a single particle to be re-scattered by other particles in the sample. This leads to a loss of information of the scattering event and hence an artificial lowering of the measured particle size. This can be observed in the graphs for Latex 223-1 and Latex 225-1.

$$r(H) = \frac{k_b T}{6\pi\eta D}$$

$(\ 15\ )$

In the case of Latex 1040 viscosity effects begin to dominate before multiple scattering is observed. Equation $(\ 15\ )$ is the Stokes Einstein Equation and can help to explain this observation. In this equation r*(H)* is the Hydrodynamic Radius of the measured particle, D is the translational diffusion coefficient, k_b is Boltzmann's constant, T is Temperature and η is the viscosity of the dispersion medium (*e.g. water)*. The variable that is measured when using DLS is D. If the particles in the system are colliding due to increased concentration, this can cause the apparent viscosity of the overall system to increase. This increase in viscosity will lead to a decrease in the measured value for D. Looking at how this would then

affect Equation (15) it can be seen that if D is decreased due to increased concentration, but the viscosity of the system is not correctly adjusted, the measured Hydrodynamic Diameter would be larger than the actual size of the particle in question. In contrast, at low concentrations the signal strength is so weak due to such small levels of scattering that uncertainty in the data leads to a poor fit of the correlation function. In turn this leads to errors in both the measured Hydrodynamic Diameter size and size distribution.

Using the data collected for Figure 5:1 it is possible to select an appropriate concentration to use for each of the three latexes when conducting any future DLS measurements. In each case there is a plateau region between $1x10^{-4}$ and $1x10^{-2}$ wt% solids. Selecting the middle of this concentration range ($\approx 1x10^{-3}$ wt%) would therefore ensure that all future measurements are as accurate as possible. At this concentration any effects from multiple scattering, viscosity changes or errors in fitting the correlation function will be reduced as much as possible. However, even if the upmost care has been taken to ensure that the sample has been run at the correct concentration, if the sample has a large variation in particle size, errors can still creep into the measured Hydrodynamic Diameter. This error arises from the way that DLS measures the size of particles. Section 2.3.1 explains this in more detail, but in short DLS weights larger particles more than it does smaller ones, meaning that the Hydrodynamic Diameter measured with DLS is not the number average, but rather a skewed number average. In Figure 5:2 the three latexes used in the concentration study have been used to show the effect that the larger particles have on the measured Hydrodynamic Diameter.
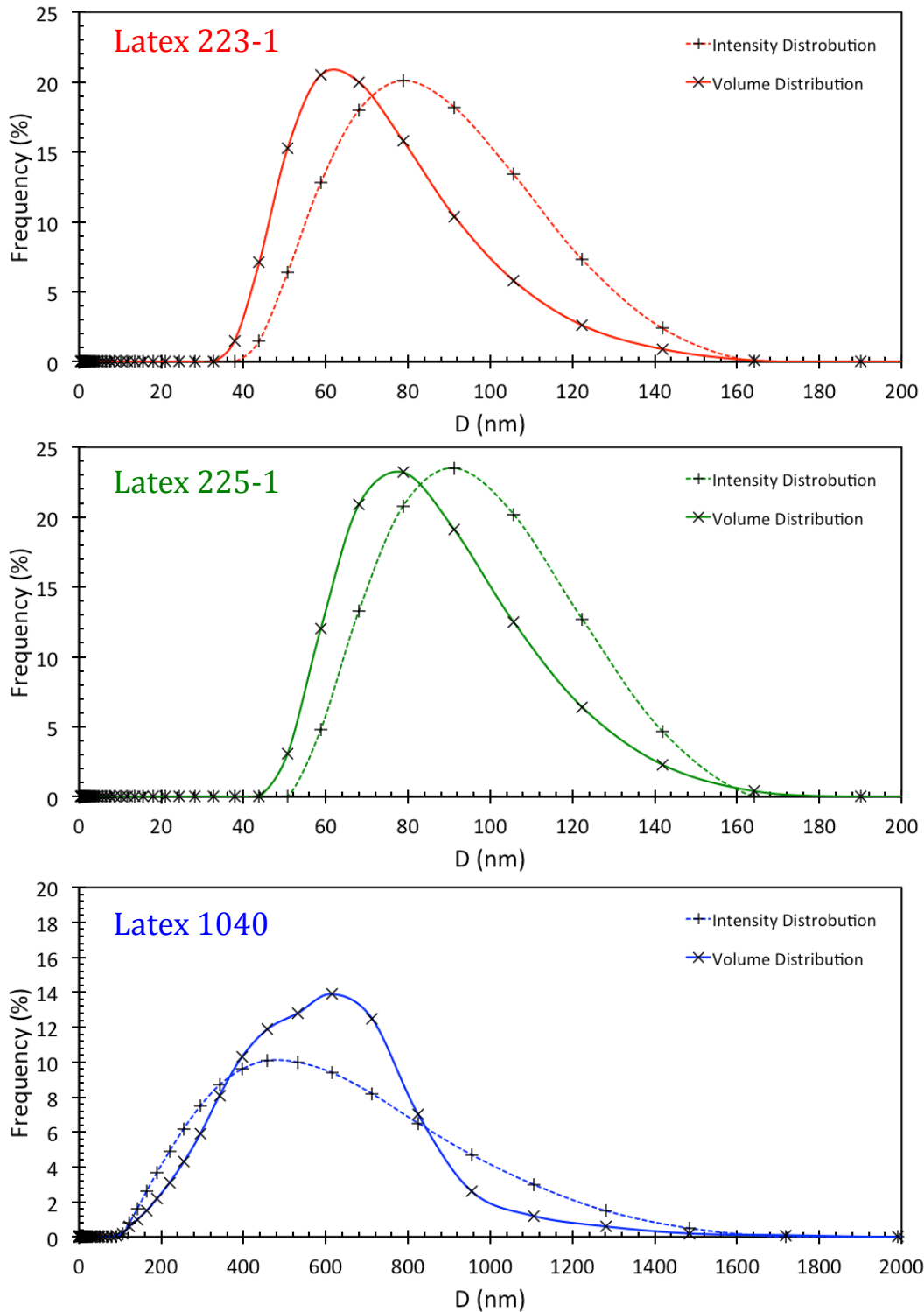
Figure 5:2 – Shows the difference between the volume and intensity distribution. It can be seen that with the intensity distribution the larger particles have more of an effect on the particle size. This is seen by a shift in measured size distribution This is why particular care needs to be taken during sample preparation for DLS as a small amount of contaminants can drastically skew the particle size distribution.

When using DLS the hydrodynamic diameter of a particle is stated as its Z-average size. A particle's Z-average size is calculated from the intensity distribution of the measured sample and is therefore weighted towards larger particles. In order to use Z-average a system needs to be monomodal with a narrow particle distribution with the particles being near spherical in shape. Below the Z average particle sizes for the three latexes have been tabulated.

Table 5:1 – Measured Z average particle size in nm

	Latex 223-1	**Latex 225-2**	**Latex 1040**
Z Average Size	*76.2*	*88.7*	*393.9*

The latexes under investigation are latex 223-2 and latex 225-2, using the information gathered above the samples were run at a suitable concentration to ensure minimal error. The measured Z average Hydrodynamic Diameter of Latex 223-2 and Latex 225-2 is 75.3 nm and 73.3 nm respectively. Now that this information has been collected it can be used as a starting point for further investigation using other complementary techniques. Even though the Hydrodynamic Diameter is larger than the actual size of the particle, the size of the particles are still an order of magnitude smaller that the wavelength of light. For this reason it is not possible to use standard light microscopy to further study the size and shape of the particles. It was therefore decided that a form of electron microscopy (*EM*) would be used to further investigate the particles ahead of SAXS. In the following section the results from this selected form of EM will be presented and discussed.

5.2.2. Transmission Electron Cryomicroscopy

Electron microscopy techniques are often used when trying to establish the size, shape and structure of many objects ranging from metal alloys to butterfly wings. However, the appropriate technique must be selected in order to obtain the best result. In the case of latex 223 and 225, where the T_g of the particles are around room temperature, performing EM experiments to get an idea of the size and shape of the particles becomes difficult. If the T_g of the particles was significantly above room temperature the experiment could be simplified. This comes as a result of the need for EM experiments to be performed under a vacuum and hence the need for water in the system to be removed to allow a good vacuum to be produced. Due to the soft nature of the particles, upon drying even a dilute solution the particles could deform and thus not give an accurate representation of the particles' native size and shape in solution. In order to combat this, the solution can be cryogenically frozen and then the frozen solution can be measured with TEM to obtain an image of the particles in their native state; this technique is Transmission Electron Cryomicroscopy (cryoTEM). In this study Latex samples were diluted from 40 wt% solid to approximately 0.1 wt% solid concentration. The solutions were then cast onto holy carbon grids before being cryogenically frozen using liquid ethane. Samples were run on a Phillips CM100 100 kV electron microscope equipped with a LaB6 gun and Gatan 1Kx1K digital camera.
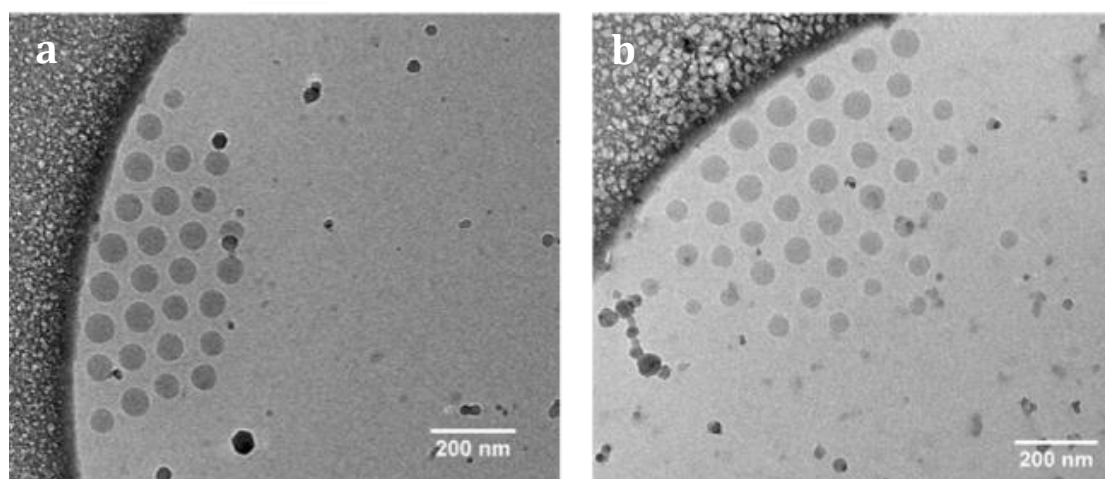
Figure 5:3 – Shows examples of images collected with cryoTEM for Latex 223-1 (a) and Latex 225-1 (b). The darker artifacts in the images are ice crystals and the large continuous artifact on the left is the carbon substrate. It can be seen that the particles occupy a regular ordered structure.

The images shown in Figure 5:3 provide a representation of the total population distribution of the particles in each system. From these images, along with the other images collected, an approximation of the size and size distribution of the particles can be gathered. As mentioned previously the latex was mounted and prepared onto holey carbon grids, this carbon grid can be seen toward the left hand side of each image. Another artefact not related to the particles are the darker spots that can be seen clearly in the bottom of Figure 5:3a. Upon closer inspection it can be seen that these crystals are slightly hexagonal in structure, indicating that they could be ice crystals. This is further backed up if a second image is taken on the same area after exposure to the electron beam. It can be seen that the larger crystals have a tendency to shrink, or in the case of the smaller crystals disappear. This indicates that the ice crystals have partially or fully melted respectively; this is shown in Figure 5:4. These re-exposed images have not been used in the data extraction, as it is not known what effect the electron beam has on the particles.
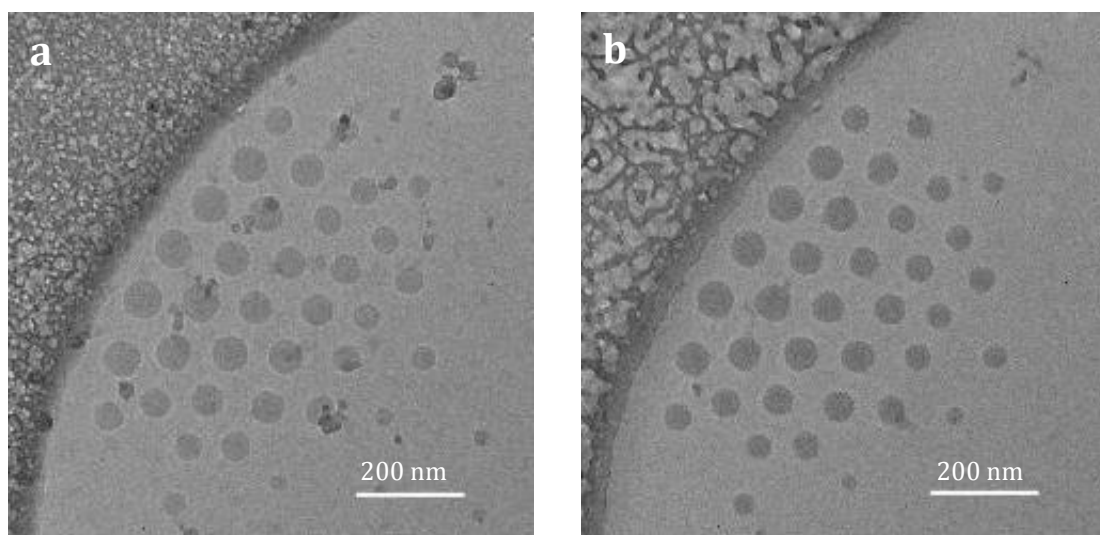
Figure 5:4 – Shows the difference between a sample before and after exposure to the electron beam. (a) shows the region of interest as it is exposed to the beam for the first time, (b) shows the same region after it had already been exposed. It can be seen that the small artifacts present have either reduced in size or completely disappeared hence indicating that they are most likely to be ice crystals.

The next interesting thing to point out from the above images is the regularity of the particle packing. At the concentrations used in this study this packing is not representative of the bulk solution, but rather due to the sample preparation. Particles tend to adopt this regular packed structure when constrained and forced near to one another. When the samples are prepared, the holey carbon grid has the dilute latex solution applied to it and then the majority of it is wicked away as, discussed in section 2.2.2. When the sample is prepared the surface tension of the solution causes a meniscus to form in the carbon well. This forces the particles to the edge of the hole if the level of the liquid in the centre is less than the diameter of the particle. This hypothesis is further supported when examining the size distribution of the particles. It can be seen that the smaller particles show a tendency to be located more towards the centre of the hole with the larger ones being located more towards the edge where the liquid level would be higher.

In order to extract some quantitative data from the images they were analysed using MATLAB. The code uses a circle finding algorithm in order to extract the radius for each particle. This code is shown in section V. b. i of the appendix. Once the particle data had been extracted the diameters were then plotted and fitted in MATLAB, this is shown in Figure 5:5. The fit used was a Gaussian distribution shown below in Equation (16) .

$$f(x|\, \overline{D}, \sigma^2) = \ Ae^{-\frac{(x-\, \overline{D})^2}{2\sigma^2}}$$

$(\ 16 \ )$

In the above equation A is a scaling constant, $\overline{D}$ is the mean particle diameter and σ is the standard deviation of the particles. By using this equation for the fit it is possible to extract the average particle diameter from the collected data. For Latex 223-2 and Latex 225-2 this comes out as 62.2 nm and 59.4 nm respectively. Comparing these values to the Hydrodynamic Diameters measured using DLS it can be seen that the actual physical diameter of the particles is indeed less than their Hydrodynamic Diameter. Latex 223-2 having a Hydrodynamic Diameter of 75.3 nm, compared to a physical Diameter of 62.2 nm, and Latex 225-2 having a Hydrodynamic Diameter of 73.3 nm, compared to a physical diameter of 59.4 nm.

This gives a difference between the two measurements as 13.1 nm and 13.9 nm respectively. More differences lie in the shapes of the distributions shown in Figure 5:5.
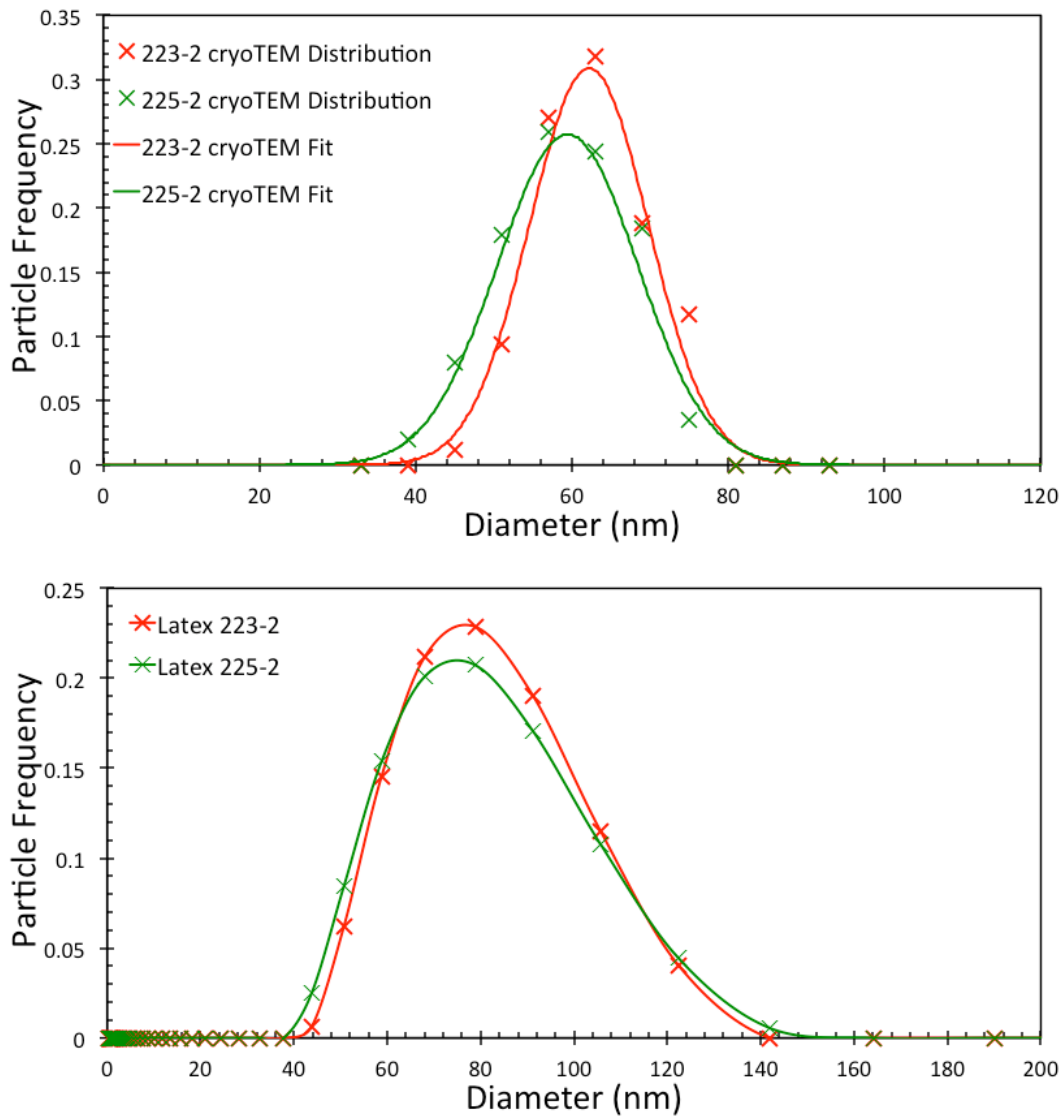
Figure 5:5 – Top – cryoTEM distribution and Fit. Bottom – DLS size distribution. It can be seen that when the shape of the two data sets are compared that the DLS data is significantly skewed with the cryoTEM data being far more symmetrical. This difference in the measured sze distribution results in the need for a different fit to be used for each.

As mentioned in section 5.2.1 and earlier in section 2.3.1, DLS weights larger particles more than it does smaller ones. This is the reason for the difference in the shapes of the distributions. Looking at Figure 5:5 it can be seen that the DLS particle size distribution appears to be skewed. For this reason if fitting this data a Log Normal distribution could be the fit best suited, as shown by Thomas. [141] whereas the cryoTEM data appears to have a more symmetrical distribution, hence the use of a Gaussian fit. This highlights the issue with relying on using one bit of supporting data when attempting to build a SAXS model. If starting to create a SAXS model for the particles under investigation using just the DLS data, it could be assumed that the particles have a Log Normal size distribution. However, in reality this is caused by the measurement technique and rather a better suited fit to use would be one with a Gaussian distribution. This illustrates the importance of using a range of techniques when gathering information on a system. Without the cryoTEM data to back up the DLS data both the exact size and distribution of the particles would not be known, both factors that are particularly important when developing a SAXS model.

Another aspect that is important for SAXS is the particle circularity. As mentioned previously, the form factor is not only determined by the size and size distribution of the particle but also by the shape of the particle. As discussed in section 2.3 the further from a sphere that a particle is, the less defined the peaks will be in the scattering pattern, an effect similar to that observed for a system with a large particle dispersity. For this reason it is important to get an idea of how regular the shape of the particles are, so that a correct model can be produced. There are a number of approaches that can be adopted when trying to quantify how spherical an object is. However, as cryoTEM images are going to be used, the assumption has to be made that the 2D shape of the particle provides a good representation of their 3D structure. The first way this can be quantified would be the particles' circularity, this is defined below in Equation (17):

$$f_{circ} = \frac{4\pi A}{P^2}$$

(17)

161

In this equation f_{circ} represents the particle's circularity, A the particles area and P its perimeter. For a circle the value of f_{circ} is 1 and for anything that is not a circle the value will be less than 1, for example the f_{circ} value for a square is $\frac{\pi}{4}$ or 0.79. This method for defining the circularity of the particles is in theory the best technique to use. However, in practice applying this method is difficult for a number of reasons. The main reason is due to the resolution of the microscope images collected - looking closer at Figure 5:3 it can be seen that the edges of the particles are fairly pixelated which would cause a problem in image analysis. In order to extract the perimeter from these images assumptions would have been made with respect to the location of the particles' edge. Attempts to gather higher resolution images were made to no avail.

The second approach, and the one that was used in this study, is to look at the particles' aspect ratio; this is defined as the smallest diameter divided by its largest diameter orthogonal to it, as represented below in equation (18):

$$A_R = \frac{D_{min}}{D_{max}}$$

$$(18)$$

In this equation A_R is the Aspect Ratio of the particle, D_{min} is the minimum particle diameter and D_{max} is its maximum diameter. Again in the case of a circle the value for A_R is 1. The reason this method has been chosen is due to the ease at which it can be applied to the measured particles. Using MATLAB a particle is selected for analysis and a rough centre of mass is found for the particle. Once this has been done the user then utilises the generated guidelines to measure a number of orthogonal particle diameters. From these selected values the minimum value is selected and used as the particles' Aspect Ratio. This process is repeated for a number of particles and an average for the population can be taken.
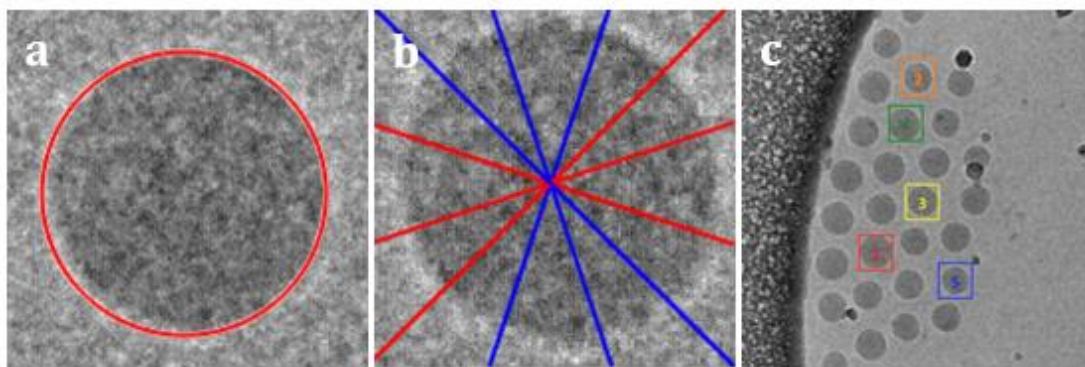
Figure 5:6 – Demonstrates three of the stages involved in measuring the aspect ratio of the particles. (a) – A rough center for the particle is found using the same circle finding algorithm as used above. (b) – Guide lines are generated and guide the user to measure a number of different orthogonal diameters. (c) – This process is repeated to gather information representative of the whole sample.

Using the process described above, an aspect ratio for both Latex 223-2 and Latex 225-2 was calculated; the values came out as 0.96±0.01 and 0.95±0.01 respectively. From these values it can be seen that the particles are in fact highly spherical. For this reason, and when in solution at least, the particles can be assumed to be perfect spheres. One final assumption that has been made ahead of the SAXS analysis is that the particles have no internal structure. In reality, due to the method by which the particles were synthesised, the particles may have a slight core-shell structure. However, as the polymer in both the core and the shell are the same then the contrast between the two will be minimal, resulting in minimal scattering at this interface. This, along with the difficulty in exploring the internal structure of these particles due to their small size and low T_g, means that initially the model used assumes that they are perfectly spherical with no internal structure.

Since a relatively extensive study has been carried out on the shape and size of the particles under investigation, the next step is to see how well the information gathered compares with the reduced scattering patterns. Figure 5:7 shows the scattering patterns collected along with the fits that have been applied to the data based upon the information gathered *via* cryoTEM. The steps taken to manipulate the raw scattering data into the form seen in Figure 5:7 is outlined in section 2.3. Looking into the fit that has been generated, it can be seen that it is a fairly good match to the data. There are some slight differences with the data both at high and low q, this error is likely caused by noise in the data and error introduced by proximity to the beam stop. The fit used modelled a Gaussian distribution of hard spheres. The starting point for the fit of each data set was taken to be the Gaussian distribution that was measured using cryoTEM. From this start point SASfit was used to fit the selected model to the scattering data. The final fits gave a distribution of particle sizes that can be compared to the size distributions measured using image analysis of the cryoTEM data. These fits were plotted for visual comparison and presented in Figure 5:8.
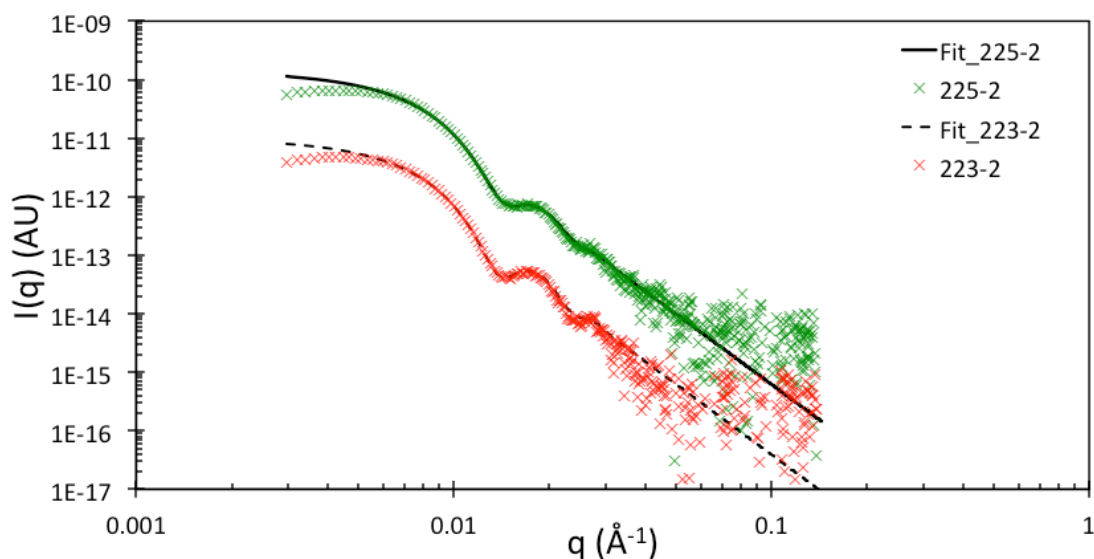
Figure 5:7 - Shows the scattering patterns for latex 223-2 and latex 225-2. The solid lines represent the fits produced using information gathered from cryoTEM and DLS. It can be seen that the fit is in strong agreement with the data apart from at low q where error could be introduced due to proximity to the beam stop.
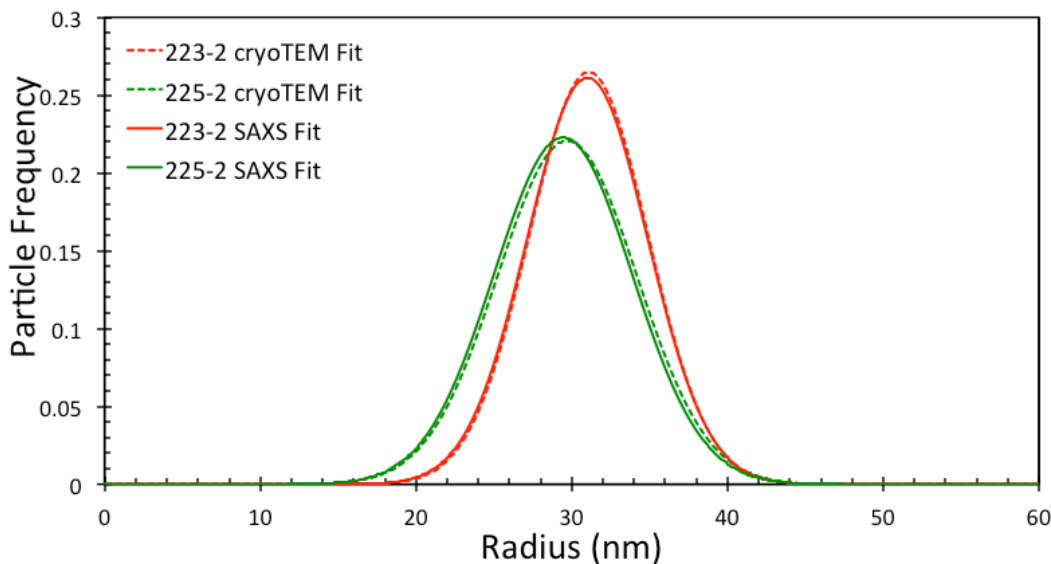
Figure 5:8 – Shows the plotted Gaussian distributions for the data collected by both cryoTEM and SAXS. It can be seen that for both experimental techniques the measured particle distributions are almost identical.

Table 5:2 – Measured radius of particles in nanometres

	Latex 223-2	**Latex 225-2**
cryoTEM	*31.09*	*29.71*
SAXS	*31.05*	*29.44*

It can be seen that the fitted size distributions for both the SAXS and cryoTEM data are in strong agreement. When extracting the measured average size from both sets of data this point is further backed up. The measured average radius for each 223-2 and 225-2 for both SAXS and cryTEM is presented in Table 5:2 One thing that can be noted when looking at the data is that, due to the small difference between the two measured sizes, the population size used when fitting the cryoTEM data is sufficient to generate a more than good enough idea of particle size. This means that in any future work conducted using different size latices a good starting point would be to gather images of approximately 100-200 particles and measure the size distribution using image analysis. This in turn will allow a better fit of the particle size using SAXS.

As previously mentioned it was assumed that the particles did not have an internal structure. In this study the latex particles are produced through a seeded emulsion polymerisation. This means that at first a seed particle is produced, the rest of the particle is then "grown" from this.[142–144] For this reason it is possible that there will be a small contrast between the initial seed particle and the further growth. However, the initial fit for the particles does not take into consideration the possibility of this structure. Despite this, the fit shown in Figure 5:7 shows it does not appear to cause any problems with the fit at this stage, indicating that the electron density of seed and the outer particle are very similar and hence have little to no contrast.

Now that the form factor of the particles has been fitted and a good understanding of the dilute system has been gathered, the application of SAXS on the more complex systems containing the additives can be investigated. In the next section SAXS will be carried out on dried films containing varying concentrations of Texanol™ as well as the additives that have been used throughout this study.

5.3.   Particle Structure Factor

It has been shown that through the addition of additives the cracking in a PS/Ac latex film can be reduced. It has been hypothesised that the additive is creating a network around the latex particle and hence altering the particle spacing. The amount of change to the particle packing is dependant on both the additive used and the concentration of the additive. In order to try to gain an understanding into the way that the additives are affecting the particle spacing within the film a number of additives have been studied. The changes in the packing of the particles can then be compared to the way that these additives change the properties of the films on the macroscopic level. With this increased understanding of the films' behaviour, the intention is to gain a better understanding of how the additives studied earlier in this thesis are causing the observed reduction in cracking.

Initially the effect of a cosolvent, Texanol™, has been studied. As previously mentioned adding an increasing concentration of cosolvent to a latex formulation plasticizes the latex. In turn this reduces the cracking within the film and allows the film to form at lower temperatures. Using SAXS a number of different concentrations of Texanol™ have been studied to try to observe the effect on the packing of the particles. The results gathered from this will hopefully provide a way to compare the effect that altering additive concentration has on the packing of the particles within the film.

5.3.1.   Texanol™ Concentration

A number of formulations of latex 223-2 have been made with varying concentrations of Texanol™ concentrations, ranging from 0 wt% to 11.6 wt%. The samples were dried in a 5 mm washer with a kapton film adhered to the back. This ensures that the surface area of the film remains constant as the films dry. The films were dried at a constant humidity of 20%RH using the humidity-controlled glove box. The reduced scattering patterns are shown below in Figure 5:9.
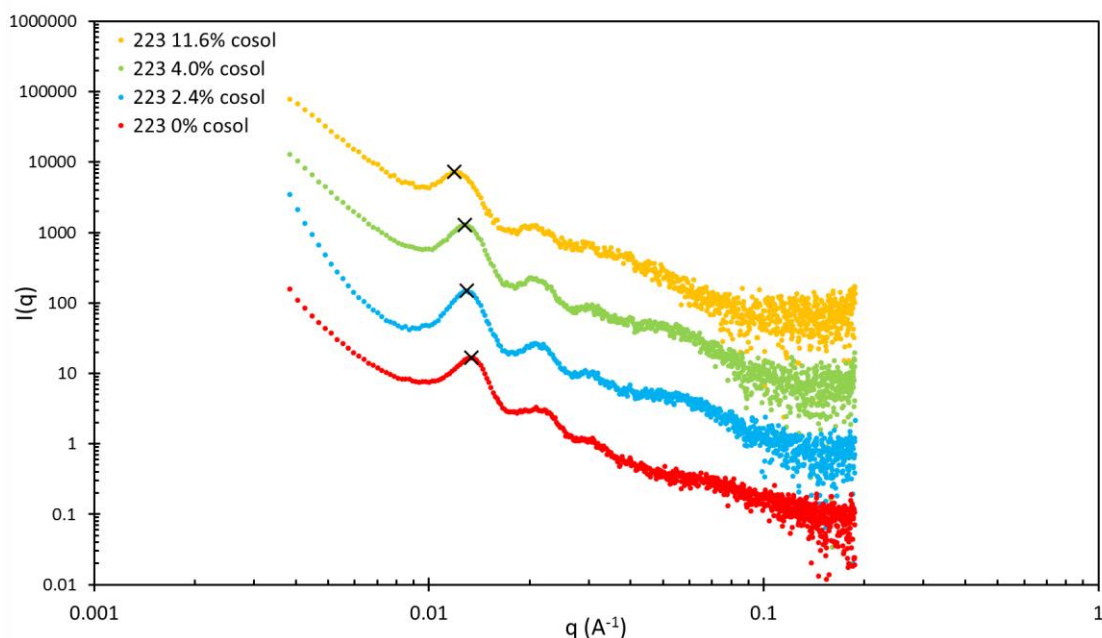
Figure 5:9 – Shows the SAXS reductions of latex 223 with varying concentrations of Texanol™. It can be seen that as the concentration of Texanol is increased the structure factor peaks shifts to lower q indicating increased particle separation.

The first thing to note when looking at Figure 5:9 is that the system has good contrast, this allows the SAXS data to be used to study how the concentration of Texanol™ is affecting the spacing of particles within the film. This contrast must come from inhomogeneities within the film which could come from several things for example: residual water, air or Texanol™ trapped at the particle-particle interface This would then provide a contrast in electron density that would provide the peak in the above graph. Due to the expected periodic honeycomb structure it could be imagined that the resulting peaks that are seen in Figure 5:9 could be Bragg peaks. However, if we look at the 2D SAXS image, Figure 5:10, there are no clear Bragg peaks but rather a set of concentric rings; these rings are likely to be Debye-Scherrer rings.[139,145] This would indicate that the dried latex film has regions of highly ordered packed particles occupying a honeycomb structure, dispersed with randomly packed regions of particles. It could almost be thought of as a semicrystalline colloidal structure rather than a full colloidal crystal.
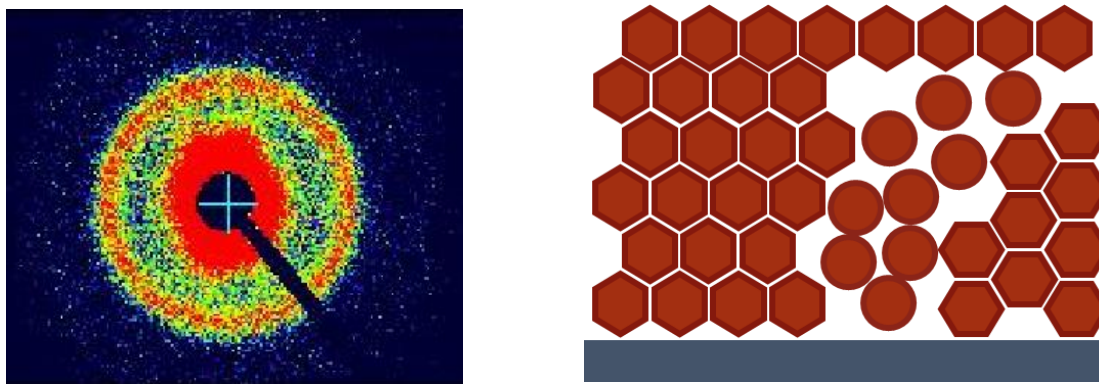
Figure 5:10 – (Left) Shows the 2D scattering pattern of Latex 223-2 without the addition of any Texanol™. It can be seen from the Debye-Scherrer rings that the colloidal structure is not completely uniform and most likely has regions of ordered crystalline structure combined with regions of more randomly packed structure. (Right) Shows a cartoon sketch of the proposed semicrystalline colloidal structure, with regions of highly ordered honeycomb structure combined with less ordered regions.

Outside of the general structure of the system it can clearly be seen that as you increase the concentration of Texanol™, the particle spacing increases. As previously mentioned the contrast in this system most likely comes from Texanol™, air or water trapped at the interface between particles. As a result the distance that is being measure in this experiment is most likely the distance between faces of the dodecahedral structure. The increases in distance between the faces of the deformed particles can be seen as a shift in the initial peak of the scattering pattern. This shift in the scattering pattern shows that the particle packing density decreases with increasing Texanol™ concentration. This reduction in packing density could be attributed to a number of things however, as the mechanism by which the coalescent solvents such as Texanol™ operates is fairly well known it can be proposed that that the Texanol™ is plasticising the particles. This in turn will swell the particles and cause the observed increase in particle separation. The change in particle separation as a result of increased Texanol™ concentration has been plotted in Figure 5:11. Figure 5:11 also shows the theoretical increase in particle separation calculated from the volume change of the system caused by the addition of the Texanol™. In order to calculate the theoretical particle separation, the particles where assumed to be regular dodecahedrons. Based upon this assumption and that the distance measured by SAXS is the distance between faces of a regular dodecahedron we can begin to

calculate the theoretical volume of an individual particle without the addition of any Texanol™. The first step is to calculate the edge length of a regular dodecahedron, a, which can be done with the following expression:

$$a = \frac{2r_i}{\sqrt{\frac{5}{2} + \frac{11}{10}\sqrt{5}}}$$

(19)

Where r_i is the radius of an inscribed sphere, or half the distance measured using SAXS. From this we can then calculate the theoretical volume of each particle (V_d) using the following expression:

$$V_d = \frac{1}{4}(15 + 7\sqrt{5})a^3$$

(20)

As the density of latex 223-2 should be $\sim$1100 kg.m^{-3} the theoretical mass of each particle can be calculated. From this the mass of Texanol™ in each sample can be calculated along with a volume of Texanol™ per particle, if this volume is added to the volume of an individual particle without Texanol then theoretical particle separation for a known mass of Texanol™ can be calculated, as is shown below in Figure 5:11.
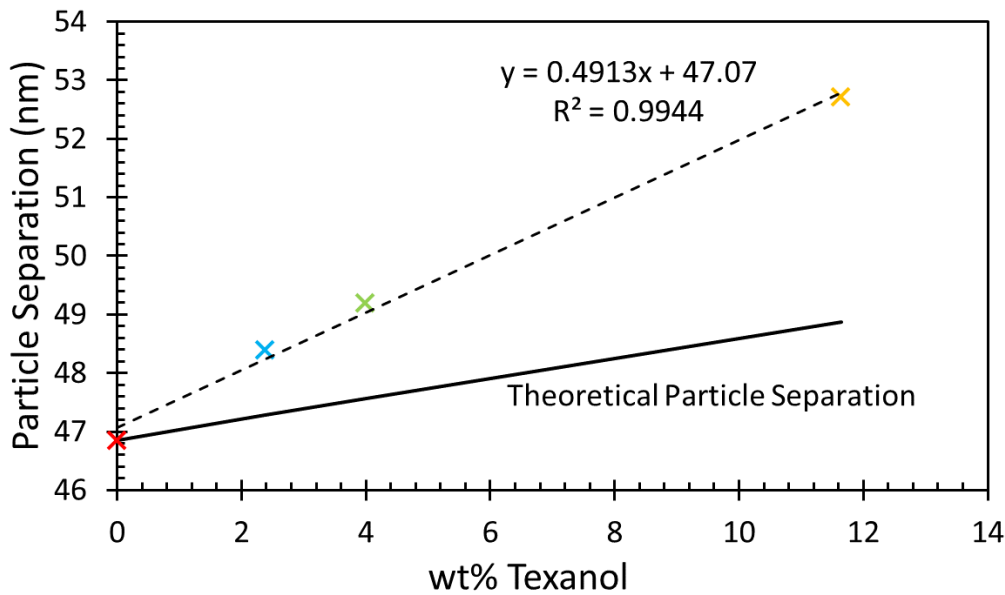
Figure 5:11 – Shows the Increase in particle separation as a result of increasing Texanol™ concentration. It can be seen that the concentration of Texanol™ is directly proportional to the particle spacing. It is known that Texanol™ and other coalescent solvents plasticise latex particles and hence reduce the MFFT. This plasticization is likely to swell the particle and hence increase the interparticle separation. A theoretical particle separation has also been plotted that is based on the increased volume change with the addition of Texanol.

Comparing the theoretical particle separation to the SAXS data it can be seen that the theoretical separation is less than the experimental values, with an increase of 2 nm and 6 nm respectively . This would indicate that along with the increase in separation caused by the increased volume of Texanol™ there is a further increase in separation that is related to the increasing concentration of Texanol™. One possible source of this could be an increase in residual water in the film that is located at the particle-particle interfaces. When looking at the effect that increasing the concentration of Texanol™ has on the macroscopic properties of the film over the concentration range being investigated, shows a drastic decrease on the MFFT of the film from around 20 °C down to around 5 °C. Figure 4:2 shows the reduction in MFFT with respect to increasing Texanol™ concentration and has been inserted below for ease of discussion. Upon review it can be seen that the reduction in MFFT is proportional to increasing particle separation. As Texanol™ is plasticising latex 223-1 then this increase in separation is likely due to particle swelling with the reduced particle T_g.
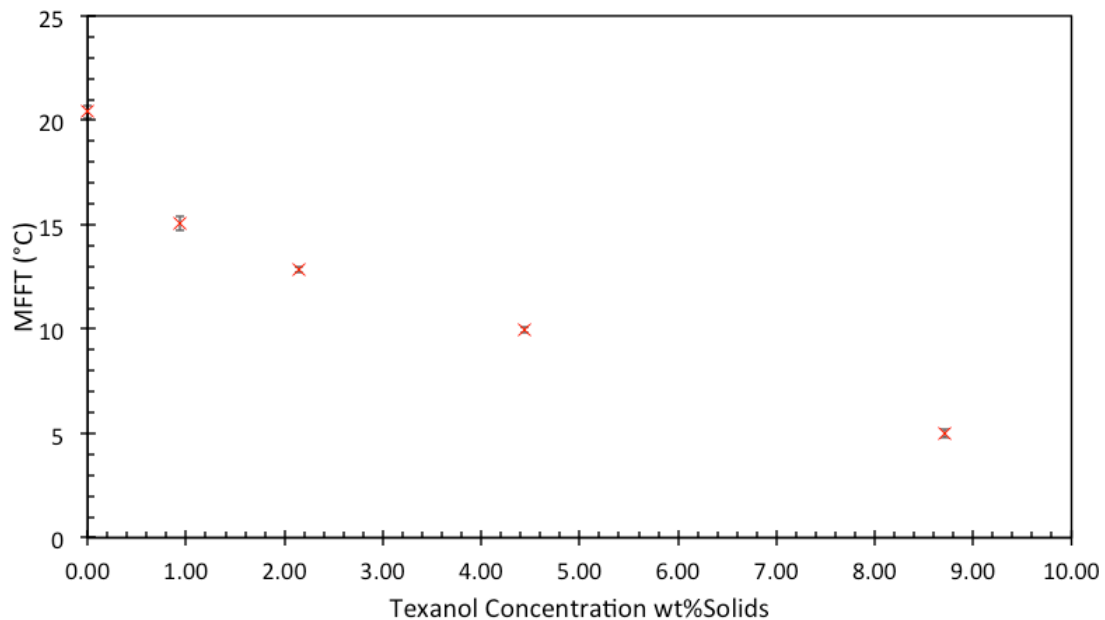
Figure 4:2 – Shows the MFFT of a system containing varying concentrations of Texanol™. It can be seen that over the concentration window used in the SAXS experiment the MFFT of the system changes around 20 ℃.

This reduction in MFFT allows the paint to be used over a wider operating window. The coalescence solvent can be thought of as creating a plasticised region that allows the release of internal stress development through the deformation of the plasticised region, rather than through the cracking of the film. The advantage to a coalescence aid such as Texanol™ is that it evaporates over time to yield a film that has a T_g close to the T_g of the polymer that makes up the latex particle. This means that a high T_g polymer with good barrier properties with a high resilience to dirt pick-up and damage can be used and still form a highly uniform homogenous film. However, the downside to the use Texanol™ that it is still classified as a VOC. This means that its use is restricted to limited concentration with the enforced reduction of VOC content of paint; in particular interior paints. Ideally VOCs would be eliminated completely due to the possible health concerns associated with VOC content. [146–148]

In contrast the additives that have shown the most promise in minimising cracking in these films are cellulose-derived and hence produced from natural products such as cotton or sugar cane.[149] In the next section a number of films with varying concentrations of additive have been studied to show how the addition of

172

additive alters the particle packing and structure within the films. This will hopefully give an insight into the mechanism by which the additives are operating and allow the production of crack free films without using as much coalescent solvents.

5.3.2.   Additive Concentrations

The effect of additives on the properties of latex films has been studied throughout this thesis. It has been found that due to the need of free water, the addition of additives as a way to increase the drying/open time of a film is poor. However, it has been shown that adding additives to latex films reduces the cracking within the films and hence provides a way to reduce the amount of cosolvent required in the films' formulation. A number of formulations with varying additive concentrations have been made. These formulations were then dried at 20%RH in a humidity-controlled glovebox in 5mm washer with a kapton backing. This allowed the samples to be dried at a constant surface area, allowing a controlled rate of evaporation. This means that any differences observed in the scattering pattern will be caused by the variation in additive and additive concentration alone. The same additives that have been studied in the previous chapters have been studied in this section. Each system has been looked at using SAXS and then the data has been analysed in order to consider the differences in packing density of the films. The reduced and fitted SAXS plots are shown below in Figure 5:12 - Figure 5:14. The concentrations of additives used in these systems are shown below in **Error! Reference source not found.** The wt% of additive in the dispersions is calculated from the mass of the polymer within the dispersion.

Table 5:3 – wt% of Additives used in the SAXS study

	Pl	MC	HPMC
1	*0.22*	*0.30*	*0.25*
2	*0.38*	*0.38*	*0.37*
3	*0.72*	*0.78*	*0.76*
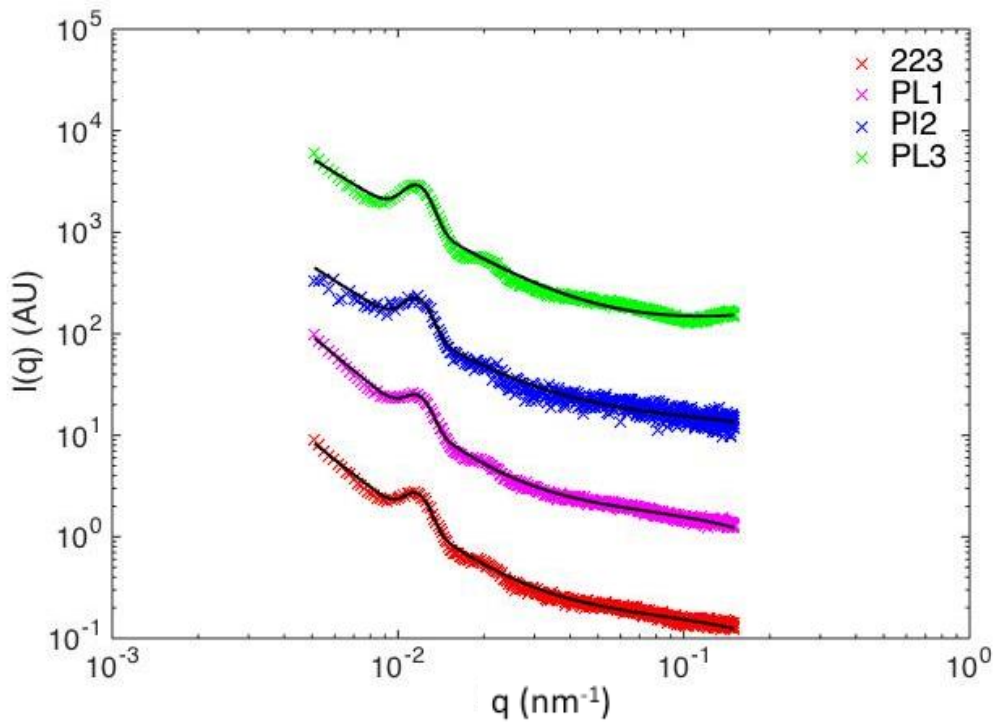
*Figure 5:12 – Shows the Scattering patterns of latex 223-2 with Pluronic additive at various concentrations according to **Error! Reference source not found.** The plots are in order of most concentrated to least concentrated Pluronic sample from top to bottom.*
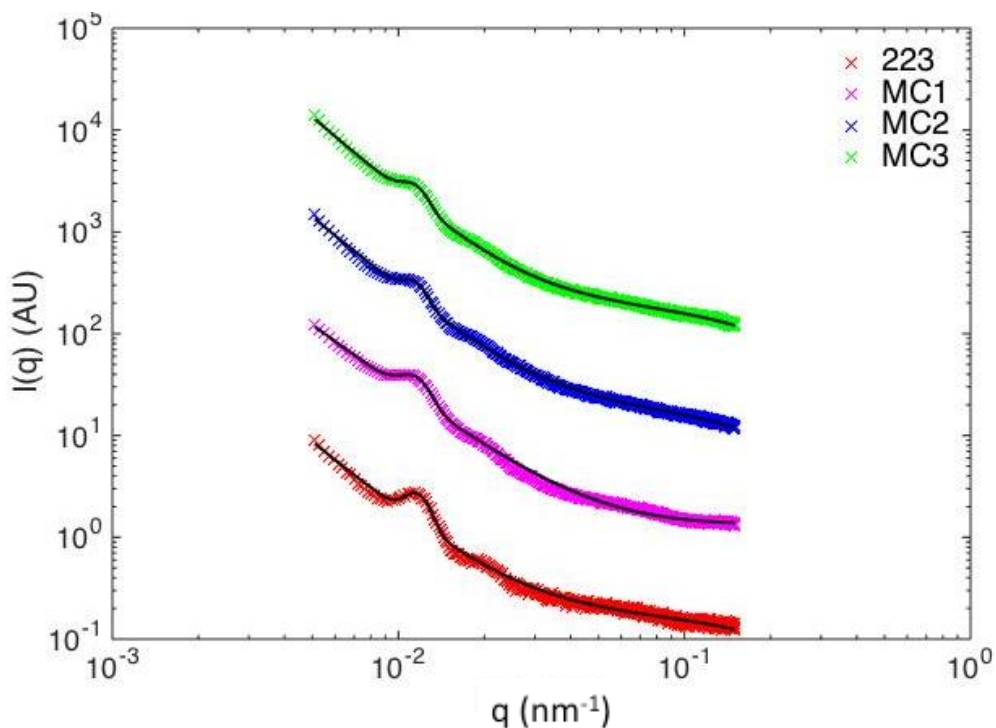
Figure 5:13 - Shows the Scattering patterns of latex 223-2 with methylcellulose additive at various concentrations according to Table 5:3. The plots are in order of most concentrated to least concentrated MC sample from top to bottom.
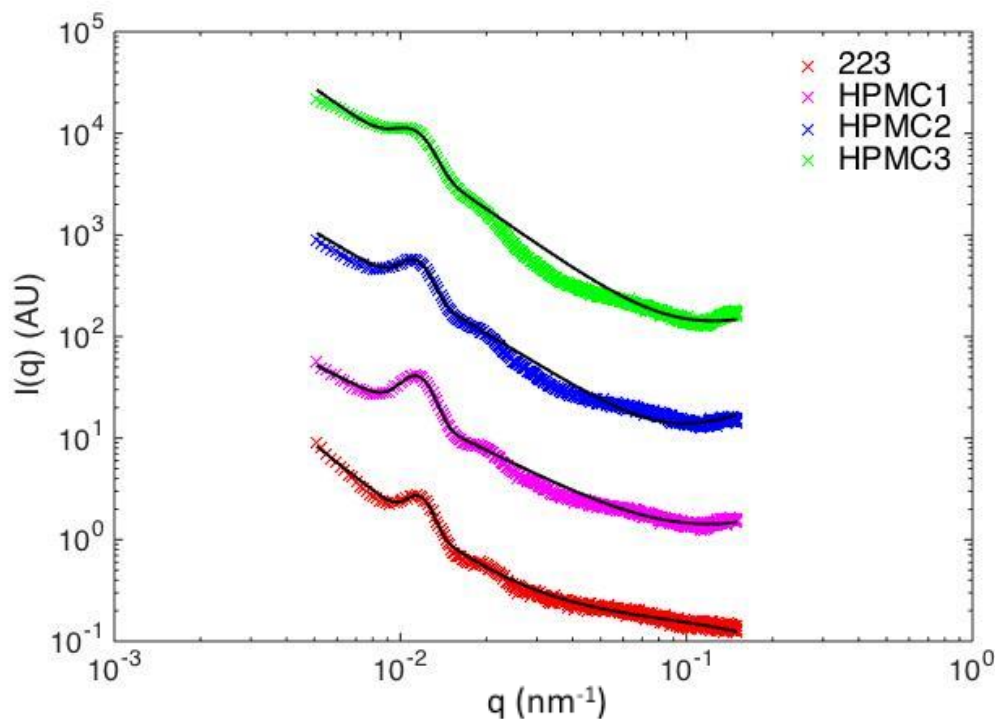
Figure 5:14 - Shows the Scattering patterns of latex 223-2 with Hydroxypropyl methylcellulose additive at various concentrations according to Table 5:3. The plots are in order of most concentrated to least concentrated HPMC sample from top to bottom

Looking at the above figures (Figure 5:12 to Figure 5:14) it can be seen that as with the Texanol™ concentration, changing the additive concentration has an effect on the scattering patterns of the latex systems. Through the addition of additive the initial structure factor peak appears to shift slightly towards lower q, which indicates that the particles' packing density has decreased. This shift in q can be seen as an effect of changing both the concentration of the additive as well as changing the additive being used. It must also be noted at this point that the humidity level in the SAXS chamber is not controlled as in the previous experiments. This could also slightly shift the structure factor peak, as at higher humidity levels the system could absorb more water and hence increase the interparticle separation. Controlling the environment that the SXS is run in is something that should be considered in any future SAXS experiments. In order to compare how the spacing of the particles changes between formulations the structure factor peak has been fitted using MATLAB. The fit consist of a background slope and a Gaussian peak, a fit for each system has been shown along

with its corresponding data above in Figure 5:12 to Figure 5:14. For each system a number of data sets were analysed and then the average peak position was taken and plotted *vs* the additive concentration below in Figure 5:15.
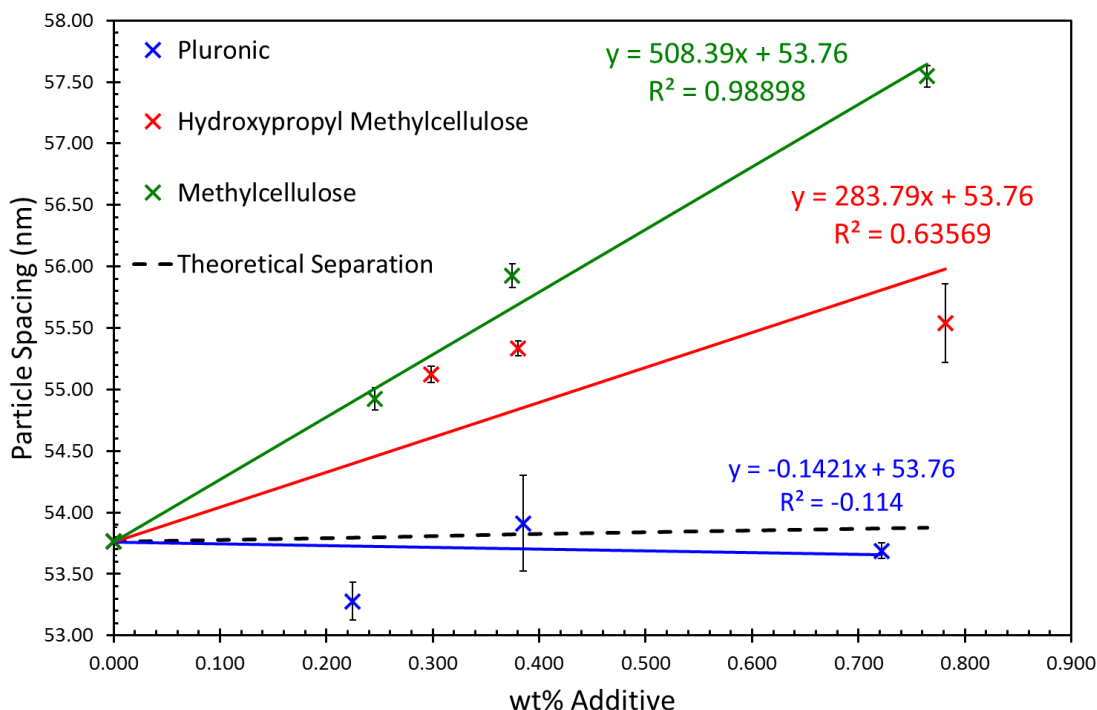
Figure 5:15 – Shows the position of the structures factor peak vs the additive concentration for each additive system. It can be seen that increasing the concentration of both the cellulose-derived additives decreases the packing density of the particles thereby increasing their particle spacing. However, the Pluronic additive does not appear to be having an effect on the particle separation. Unlike Texanol™ it has been shown through the use of AFM that the additives are not plasticizing the latex particles and therefore it has been hypothesised that the additives are located in between the latex particles. The data above agrees with this hypothesis. A theoretical particle separation has also been presented based on the increased volume of additive alone.

In Figure 5:15 there are a number of clear observations that can be made. The first observation is that with an increase in additive concentration there is typically an increase in the particle spacing. However, this is not the case with the Pluronic additive where the particle spacing remains fairly consistent with increasing additive concentration. As was the case earlier in section 5.3.1 it is possible to calculate the theoretical particle separation based on the increased volume of the additives alone. In this instance, even at the highest concentration of additive the predicted particle separation would be ~0.1 nm compared to the measured value of ~3.75 nm, this data is plotted along with the experimental data in Figure 5:15. It is also worth noting at this point how the particle spacing could affect the film's thickness. Earlier in section 4.2 it was discussed how the dried film's thickness could increase by around 4 μm through the inclusion of the hydrophilic additives. However, the SAXS has shown that the particle spacing had increased by more than was predicted. The SAXS data has shown that particle spacing can increase by as much as ~3.75 nm in the case of systems containing methylcellulose. Using equations (19) and (20), it could be expected that based on the SAXS data a thickness change of ~ 40 μm would be observed. With the available equipment, this would be on the very limit that could be measured. To conduct a study that looked at the thickness change of these films a more sensitive technique such as ellipsometry would have to be used.

As has just been mentioned for the cellulose based additives there is a discrepancy between the theoretical increase in particle spacing and the spacing measured by SAXS, as is shown in Figure 5:15. It is also important to note that the Pluronic additive do not share this trend and instead shows no real increase with increasing additive concentration. With the cellulose based additives, there must me a mechanism that provides this increase in separation over the volume based prediction, this most likely comes from the physical properties of the chosen cellulose based additives. As the additives are hydrophilic in nature then as water evaporates from the system some water could be held back by the additives. As the additives, will be forced to the particle-particle interfaces during film formation, then the hydrated, swollen additive will force the particles apart more than the volume based calculation predicts. However, as with the cellulose based

additives the Pluronic additive is also a hydrophilic molecule, and therefore a similar trend should be expected. There are several things that could cause the differences observed in the SAXS data between it and both the cellulose based additives. The first possibility could be that the Pluronic additive does not mix with the Latex particle network and either forms a Pluronic dense region at the top or bottom of the film. This would hence not affect how the particles in the bulk of the film pack and would therefore not show in the SAXS data. As was discussed earlier in section 4.4, as the concentration of cellulose derived additives were increased, the MFFT of the film appeared to decrease with the MFFT of the films containing various amounts of Pluronic additive remaining largely unaffected. Figure 4:6 has been added in for ease of comparison.
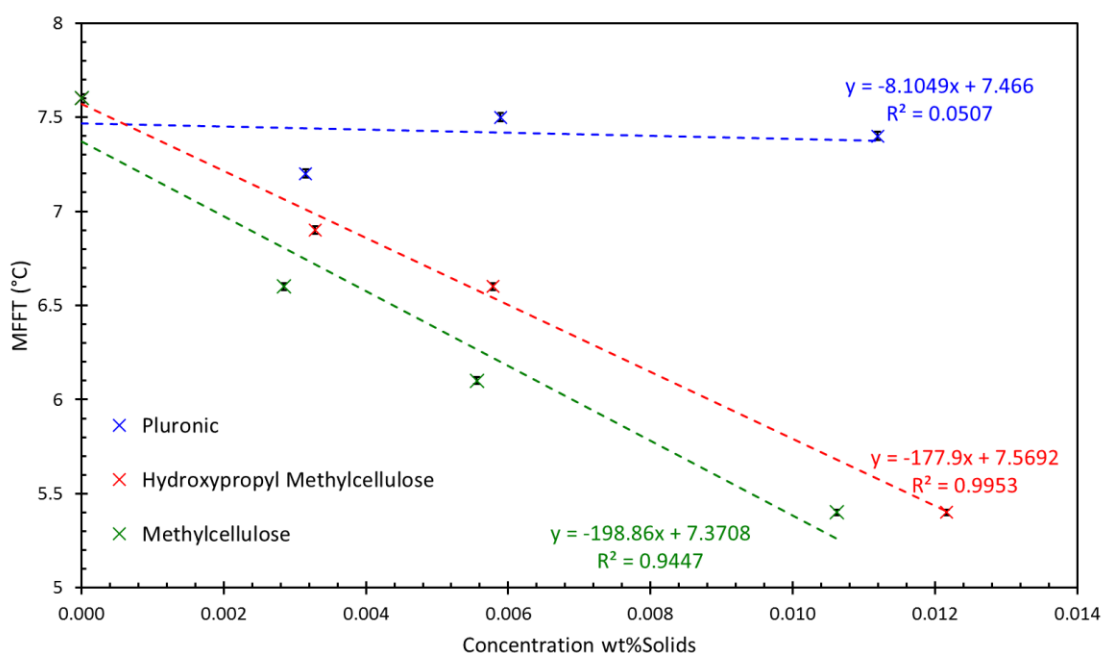
Figure 4:6 - Shows the films' MFFT vs the concentration of additive as a percentage of the films' mass of solids. It can be seen that the cellulose based additives lower the MFFT as the concentration increases. In comparison, the Pluronic additive does not have a large effect on the MFFT.

Looking at Figure 4:6 the affect that the additives are having on the MFFT mirrors the effect on particle spacing measured using SAXS. If the Pluronic additive was not incorporated into the latex network as the SAXS data may suggest, then it would be expected that the film formation properties would remain unaffected. The MFFT data presented in Figure 4:6 shows strong agreement with this hypothesis.

Due to the small concentrations of additives used in this study, there is another potential hypothesis that may explain the minimal change in particle spacing with increasing concentrations of Pluronic additive. Looking back at Figure 5:15 the theoretical increase in particle spacing is shown, this calculation assumes that the additive causes particle spacing to change through the increased volume of additive alone. It can be seen that at the low additive concentrations the volume based calculation would predict minimal change in particle spacing, comparing this to the SAXS data for the Pluronic additive we can see that there is some agreement to the volume based model. This minimal change in particle spacing caused by the Pluronic additive would indicate that the Pluronic additive is not absorbing water and that all that is present at the particle-particle interface is the additive. In contrast the cellulose derived systems show that the increase in spacing is much larger than the volume based model predicts, and hence must be holding water at the particle-particle interface. This would suggest that the cellulose derived additives had a greater affinity for water than the Pluronic additive. Looking back at the water activity measurements for the dilute additive solutions, Figure 3:2, it can be seen that there is minimal difference between the different additives. However, this does not provide any information of the affinity for water in a more concentrated state, such as in the dried latex film. Turning to the literature and the existing work around water vapour sorption of cellulose and Pluronic additives, there is some information that could be useful when drawing conclusions on this hypothesis. Looking at the work by George *et al.* it was seen that a film of HMPC had an equilibrium moisture content of between 2 – 6 wt% based on the 20 - 60 %RH humidity range studied in this investigation.[150] However, over the same humidity range Gu *et al.* showed that a hydrogel film of a similar Pluronic to the one studied in this investigation gained less that 2 wt%

water.[94] As the Pluronic has been shown to absorb less water than HPMC then it could be imagined that the films containing MC and HPMC have an increased water content at the particle-particle interface in comparison to the film containing the Pluronic additive. This could explain the difference in particle spacing observed in the SAXS study. To further investigate what is causing the difference in measured particle spacing, and in turn test which of the two hypotheses is correct, further experimentation would be required. The simplest way to test each hypothesis would be to section the film and try to measure the vertical distribution of the additive throughout the film. If the additives distribution is uniform throughout the film then it is likely that a difference in hydrophilicity is causing the observed difference in particle spacing. If this is the case then DVS could be used to measure the equilibrium moisture uptake of each film at various humidity levels, in turn SAXS could be used to measure the particle spacing to test for humidity dependency.

However, the alignment in trends between particle spacing and MFFT in all cases, raises the question of the relevance of particle spacing in producing a uniform crack-free film. In Chapter 4: a model for this system was presented (Figure 4:12), in this model the additive created a network around the latex particles. As the concentration of additive is increased it is likely that the additive network forces the latex particle to pack less densely, especially if there is increased water content at the particle-particle interface. This network is thought to be providing a way for the stress build up that develops during particle consolidation to be relieved. This alternative mechanism of stress relief, other than cracking, is the reason that the films containing the cellulose-derived additives are producing a crack free film. It was mentioned previously that the network of additive around the particles could be creating a way for the particles to rearrange slightly to relive stress build up. The softer additive would also deform without yielding if bound to the latex particles. However, without further experimentation the exact mechanism by which stress is relieved and hence cracking is reduced can only be hypothesised. Figure 5:16 illustrates how particle packing is changing with respect to increasing concentration of the cellulose-derived additive.
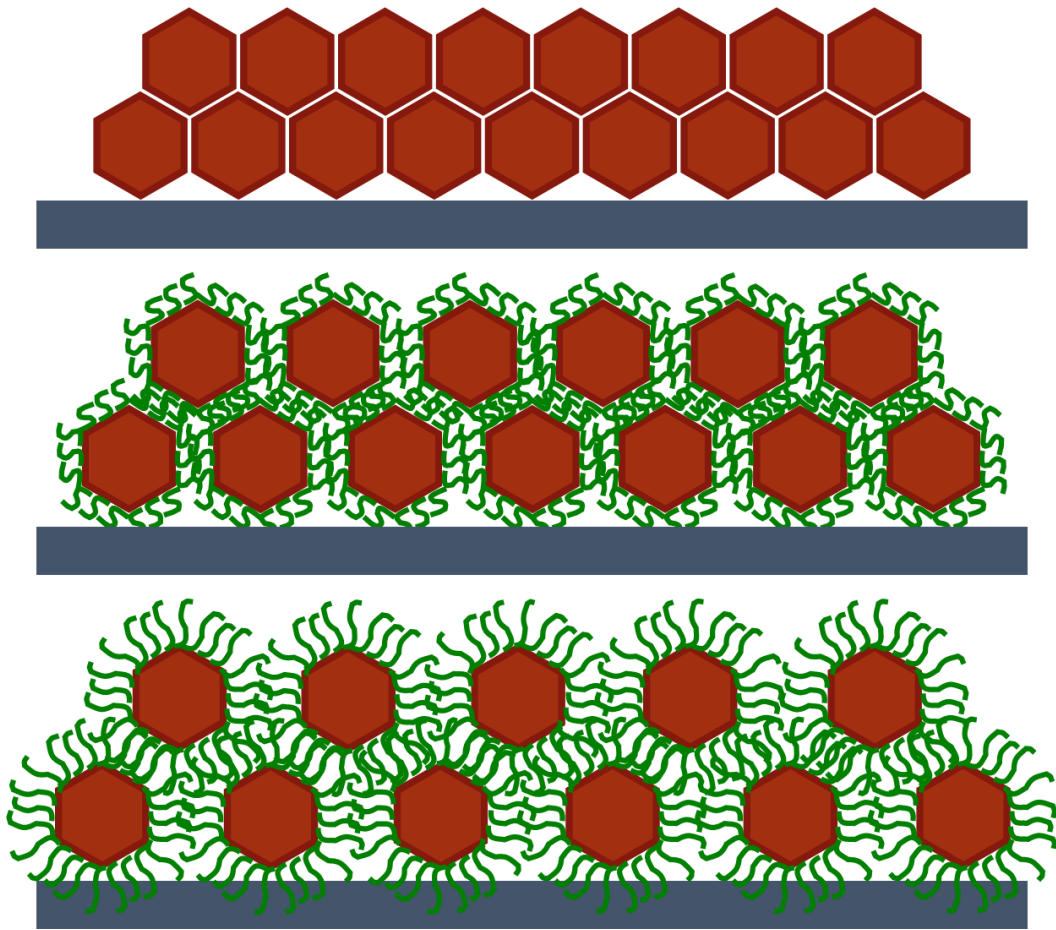
Figure 5:16 - Shows the proposed effect that increasing additive (top to bottom) is having on the structure of the particles in the system. The cellulose derived additives are thought to be forming a network around the additives, as the concentration of additive increases the latex particles are being forced further apart and hence the interparticle separation measured with SAXS is increased. The network surrounding the particles is thought to be providing a mechanism to relieve stress other than cracking.

5.4.   Conclusions

At the start of this chapter it was hypothesised that the cellulose-derived additives were producing a network around the latex particles. This network is believed to be reducing the cracking by providing an alternative mechanism for stress relief instead of cracking. In order to look at the particle packing throughout the depth of the film a method was needed enabling the study of the film from top to bottom. This can be achieved through techniques such as microscopy, however, this requires sectioning the film into slices. Sectioning the film increases the risk of damaging the internal structure due to excessive heat build-up caused by the device used to slice the film. For this reason SAXS was used to investigate the film as a whole. SAXS enables the whole depth of the film to be studied at one time.

Using SAXS films multiple concentrations of the three additives used in the rest of the study (Pluronic, MC and HPMC) were examined. It was found that increasing concentration of additive gave rise to increasing particle separation. These results actually mirror the results from an experiment presented in section 5.3.1, in which SAXS was used to investigate the particle separation in films with increasing concentration of Texanol™. However, it has already been shown that the films containing the cellulose-derived additives do not appear to plasticise the latex like Texanol™. On the contrary Texanol™ is known to plasticise latex particles. For this reason, the increased particle separation in the films containing increased concentration of Texanol™ is likely to be caused by Texanol™ swelling the latex particles. The increased particle separation measured with SAXS on the films with higher concentration of MC and HPMC is therefore likely to be caused by the hypothesised additive network surrounding the latex particles. The additive network is likely allowing the particles to rearrange slightly upon consolidation, this will aid in the relief of stress as the film enters the later stages of film formation. The softer additive molecules bridging the gaps between the latex particles will also allow slight deformation without yielding due to internal stress build-up. However, the exact mechanism by with stress is being relived can only be hypothesised without further experimentation. In section 4.7 further work that could examine the stress development in these drying films was proposed. With

this information the correlation between increasing additive concentration and increasing stress relaxation could be studied and compared to other common coalescent aids.

In order to study the location of the additives in these systems SAXS could be used as part of a more extensive investigation. In this study the location of the additives in the film may be compared and studied at various concentrations throughout the entire film formation process. This internal structure could then be compared to various physical points in the film formation process, such as opentime. It is necessary to use a method that quantifies the amount of water at the point that the SAXS measurement is taken. Using the gravimetric technique from section 3.6 would not work due to the inhomogeneity during film formation. In the next section future work that could be carried out to further investigate particle packing and internal structure has been proposed.

5.5.　　Future Work

Studying particle packing throughout the entire film formation process using SAXS is not a novel concept. A number of studies have been carried out on this area, including the work by Hu *et el.* and Chen *et al.*[54,151] However, one thing that neither of these studies looked at is the real-time water content of the drying film/droplet at the point of investigation. In order to achieve the best possible fit for the data the volume fraction of particles needs to be known. One way of achieving this is through a spectroscopic technique such as Near Infrared Spectroscopy *(NIR).*

5.5.1.　　Water Content with Near Infrared Spectroscopy

In order to investigate the particle packing and additive distribution in real-time throughout film formation it is necessary to ascertain a way to monitor the water content of the film at the point the beam passes through the sample. One way to achieve this is to use a spectroscopic technique such as Raman or Infrared.[152] Another way that water content has been investigated using a spectroscopic technique is with NIR. In the work by Cho *et al.* a miniaturised NIR set-up was developed to monitor the water content in water/ethanol mixtures.[153] In a future investigation a NIR probe could be used to study the water content of a drying film at the point the x-ray beam passes though the sample. With this additional information on the evolution of the volume fraction of particles in the film, a better picture of the system could be created. This would then allow a SAXS model to be fitted to the reduced data, enabling the structural evolution of the film to be tracked in real time. The NIR probe could also be used to tie together a number of experiments and fully correlate the internal structure and additive distribution within the film with physical properties such as those measured by a linear drying time recorder as mentioned in section 3.8.1. In order to assess whether this proposed future direction is possible, a preliminary experiment was conducted that compares the evolution of wt% solids *vs* time of a drying film of latex 223-2 both gravimetrically and through the use of a NIR probe. In this experiment a wet film of latex 223-2 was produced using a 100 μm drawdown cube onto a 25 mm x 75 mm microscope slide. The sample was then placed onto a A&DHR-250AZ 4.d.p balance to monitor the mass loss gravimetrically, It must be noted that in this experiment no precautions to mitigate the effects of balance drift were used. Using

184

an OceanOptics NIRQUEST 256-2.5 NIR spectrometer fitted with a reflectance probe, the NIR spectrum was collected for the centre of the sample *vs.* time. To extract the relevant data from the NIR spectra, the ratio of the height of the polymer and the water peaks were examined. Assuming the start point was 40 wt% polymer and the endpoint was 0 wt% water, a rough idea of how the water content at the centre of the sample was evolving *vs.* time could be established and compared to the data collected gravimetrically; this data is shown in Figure 5:17.
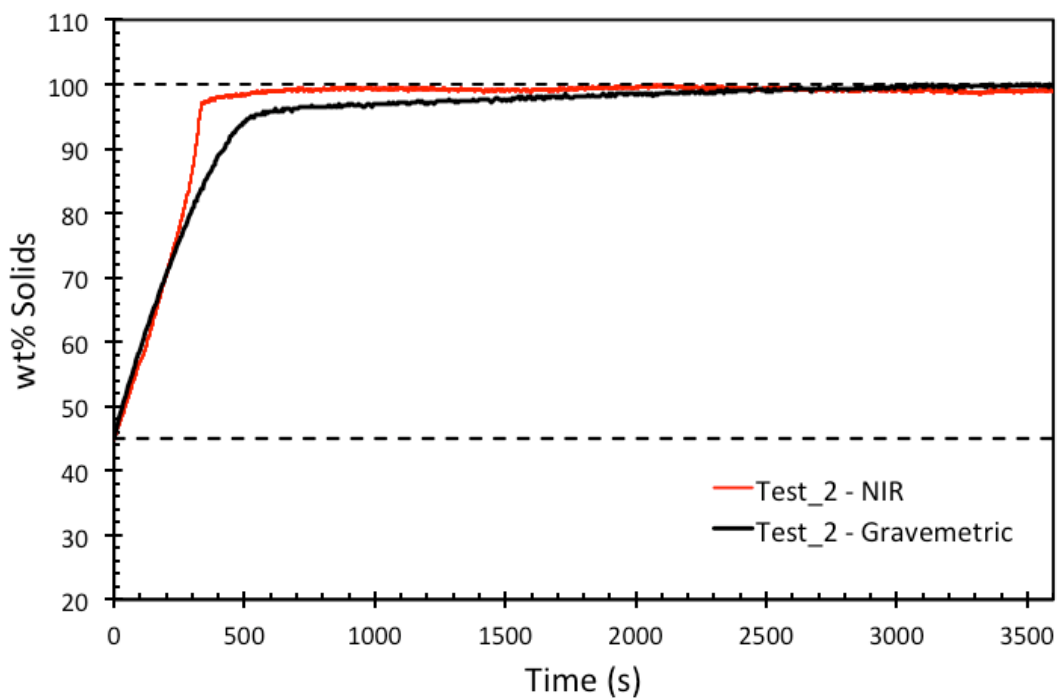
Figure 5:17 – Shows the wt% solids of a drying film of latex 223-2 measured both gravimetrically and with a NIR probe. It can be seen that as the NIR probe is measuring the water content at a very small point and not the average of the whole film the transition from the constant rate period to the plateau is much sharper. This transition likely occurs as the drying front moves over the position where the NIR is being taken.

Upon examination of Figure 5:17 it is clear that the measurement taken with NIR is significantly different to the data produced using a traditional gravimetric technique. The transition from the constant rate period in the NIR data is significantly sharper than that displayed by the data using the gravimetric technique. This is because the NIR looks at the water content at a small point - when the drying front moves over this point the drastic reduction in water content is observed. This data shows that NIR would provide a way for water content to be monitored at a single point, making it possible to study real-time structural evolution within a drying colloidal film. This provides valuable information about the way that additives and other additives change their drying behaviour and, in turn, the properties of water-borne paints.

Chapter 6:   Conclusions

Legislative pressure is forcing VOC content in paint to be reduced. Pursuant to EU directive 2004/42/CE the levels of VOC in all categories of paint are required to be reduced significantly as part of a two-part initiative. The biggest reduction in VOC content affects interior paints, with the reduction of VOCs in interior solvent-borne paints being required to match that in water-borne paints. This legal pressure has driven the development of water-borne paints resulting in a significant increase in research in the area of latex film formation.

In comparison with traditional solvent-borne latex paints, water-borne latex paints have undesirable drying characteristics. In short, they dry far too quickly. This means that there is inadequate time for corrections to be made to a finished coating of water-borne latex paint without leaving marks. This property is called open time and is currently the area of water-borne paint that requires the most improvement. It has been necessary to consider whether the drying time of water-borne latex paints can be sufficiently slowed to enable optimum drying, leaving sufficient opportunity for this self-correction exercise.

Fundamentally, altering the drying time of water-borne latex paint requires changing the vapour pressure of water. This can be achieved through the addition of salt and other additives. In this study a number of additives were investigated for their potential use as humidifying agents in order to modify the drying properties of water-borne paints. The additives chosen to study in this investigation were Methylcellulose, Hydroxypropyl Methylcellulose and a Pluronic. Initially the investigation focussed on characterising the water activity of these additives in order to deduce their affinity to water. It was observed that the water activity of the additives in their pure state was low, meaning that they were effectively holding back the evaporation of water contained within them. However, when these additives were diluted to 2 wt% with both latex 223-2 and water the change in water activity in comparison to the samples without additive was minimal. As paint needs to be of a suitable viscosity, it was not possible to

significantly increase the concentration of the additives. The minimal changes observed in the water activity provided early indications that changing the vapour pressure of water through the addition of such additives, and hence prolonging the paints open time, was not going to be an easy task. Notwithstanding this, the effect of these additives on the film formation of water-borne latex paint was more encouraging.

As mentioned, the open time of water-borne latex paints requires improvement. The ASTM standard for measuring open time is ASTM D7488-11. This outlines the procedure used to measure the open time of decorative coatings; this technique is susceptible to user error and poor time resolution. As set out above, the additives chosen for this study appear to have a minimal effect on the water activity of the samples. For this reason it is necessary to use a technique that can measure small changes in the early stages of film formation, a benefit that perhaps the standard ASTM test method does not offer. A decision was therefore made to study monitor the rate of evaporation of water gravimetrically in order to more accurately understand the effects of the additive on the early stages of film formation.

Humidity levels in the UK fluctuate on all time scales, from seasonal to daily; the observed range is around 40 %RH. In order to study how the additives influence drying time across a variety of conditions it was necessary to perform the gravimetric studies at humidity levels of 20, 40 and 60 %RH. In order to use a standard analytical balance across the range of humidity levels it was necessary to modify this equipment in order to combat variation in the zero point drift *(ZPD)*. Although seemingly small this variation in ZPD can be significant when monitoring the mass loss in small samples. By using a linear stage to move the sample on an off the balance it was possible to track the ZPD of a standard 10 g mass. This ZPD could then be subtracted from the observed mass change caused by evaporation. Although simple, this modification could prevent the misanalysis of small changes in the drying profiles of latex films, a consideration that has not been taken into account in existing literature. Using this technique, along with a PTFE o-ring to control the surface area and thickness of samples with drastically changing viscosity levels, a study was carried out to monitor the evaporation of

water at the three aforementioned humidity levels. It was immediately apparent that the additives did not have an effect on the rate of evaporation from these systems. In contrast, it was clear that the changing humidity levels caused the rate of evaporation to change drastically. In order to try and extract information on any small changes that the additives could be having on the rate of evaporation, the initial rate of evaporation was fitted. When this constant rate period was fitted, it was possible to see some changes in the rate of evaporation caused by increasing additive concentration. However, this change was negligible in comparison to the changes in rate of evaporation caused by humidity fluctuation. Further, by increasing the concentration of the additives their viscosity also increases. Therefore, there is a practical limit on the extent to which the levels of concentration of the additives may be increased. Taking into account this limit, the effect of the additives on the rate of evaporation has no real practical use as a method of extending the open time of water-borne latex paints. However, during the drying time investigation it materialised that for the cellulose-derived additives the level of cracking in the films decreased with increasing additive concentration.

Legislation prescribes that water-borne paints are allowed to contain between 40 and 100 g.l^{-1} of VOC depending on whether they are matte/eggshell or a gloss paint respectively. This allocation of the levels of VOC allows the use of a coalescent solvent in water-borne paints. The role of a coalescent solvent is to plasticise the latex particles, allowing a film to form below the native T_g of the constituent particles. One of the most widely used coalescent solvents is Texanol™. It was shown that in a film made of latex 223-2 with varying concentrations of Texanol™ the minimum film formation temperature was lowered from around 20 °C to 5 °C with an increase in Texanol™ concentration of 0 to 11.6 wt%. The issues with using a paint that contains even small amounts of VOC lie with associated health concerns, such as increased risk of respiratory issues in children such as asthma and/or increased risk of allergies.[154–156] The additives initially selected for their potential use as drying time extenders showed some promise when it came to reducing cracking in drying latex films. Moreover, by using optical microscopy on the films it was clear that the cellulose-derived additives reduced cracking

significantly in the dried latex 223-2 films. Unlike Texanol™ the cellulose derived additives are not classified as a VOC and they are not (so far as the writer is currently aware) associated with health concerns. These cellulose-derived additives are also produced from a natural product with most of their production deriving from materials such as cotton or sugar cane.[149] This means that the reduction in cracking observed in films containing MC and HPMC is promising from an environmental and health standpoint.

Although it was observed that the films containing the cellulose-derived additives exhibited less cracking, it was not immediately obvious why this was the case. Initially it was thought that the additives could be plasticising the latex particles, thereby acting as a traditional coalescent solvent. Initially films with varying concentration of Methylcellulose were studied with DMA in order to identify any changes in the films' T_g. However, upon analysis no such change was observed. It was therefore concluded that the additives were not acting as traditional coalescent solvents and plasticising the latex particles. A decision was therefore made to investigate the MFFT of the systems; if the additives were altering the film formation to reduce cracking in the system this would be observed through the MFFT. MFFT was studied for films with varying MC, HPMC and Pluronic Additives. As was seen in previous experiments the films containing the cellulose derived-additives showed a decrease in MFFT of around 3 °C, whereas no reduction was seen with the pluronic additive. This informed the hypothesis that the additives were operating *via* a different mechanism to reduce cracking, perhaps partial plasticisation that did not lower the T_g of the whole film or perhaps an alternative mechanism not related to the alteration of the T_g of the particle. It was necessary to observe the process on a particulate level, the chosen technique to do so was Atomic Force Microscopy *(AFM).*

Applying AFM to films containing various concentrations of the additives produced interesting results. Despite an obvious trend in the reduction of cracking between films containing no additive ,1.2 wt% Pluronic, 1.2 wt% MC and 1.2 wt% HPMC, no obvious trend in the particle structure was seen. When comparing the films containing no additive it could be seen that the particles were arranged in a

close packed array with minimal deformation and coalescence as could be expected from a film that contains a high level of cracking. When the film containing 1.2 wt% HPMC (a film with a crack free homogeneous finish) was reviewed, the result was unexpected. When a film is dried above its T_g or dried in the presence of a coalescent solvent such as Texanol™, it is expected that the particles will exhibit a high degree of deformation and coalescence. However, it a structure very similar to the film containing no additive was observed. It appeared that the particles exhibited no coalescence at all. From this result it became clear that the additives were operating *via* a different mechanism to reduce cracking over a standard coalescent solvent. It was initially hypothesised that the additives were producing a network that surrounded the particles and provided a mechanism by which intrinsic stress that evolves during the film formation process was relieved. However, as AFM only looks at the surface of a film, an alternative technique was used to investigate the particle structure throughout the entirety of the film's thickness. This technique is Small Angle X-ray Scattering *(SAXS)*.

SAXS was used to observe particle packing in a number of films containing a variety of additive concentrations. Upon analysis of the data it was clear that there was a strong agreement with the hypothesis. The interparticle separation in films containing both MC and HPMC increased proportionally with concentration, whereas, as with previous results, the Pluronic additive appeared to have no effect on particle packing. Therefore, in the presence of additive the interparticle separation is proportional to the films' reduction in cracking and hence MFFT. Without further investigation it may be hypothesised that the cellulose-derived additives are indeed producing a network around the latex particle during film formation. In samples with higher concentrations of additive the separation is increased, as is shown in in the schematic of Figure 5:16. This network is created by the additive allowing an alternative mechanism of stress relief, rather than cracking. It is hypothesised that this occurs through a number of mechanisms, or a combination of a few. The increased separation between particles as a result of the additive network surrounding the particles could allow the particles to remain slightly mobile to the very final stages of the film formation process. This

increased mobility could allow particle rearrangement as a method to alleviate stress build-up.[122] As the additive network is made up of a softer material, this could also allow deformation of the particle-additive network as a whole without the yield point of the system being reached. This therefore reduces cracking.

To conclude, the use of additives did not slow down the rate of evaporation, at least not at the concentration levels consistent with the viscosity of a useable water-borne paint. In any event, the study did indicate that these additives could act in a way to reduce cracking and hence lower the MFFT of water-borne latex paints. It has been hypothesised that the reason for this is that the additive forms a network surrounding the latex particles; this provides an alternative mechanism for stress relief other than cracking. With existing legislative pressure to reduce VOC levels combined with increasing awareness of environmental impact, the prospect of using cellulose-derived additives as an alternative to coalescent solvents in order to reduce cracking is an avenue worthy of further investigation.

Chapter 7:   Future Work

As has been discussed throughout this work, there are a number of further studies that could be carried out as a result of the findings in this thesis.

In order to study how the rate of evaporation from the latex was affected by additive concentration a gravimetric approach was used. This approach showed that additive concentration had little impact on the initial rate of evaporation at the early stages of film formation. Later in the thesis it was hypothesised that the addition of the additive created a network around the particles, reducing cracking. One of the proposed mechanisms by which this reduced cracking occurred was through increased mobility of the particles. Open time was discussed as being the property of a paint that provides the best indication of its drying performance. Due to the poor time resolution of the ASTM method for measuring open time, it was not used. If the additives are increasing particle mobility in the later stages of film formation, this could be a means of increasing the paint's open time. It was proposed that a linear drying time recorder would provide a way to observe the physical properties of a paint throughout film formation whilst at the same time avoiding the downfalls of the ASTM method for measuring open time. A future study that looks at how such physical properties change as a result of additive concentration would potentially demonstrate the extent to which additives are suitable for this purpose. Combining this physical study with an in-depth investigation into particle mobility using adaptive speckle imaging would assist in uncovering: (i) how changing the mobility of particles affects the film formation process and (ii) whether the cellulose-derived additives are in fact a viable open time extender, if not through reducing the rate of evaporation.

In order to further study how the cellulose-derived additives are reducing cracking an investigation into the stress development of these systems needs to be conducted. A potential method to study this has been outlined. In particular, that study would initially focus on the stress development profiles of films containing a number of known coalescent solvents at a number of different concentrations. Once a good understanding of this had been gathered, the effect

that each additive has on stress development could be compared. This would potentially enable a better understanding of how and why additives operate so as to reduce stress development and cracking.

SAXS was used to investigate particle packing in systems containing various concentrations of additives. In order to study the location of the additive throughout the film formation process it is proposed that real-time SAXS would need to be conducted. In order to carry out such an investigation the concentration of water at each time frame would need to be known to aid in data analysis and data fitting. To do this a technique such as NIR could be used in conjunction with a fibre optic probe to monitor water content at the point the beam passes through the sample. This spectroscopic technique could also be used in conjunction with a number of other techniques in which the water content of the drying film is not known, such as when using a linear drying time recorder.

It was found in this study that cellulose–derived additives provide a way to reduce cracking in films, with the Pluronic additive not providing any noticeable changes. A further study could be conducted into which range of cellulose-derived additives are most effective at reducing cracking. Once it is determined which chemical properties of the molecules lead to the biggest observed effect with respect to the reduction of cracking in films, attempts could then be made to create and develop an optimal film additive.

# V.	Appendix

## V. a.	Fitted Drying Data
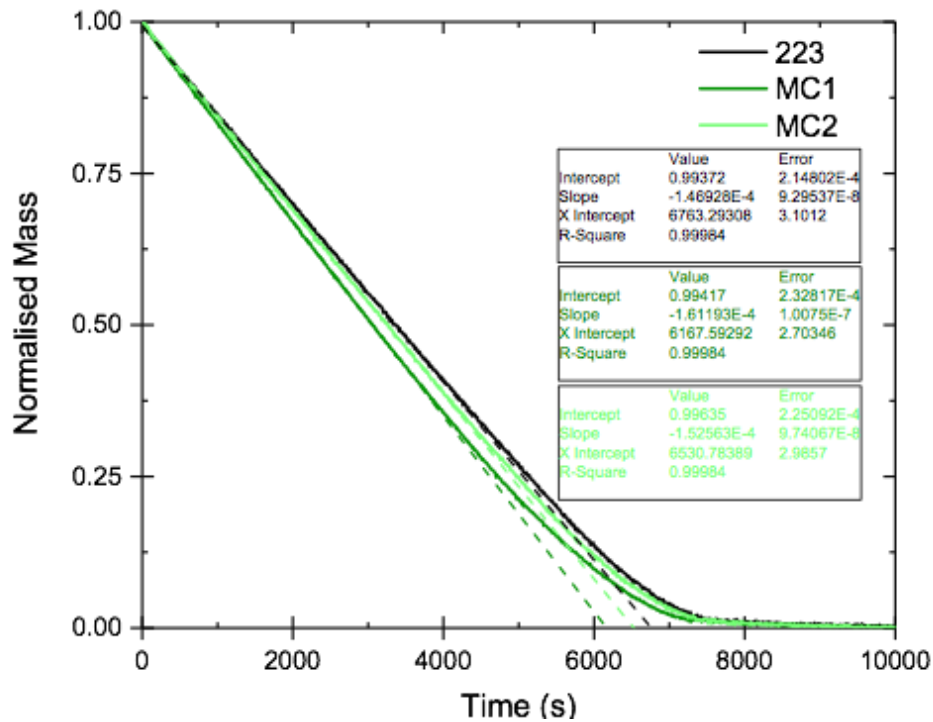
Figure 7:1 – Shows the initials constant rate period fitted for a sample of latex 223-2 with varying concentration of methylcellulose dried at 20 %RH.
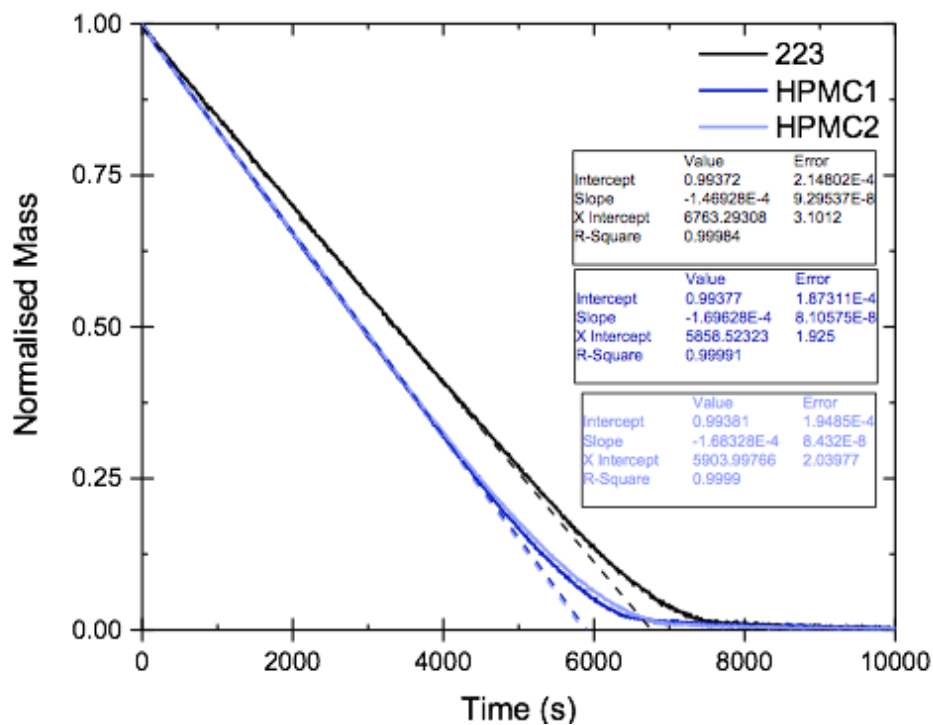
Figure 7:2 – Shows the initials constant rate period fitted for a sample of latex 223-2 with varying concentration of hydroxypropyl methylcellulose dried at 20 %RH.
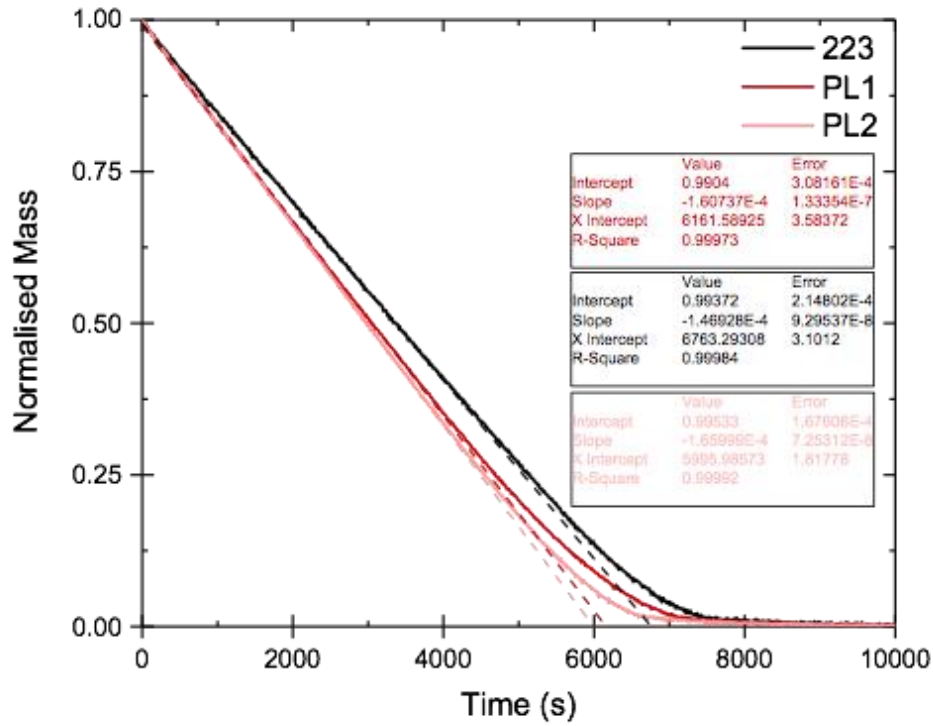
Figure 7:3 – Shows the initials constant rate period fitted for a sample of latex 223-2 with varying concentration of Pluronic PE9200 dried at 20 %RH.
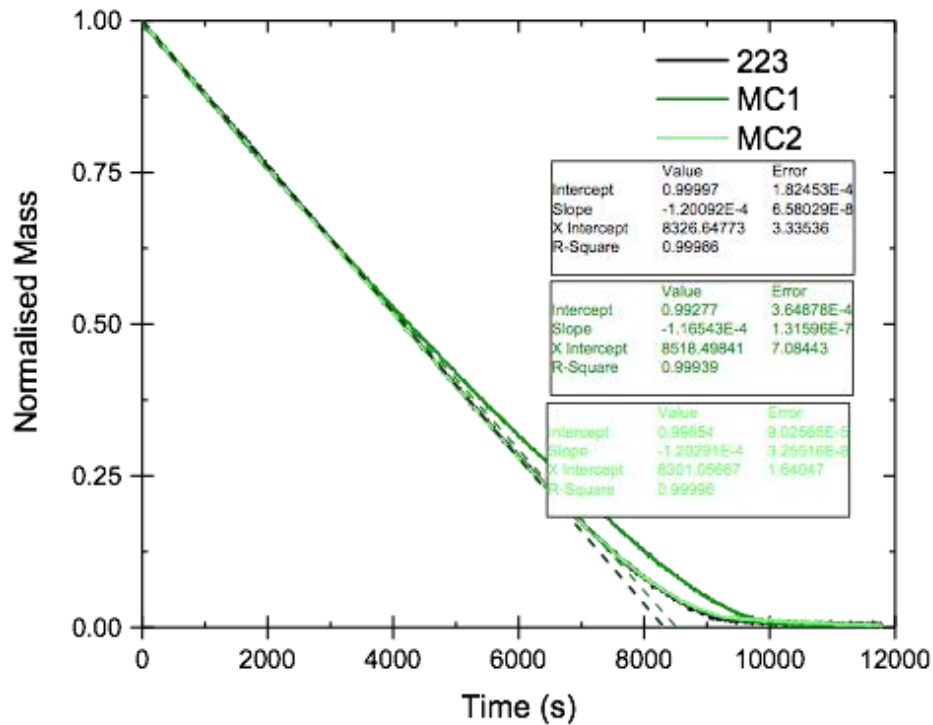
Figure 7:4 – Shows the initials constant rate period fitted for a sample of latex 223-2 with varying concentration of methylcellulose dried at 40 %RH.
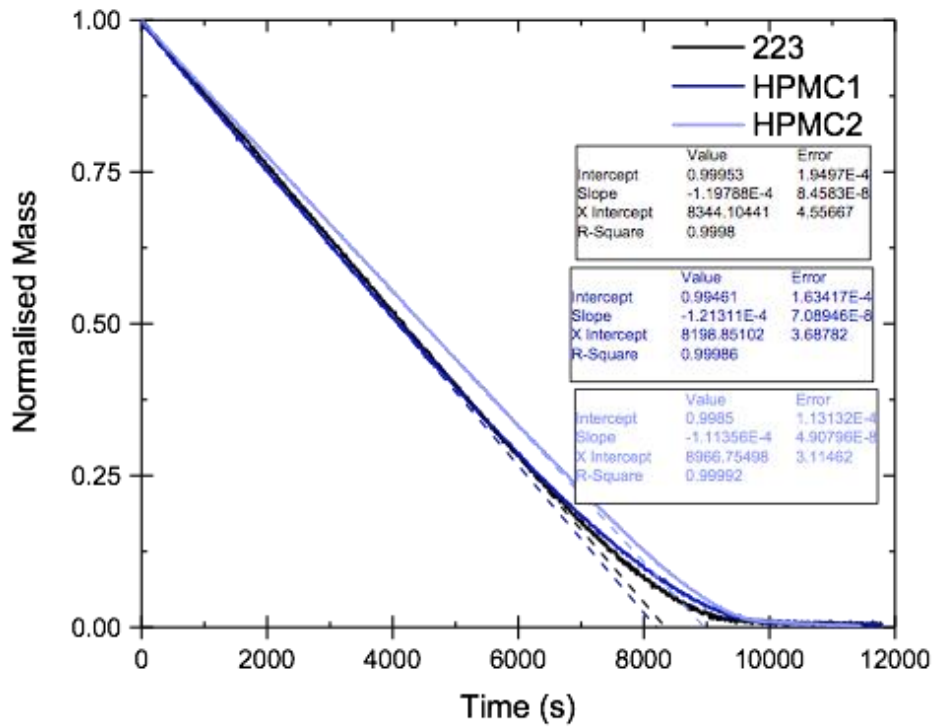
Figure 7:5 – Shows the initials constant rate period fitted for a sample of latex 223-2 with varying concentration of hydroxypropyl methylcellulose dried at 40 %RH.
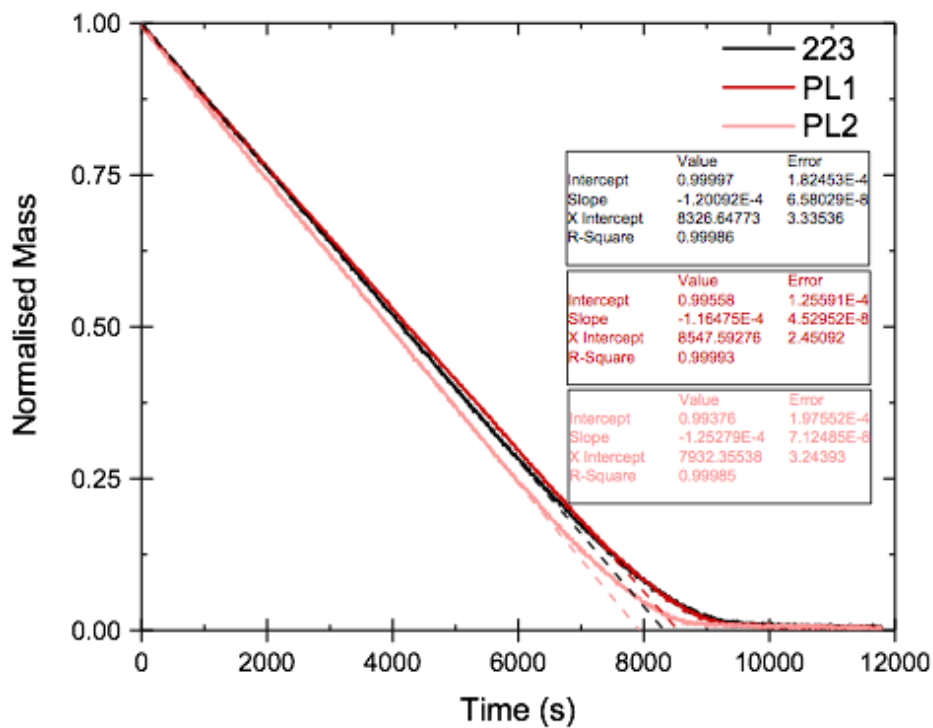
Figure 7:6 – Shows the initials constant rate period fitted for a sample of latex 223-2 with varying concentration of Pluronic PE9200 dried at 40 %RH.
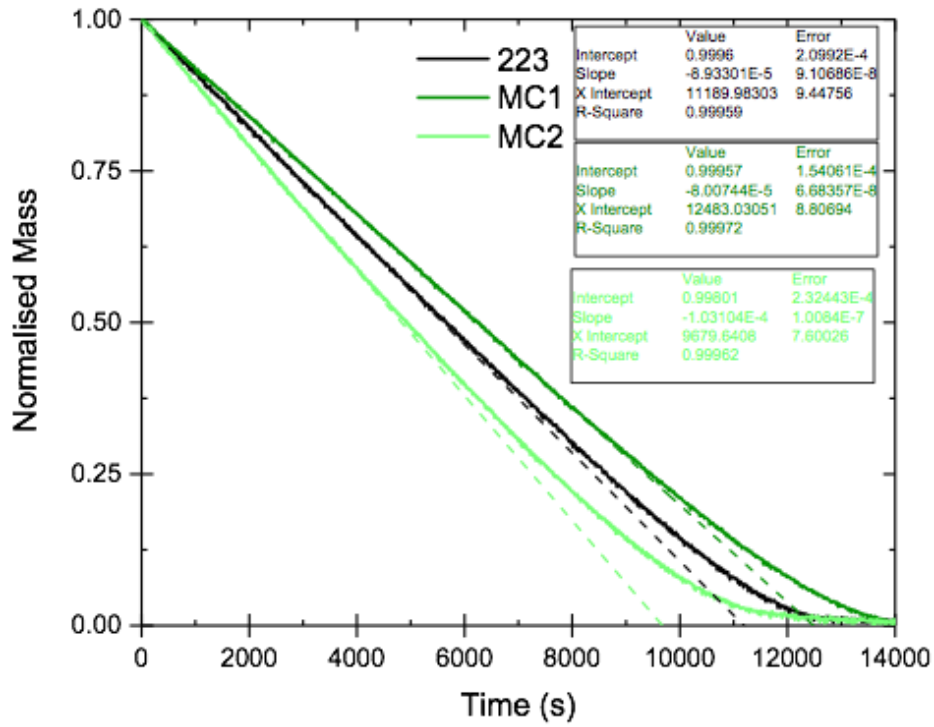
Figure 7:7 – Shows the initials constant rate period fitted for a sample of latex 223-2 with varying concentration of methylcellulose dried at 60 %RH.
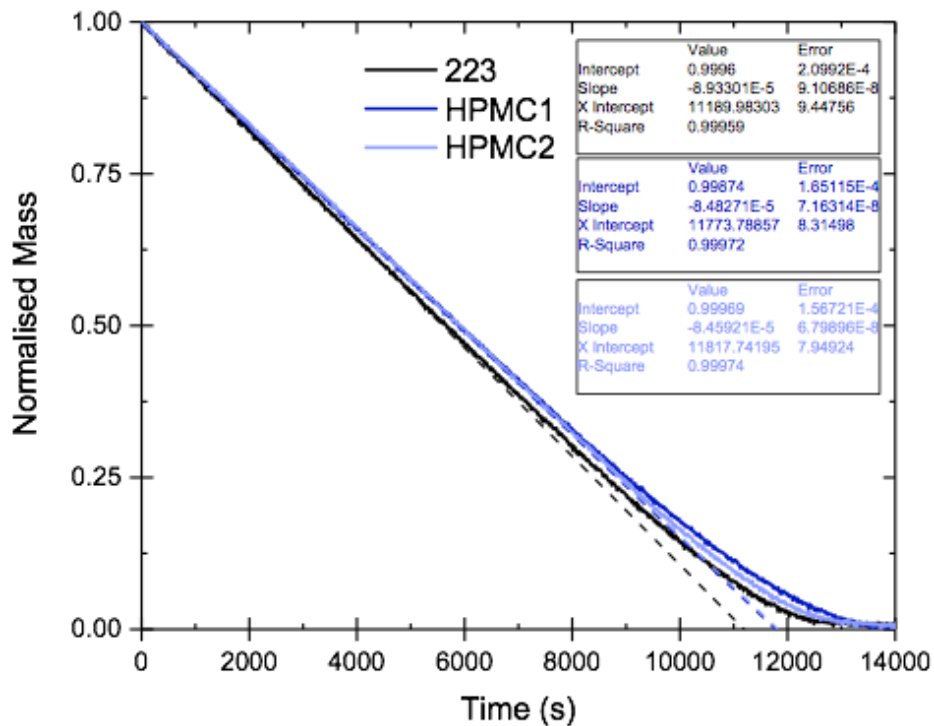
Figure 7:8 – Shows the initials constant rate period fitted for a sample of latex 223-2 with varying concentration of hydroxypropyl methylcellulose dried at 60 %RH.
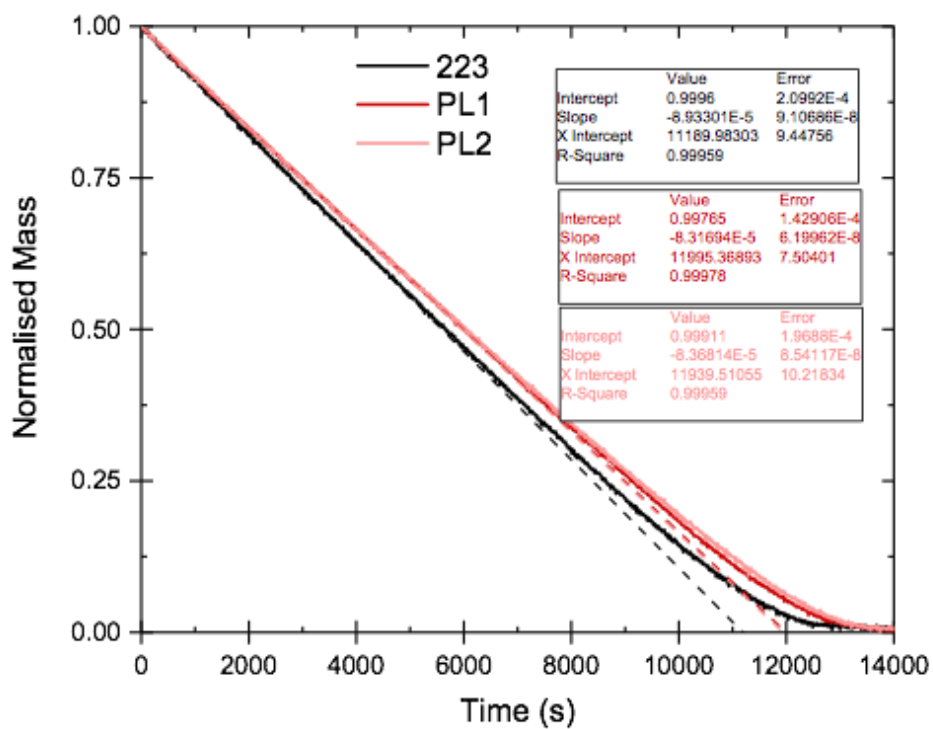
Figure 7:9 – Shows the initials constant rate period fitted for a sample of latex 223-2 with varying concentration of Pluronic PE9200 dried at 60 %RH.

V. b.   MATLAB Code

V. b. i.   cryoTEM Particle Counter

```matlab
%Clears Workspace for Start
clear

%input file name
file = ['223_13000_4.dm3']

%sets j equal to one for removing unwanted circles
j = 1;

%runs converter, need to put DM3Import into TEM folder
DM3Import(file)

%Gets scale of image to allow particles to be converted to nm from
pixels
scale = ans.yaxis.scale(1,1);

%imports raw image
imRaw = ans.image_data;

%Detects average image intensity and produces a normalization value
imAve_Col = mean(imRaw);
imAve_Tot = mean(imAve_Col);
Norm = 1.5/imAve_Tot;

%Normalizes image to allow selection of blank region
imAdjust = (imRaw*Norm) - 1;

%Select region of background
uiwait(msgbox('Select Area of Background'));
BKD = imcrop(imAdjust);

%Averages the ROI
imAve_Col = mean(BKD);
imAve_Tot = mean(imAve_Col);
Norm = 1.5/imAve_Tot;

%Normalises image with respect to selected region
imAdjust = (imAdjust*Norm) - 1;

%Select Suitable square region around particles
uiwait(msgbox('Select Rectangle arouind Particles'));
imCrop = imcrop(imAdjust);

%Stores a free hand region
imCrop_FH = imCrop;

%Displays cropped image
imshow(imCrop_FH);

%masks out unwanted background
uiwait(msgbox('Draw Around unwanted Background'));
h = imfreehand;
```

```matlab
M = ~h.createMask();
imCrop_FH(M) = 0;

%Converts image to black and white
BW = im2bw(imCrop_FH, 0.5);

%Finds circles in image
[centers, radii] = imfindcircles(BW,[40
70],'ObjectPolarity','dark',...
    'Sensitivity',0.94, 'Method','twostage', 'EdgeThreshold',0.3);

%Saves centers and radii of circles
[m, n] = size(centers);
storeCenters = centers;
storeRadii = radii;

%Resets centers and radii to allow unwanted circles to be filtered
centers = 0;
radii = 0;

%loop filters out unwanted circles
for i = 1 : m

    x = storeCenters(i, 1);
    y = storeCenters(i, 2);
    r = storeRadii(i, 1);

    [xgrid, ygrid] = meshgrid(1:size(BW,2), 1:size(BW,1));

    mask = ((xgrid-x).^2 + (ygrid-y).^2) <= r.^2;

    values = BW(mask);

    Average(i,:) = mean(values);

    if Average(i,1) < 0.35 && Average(i,1) > 0.02

        AdjCenters(j, 1) = x;
        AdjCenters(j, 2) = y;
        AdjRadii(j, 1) = r;

        j = j + 1;
    end
end

%Shows circles found before unwanted circles have been filtered out
imshow(imCrop);
centers = storeCenters;
radii = storeRadii;
h = viscircles(centers,radii);

%Pauise and clears old image and circles
pause(4);
close all

%Shows circles after un wanted circles have been filtered
centers = AdjCenters;
radii = AdjRadii;
```

```matlab
imshow(imCrop);
h = viscircles(AdjCenters, AdjRadii);

%Converts circles to nm
Output = radii * scale;
```

V. b. ii.   cryoTEM Particle Circularity

```
%Clears Workspace for Start
clear

%input file name
file = ['223.jpg'];

%Converts File to an array for image analysis
img = imread(file);

%Display cropped image
imshow(img)

%Select Suitable square region around particle for circularity
analysis
uiwait(msgbox('Select Rectangle around Particles'));
imCrop = imcrop(img);

%Display cropped image
imshow(imCrop)

%Converts image to black and white
BW = im2bw(imCrop, 0.575);

%Finds circles in image
[centers, radii] = imfindcircles(BW,[40
70],'ObjectPolarity','dark',...
    'Sensitivity',0.94, 'Method','twostage', 'EdgeThreshold',0.3);

%Saves centres and radii of circles
[m, n] = size(centers);
storeCenters = centers;
storeRadii = radii;

%Shows circles found before unwanted circles have been filtered out
imshow(imCrop);
centers = storeCenters;
radii = storeRadii;
h = viscircles(centers,radii);

%Retrieves the center of the fitted circle
x = centers(1,1);
y = centers(1,2);

%Crops the image around the particle
imCrop2 = imcrop(imCrop,[(x-(1.1*radii)) (y-(1.1*radii)) (2.2*radii)
(2.2*radii)]);

%Length of sides
L = 2.2*radii;
%Number of Steps
Step = 3;
%Step Size
SS = L/Step;

%Displays the image
    imshow(imCrop2)
```

```matlab
    hold on

for i = 0 : Step

    %Sets the two sets off line coordinates
    Y_A = [(0+(SS*i)) (L-(SS*i))];
    X_A = [0 L];

    Y_B = [0 L];
    X_B = [(L-(SS*i)) (0+(SS*i))];

    %Plots Fist line and promts to select the length
    plot(X_A,Y_A,'Color','r','LineWidth',2)

    %User selects line
    [xA,yA] = getline();

    %Calculation for line length
    DxA = xA(2,1) - xA(1,1);
    DyA = yA(2,1) - yA(1,1);

    LengthA = sqrt((DxA^2)+(DyA^2));

    Plots the second line and promts to selct the length
    plot(X_B,Y_B,'Color','b','LineWidth',2)

    %User selects line
    [xB,yB] = getline();

    %Calculation for line length
    DxB = xB(2,1) - xB(1,1);
    DyB  = yB(2,1) - yB(1,1);

    LengthB = sqrt((DxB^2)+(DyB^2));

    %Stores line lengths in an array
    LL(i+1,1) = LengthA;
    LL(i+1,2) = LengthB;
    Ratio(i+1,1) = (min(LL(i+1,:)))/(max(LL(i+1,:)));

end

hold off

%Calculates the Ratio Between the Min and Max length
Min = min(LL);
Max = max(LL);

RatioT = Min/Max
Rave = mean(Ratio)
```

V. b. iii.   Stress Development

```matlab
%Clear workspace before starting
clear

%set webcam for use
cam = webcam;

%take image for spatial calibration
calib = snapshot(cam);
fig1 = figure('Name', 'Select Calibration Region', 'NumberTitle',
'off');
set(fig1, 'Position', [100, 200, 1700, 600])
imshow(calib);
hold on

%select region for spatial calibration
[xc,yc] = getline(fig1);

xc1 = xc(1);
xc2 = xc(2);
yc1 = yc(1);
yc2 = yc(2);

%calulate length of claibration
caliblength = (((xc2-xc1).^2)+((yc2-yc1).^2)).^0.5;

%keeps line up to help user inpuit claibration length
line([xc1,xc2],[yc1,yc2]);

prompt = {'Calibration Length (mm):'};
dlg_title = 'Image Aquistion Parameters';
num_lines = 1;
def = {'20'};
input = inputdlg(prompt,dlg_title,num_lines,def);

%takes user input and converts to input
cl = str2num(input{1});

%calibration factor
CF = cl/caliblength;

%set parameters for image aquisition
prompt = {'Number of Frames:','Frame Rate:'};
dlg_title = 'Image Aquistion Parameters';
num_lines = 1;
def = {'20','1'};
input = inputdlg(prompt,dlg_title,num_lines,def);

%number of frames
Fr = str2num(input{1});

%Aquisition rate
FR = str2num(input{2});

%insert painted substrate here
uiwait(msgbox('Please Insert Sample Now', 'Warning', 'warn'));
```

```matlab
%previews image used for line selection and image calibration camera
for calibration
ROI = snapshot(cam);


fig = figure('Name', 'Select Region of Interest', 'NumberTitle',
'off');
set(fig, 'Position', [100, 200, 1700, 600])
imshow(ROI);


[xn,yn] = getline(fig);

%Select line width in Pixels and start and end coordinates
W = 20;

%line coordinates
x1 = xn(1);
x2 = xn(2);
y1 = yn(1);
y2 = yn(2);

%length of line for line profile
yn = (y2 - y1);

%Calulates angle of line from x axis
Theta = atan((x2-x1)/(y2-y1));

%loop for drawing area for lineprofiling
for i = 1 : W+1;
    f = (W/2) - (i-1);

    %Modified Coordinates using angle of line
    x1_2 = x1 + (f*cos(Theta));
    x2_2 = x2 + (f*cos(Theta));
    y1_2 = y1 - (f*sin(Theta));
    y2_2 = y2 - (f*sin(Theta));

    %Line start and line end
    A = [x1_2 x2_2];
    B = [y1_2 y2_2];

    %Plot line on image
    line(A,B);
end

pause(1);
close('Select Region of Interest');

%start loop for image aquisition
for j = 1 : Fr

    %Takes image from camera
    img = snapshot(cam);

    %Converst image to grayscale for simplification
    GS = rgb2gray(img);

    %puts all images into an array of dimensions (:,:,Frame number)
    F(:,:, j) = GS;
```

```matlab
    %create an array (d) of size k with the information in the image
difference
    d(:, :, j) = imabsdiff(F(:, :, 1), F(:, :, j));

    %sets a threshold on the grey level
    thresh = graythresh(d);
    bw = (d >= thresh * 300);

    % line for taking line profile for deflection measurement
     for i = 1 : W+1;
            f = (W/2) - (i-1);

            %Modified Coordinates using angle of line
            x1_2 = x1 + (f*cos(Theta));
            x2_2 = x2 + (f*cos(Theta));
            y1_2 = y1 - (f*sin(Theta));
            y2_2 = y2 - (f*sin(Theta));

            %Line start and line end
            A = [x1_2 x2_2];
            B = [y1_2 y2_2];

            %Now run lineprofile on each line plotted
            r = improfile(GS,A,B);

            %Save lineprofile data to an array
                y = r([1:yn],:,1);
                Y(:,i) = y;
                x = 1:yn;

     end

    %Average lineprofile data
    Ybar = mean(Y, 2);

    %Finds peaks in intensity plot(used to locte shim position)
    [pks,locs] = findpeaks(Ybar,'MinPeakProminence',50);

    %h is shim position, H is deflection, J is time elapsed
    h(j,:) = locs*CF;
    H(j,:) = h(j,:)- h(1,:);
    J(j,:) = (j-1)/FR;

    fig = figure(1);
    set(fig, 'Position', [100, 200, 1700, 600])
    subplot(4,6,[13:18]);
    plot(x,Ybar);
    subplot(4,6,[19:24]);
    scatter(J, H, 100, 'x', 'r')
    subplot(4,6,[(1:3),(7:9)]);
    imshow(bw(:, :, j));
    subplot(4,6,[(4:6),(10:12)]);
    imshow(img);

    %Used to set the aquisition rate (FPS)
    pause(1/FR);
end
```

VI.   References

1   H. Bocherens, D. G. Drucker, D. Billiou, J. M. Geneste and J. van der Plicht, *J. Hum. Evol.*, 2006, **50**, 370–376.

2   H. Valladas, J. Clottes, J. M. Geneste, M. a Garcia, M. Arnold, H. Cachier and N. Tisnérat-Laborde, *Nature*, 2001, **413**, 479.

3   J. Clottes, *Antiquity*, 1995, **70**, 276–288.

4   M. P. Colombini, A. Ceccarini and A. Carmignani, *J. Chromatogr. A*, 2002, **968**, 79–88.

5   USRE3597, 1869.

6   US222995, 1879.

7   F. Hoffmann, *Angew. Chemie*, 1912, **29**, 1462.

8   254 672, 1912.

9   A. Tiwari, A. Galanis and M. Soucek, *Biobased and Environmentally Benign Coatings*, 2016.

10   A. Hutchinson, *Big Ideas: 100 Modern Inventions That Have Transformed Our World*, Hearst Books, 2009.

11   S. G. Croll, History of Paint Science and Technology, https://www.ndsu.edu/fileadmin/croll/HistoryofPaintSGC.pdf, (accessed 27 April 2020).

12   P. Atkins and J. De Paula, *Atkins' Physical Chemistry*, Oxford University Press, 9th edn., 2010.

13   D. J. Shaw, *Introduction to Colloid and Surface Chemistry: Fourth Edition*, 2013.

14   R. E. Dillon, L. A. Matheson and E. B. Bradford, *J. Colloid Sci.*, 1951, **6**, 108–117.

15   G. L. Brown, *J. Polym. Sci.*, 1956, **22**, 423–434.

16   D. P. Sheetz, *J. Appl. Polym. Sci.*, 1965, **9**, 3759–3773.

17   R. D. Deegan, O. Bakajin and T. F. Dupont, *Nature*, 1997, **389**, 827–829.

18   T. Kanai and T. Sawada, *Langmuir*, 2009, **25**, 13315–13317.

19   H. Fudouzi, *J. Colloid Interface Sci.*, 2004, **275**, 277–283.

20   A. F. Routh, *Rep. Prog. Phys.*, 2013, **76**, 046603.

21   J. L. Keddie and A. F. Routh, *Fundamentals of Latex Film Formation*, Springer Laboratory, 2010.

22   P. a Steward, J. Hearn and M. C. Wilkinson, *Adv. Colloid Interface Sci.*, 2000, **86**, 195–267.

23   J. L. Keddie, *Mater. Sci. Eng.*, 1997, **21**, 101–170.

24   S. G. Croll, *J. Coatings Technol.*

25   S. G. Croll, *J. Coatings Technol. Res.*

26   J. L. Keddie, P. Meredith, R. a. L. Jones and a. M. Donald, *Macromolecules*,

1995, **28**, 2673–2682.

27   F. Molenaar, T. Svanholm and a. Toussaint, *Prog. Org. Coatings*, 1997, **30**, 141–158.

28   L. Brunel, a Brun, P. Snabre and L. Cipelletti, *Opt. Express*, 2007, **15**, 15250–15259.

29   A. M. Donald, *Curr. Opin. Colloid Interface Sci.*, 1998, **3**, 143–147.

30   J. W. Vanderhoff, E. B. Bradford and C. W.K., *J. Polym. Sci.*, 1973, **41**, 155–174.

31   A. Herzog Cardoso, C. A. P. Leite, M. E. D. Zaniquelli and F. Galembeck, *Colloids Surfaces A Physicochem. Eng. Asp.*, 1998, **144**, 207–217.

32   T. L. Crowley, a. R. Sanderson, J. D. Morrison, M. D. Barry, a. J. Morton-Jones and a. R. Rennie, *Langmuir*, 1992, **8**, 2110–2123.

33   Y. Chevalier, C. Pichot, C. Graillat, M. Joanicot, K. Wong, J. Maquet, P. Lindner and B. Cabane, *Colloid Polym. Sci.*, 1992, **270**, 806–821.

34   S. T. Eckersley and a. Rudin, *Prog. Org. Coatings*, 1994, **23**, 387–402.

35   J. L. Keddie, P. Meredith, R. A. L. Jones and A. M. Donald, *Macromolecules*, 1995, **28**, 2673–2682.

36   J. L. Keddie and A. . Routh, *Fundamentals of Latex Film Formation*, Springer Laboratory, 1st edn., 2010.

37   Y. Ma, H. T. Davis and L. E. Scriven, *Prog. Org. Coatings*, 2005, **52**, 46–62.

38   C. C. Roberts and L. F. Francis, *J. Coatings Technol. Res.*, 2013, **10**, 441–451.

39   C. Carelli, F. Déplace, L. Boissonnet and C. Creton, *J. Adhes.*, 2007, **83**, 491–505.

40   K. C. Wood, H. F. Chuang, R. D. Batten, D. M. Lynn and P. T. Hammond, *Proc. Natl. Acad. Sci. U. S. A.*, 2006, **103**, 10207–10212.

41   A. N. Zelikin, *ACS Nano*, 2010, **4**, 2494–2509.

42   Q. Xu, Y. Lv, C. Dong, T. S. Sreeprased, A. Tian, H. Zhang, Y. Tang, Z. Yu and N. Li, *Nanoscale*, 2015, **7**, 10883–10895.

43   M. Schulz and J. L. Keddie, *Soft Matter*, 2018, **14**, 6181–6197.

44   J. C. H. Hwa, *J. Polym. Sci. Part A Gen. Pap.*, 1964, **2**, 785–796.

45   V. Divry, a. Gromer, M. Nassar, C. Lambour, D. Collin and Y. Holl, *J. Phys. Chem. B*, 2016, **120**, 6791–6802.

46   M. Nassar, a. Gromer, D. Favier, F. Thalmann, P. Hébraud and Y. Holl, *Soft Matter*, 2017, **13**, 9162–9173.

47   F. Routh and W. B. Russel, *Aiche J.*, 2002, **48**, 917–918.

48   A. F. Routh and W. B. Russel, *Langmuir*, 1999, **15**, 7762–7773.

49   ASTM International, 2016, 11, 3–5.

50   Z. Zong, S. Wall, Y.-Z. Li, J. Ruiz, H. Adam, C. Badre and F. Trezzi, *Prog. Org. Coatings*, 2011, **72**, 115–119.

51   US527380, 1993.

52   US6303189, 2001.

53   H. M. Van Der Kooij, M. De Kool, J. Van Der Gucht and J. Sprakel, *Langmuir*, 2015, **31**, 4419–4428.

54   X. Chen, S. Fischer and Y. Men, *Langmuir*, 2011, **27**, 12807–14.

55   European Parliament and Council, *Off. J. Eur. Union*, 2004, 10.

56   V. Lazarus and L. Pauchard, *Soft Matter*, 2011, **7**, 2552–2559.

57   S. Bucklow, *Stud. Conserv.*, 1999, **44**, 233–243.

58   W. P. Lee and A. F. Routh, *Langmuir*, 2004, **20**, 9885–9888.

59   R. C. Chiu, T. J. Garino and M. J. Cima, *J. Am. Ceram. Soc.*, 1993, **76**, 2257–2264.

60   R. C. H. Chiu and M. J. Cima, *J. Am. Ceram. Soc.*, 1991, **6**, 234–243.

61   K. B. Singh and M. S. Tirumkudulu, *Phys. Rev. Lett.*, 2007, **98**, 1–4.

62   Z. Néda, K. T. Leung, L. Józsa and M. Ravasz, *Phys. Rev. Lett.*, 2002, **88**, 955021–955024.

63   M. Despotovic and M. Babic, *Energy Effic.*, 2018, **11**, 877–891.

64   C. Geipel and P. Stephan, *Appl. Therm. Eng.*, 2005, **25**, 2578–2590.

65   J. Domnick, D. Gruseck, K. Pulli, a. Scheibe, Q. Ye and F. Brinckmann, *Chem. Eng. Process. Process Intensif.*, 2011, **50**, 495–502.

66   J. L. Keddie, P. Meredith, R. A. L. Jones and A. M. Donald, *ACS Symp. Ser.*, 1996, **648**, 332–348.

67   A. F. Routh and W. B. Russel, *Ind. Eng. Chem. Res.*, 2001, **40**, 4302–4308.

68   W. P. Lee and A. F. Routh, *Ind. Eng. Chem. Res.*, 2006, **45**, 6996–7001.

69   a. Tzitzinou, J. L. Keddie, J. M. Geurts, a. C. I. a. Peters and R. Satguru, *Macromolecules*, 2000, **33**, 2695–2708.

70   E. R. Dufresne, E. I. Corwin, N. A. Greenblatt, J. Ashmore, D. Y. Wang, A. D. Dinsmore, J. X. Cheng, X. S. Xie, J. W. Hutchinson and D. A. Weitz, *Phys. Rev. Lett.*, , DOI:10.1103/PhysRevLett.91.224501.

71   W. Man and W. B. Russel, *Phys. Rev. Lett.*, 2008, **100**, 1–4.

72   B. Lawn, *Fracture of Brittle Solids*, 1993.

73   P. R. Sperry, B. S. Snyder, M. L. O'Dowd and P. M. Lesko, *Langmuir*, 1994, **10**, 2619–2628.

74   F. Dobler, T. Pith, M. Lambla and Y. Holl, *J. Colloid Interface Sci.*, 1992, **152**, 1–11.

75   D. C. Sherrington, *React. Funct. Polym.*, 1998, **36**, 104–105.

76   *Nat. Photonics*, 2009, **3**, 361.

77   P. Atkins and J. De Paula, *Chemistry (Easton).*, 2009, 430–468.

78   K. I. Dragnevski and A. M. Donald, *Colloids Surfaces A Physicochem. Eng. Asp.*, 2008, **317**, 551–556.

79   T. F. Protzman and G. L. Brown, *J. Appl. Polym. Sci.*, 1960, **4**, 81–85.

80   ASTM International, 2013, 98–100.

81   K. Price, W. Wu, K. Wood, S. Kong, A. McCormick and L. Francis, *J. Coatings Technol. Res.*, 2014, **11**, 827–839.

82   E. K. Rideal, *J. Phys. Chem.*, , DOI:10.1021/j150258a011.

83   V. K. La Mer and T. W. Healy, *Science (80-.).*, , DOI:10.1126/science.148.3666.36.

84   G. N. Brink, A. P. Wandel, N. H. Hancock and S. Pather, *Exp. Therm. Fluid Sci.*, , DOI:10.1016/j.expthermflusci.2017.05.007.

85   A. P. Wandel, G. N. Brink, N. H. Hancock and S. Pather, *Exp. Therm. Fluid Sci.*, , DOI:10.1016/j.expthermflusci.2017.05.006.

86   M. Tsuji, H. Nakahara, Y. Moroi and O. Shibata, *J. Colloid Interface Sci.*, , DOI:10.1016/j.jcis.2007.10.047.

87   L. Roussel and N. Atrux-Tallau, in *Treatment of Dry Skin Syndrome*, Spiringer, 2012, pp. 473–480.

88   6,322,829 B1, 2001.

89   K. W. McCreight, R. Stockl and K. S. Seo, *Prog. Org. Coatings*, 2011, **72**, 102–108.

90   7119133 B2, 2003.

91   349225 2A, 1963.

92   20110166287 A1, 2011.

93   R. H. Stokes, R. a. Robinson, R. H. Stples and R. a. Robinson, *J. Am. Chem. Soc.*, 1948, **70**, 1870–1878.

94   Z. Gu and P. Alexandridis, *J. Dispers. Sci. Technol.*, , DOI:10.1081/DIS-200027312.

95   C. Fiorio, *Riv. Ist. Sieroter. Ital.*, 1948, **23**, 53–66.

96   P. Pichniarczyk and G. Malata, *J. Therm. Anal. Calorim.*, 2017, **128**, 771–778.

97   P. Pichniarczyk and M. Niziurska, *Constr. Build. Mater.*, 2015, **77**, 227–232.

98   P. Pichniarczyk, *Procedia Eng.*, 2015, **108**, 220–230.

99   S. Kiil, *Prog. Org. Coatings*, 2006, **57**, 236–250.

100   D. Bouyer, K. Philippe, S. Wisunthorn, C. Pochat-Bohatier and C. Dupuy, *Dry. Technol.*, 2009, **27**, 59–70.

101   T. M. Fieback and R. Span, *Energy Procedia*, 2014, **61**, 1501–1504.

102   M. S. Tirumkudulu and W. B. Russel, *Langmuir*, 2005, **21**, 4938–4948.

103   F. T. Carter, R. M. Kowalczyk, I. Millichamp, M. Chainey and J. L. Keddie, *Langmuir*, 2014, **30**, 9672–9681.

104   *Qual. Assur.*, 1996, 80, 19428–19428.

105   ASTM International, 2013, 1–4.

106   E. Todorovich, A. L. Dai Pra, L. I. Passoni, M. Vázquez, E. Cozzolino, F. Ferrara and G. Bioul, *J. Real-Time Image Process.*, 2016, **11**, 535–545.

107   a. Brun, H. Dihang and L. Brunel, *Prog. Org. Coatings*, 2008, **61**, 181–191.

108   M. C. Péron, S. Guyot and E. Deléchelle, *Opt. Laser Technol.*, 2007, **39**, 40–45.

109 J. Yoon, K. Lee and Y. Park, .

110 J. F. Asmus, *Mater. Charact.*, 1992, **29**, 119–128.

111 Y. Wang and M. a. Winnik, *Macromolecules*, 1990, **23**, 4731–4732.

112 F. Boulogne, F. Giorgiutti-Dauphiné and L. Pauchard, *Oil Gas Sci. Technol.*, 2014, **69**, 397–404.

113 K. Piroird, V. Lazarus, G. Gauthier, a. Lesaine, D. Bonamy and C. L. Rountree, *Epl*, 2016, **113**, 1–6.

114 S. Rakers, L. F. Chi and H. Fuchs, *Langmuir*, 1997, **13**, 7121–4.

115 W. L. Ng, C. K. Chua and Y. Shen, *Prog. Polym. Sci.*, 2019, 101145.

116 H. a. Edelhauser, *J. Polym. Sci. Part C Polym. Symp.*, 1969, **27**, 291–309.

117 B. R. Vijayendran, T. Bone and C. Gajria, *J. Appl. Polym. Sci.*, 1981, **26**, 1351–1359.

118 B. R. Vijayendran, L. C. Sawyer and T. Bone, *J. Dispers. Sci. Technol.*, 1982, **3**, 81–97.

119 D. Juhué and J. Lang, *Macromolecules*, 1994, **27**, 695–701.

120 D. Juhué, Y. Wang, J. Lang, O. -M Leung, M. C. Goh and M. A. Winnik, *J. Polym. Sci. Part B Polym. Phys.*, 1995, **33**, 1123–1133.

121 D. Juhué and J. Lang, *Langmuir*, 1993, **9**, 792–796.

122 L. Goehring, W. J. Clegg and A. F. Routh, *Phys. Rev. Lett.*, 2013, **110**, 1–5.

123 C. Petersen, C. Heldmann and D. Johannsmann, *Langmuir*, 1999, **15**, 7745.

124 A. Bouchaudy and J. B. Salmon, *Soft Matter*, 2019, **15**, 2768–2781.

125 M. S. Tirumkudulu and W. B. Russel, *Langmuir*, 2004, **20**, 2947–2961.

126 L. F. Francis, A. V. M. C. Cormick, D. M. Vaessen and E. K. Company, *J. Mater. Sci.*, 2002, **37**, 4717.

127 CORCORAN EM, *J Paint Technol*, 1969, **41**, 635–640.

128 Young's Modulus of Elasticity for Metals and Alloys, https://www.engineeringtoolbox.com/young-modulus-d_773.html, (accessed 15 April 2020).

129 H. Lei, L. F. Francis, W. W. Gerberich and L. E. Scriven, *AIChE J.*, 2002, **48**, 437–451.

130 J. Fairclough, J. Desbrières and V. G. Babak, *Polym.*, 2006, **55**, 1177–1183.

131 I. Martín-Fabiani, D. K. Makepeace, P. G. Richardson, J. Lesage De La Haye, D. A. Venero, S. E. Rogers, F. D'Agosto, M. Lansalot and J. L. Keddie, *Langmuir*, , DOI:10.1021/acs.langmuir.8b04251.

132 K. D. Kim, L. H. Sperling, A. Klein and G. D. Wignall, *Macromolecules*, , DOI:10.1021/ma00069a032.

133 J. N. Yoo, S. L. H. Sperling, C. J. Glinka and A. Kleina, *Macromolecules*, , DOI:10.1021/ma00010a036.

134 J. N. Yoo, L. H. Sperling, A. Klein and C. J. Glinka, *Macromolecules*, , DOI:10.1021/ma00219a017.

135   S. D. Kim, A. Klein and L. H. Sperling, *Polym. Adv. Technol.*, , DOI:10.1002/pat.165.

136   N. Dingenouts and M. Ballauff, *Macromolecules*, 1998, **31**, 7423–7429.

137   N. Dingenouts and M. Ballauff, *Langmuir*, 1999, **15**, 3283–3288.

138   N. Dingenouts, C. Norhausen and M. Ballauff, *Macromolecules*, , DOI:10.1021/ma980985t.

139   S. Förster, A. Timmann, C. Schellbach, A. Frömsdorf, A. Kornowski, H. Weller, S. V. Roth and P. Lindner, *Nat. Mater.*, , DOI:10.1038/nmat1995.

140   E. A. Sulyanova, A. Shabalin, A. V. Zozulya, J. M. Meijer, D. Dzhigaev, O. Gorobtsov, R. P. Kurta, S. Lazarev, U. Lorenz, A. Singer, O. Yefanov, I. Zaluzhnyy, I. Besedin, M. Sprung, A. V. Petukhov and I. A. Vartanyants, *Langmuir*, , DOI:10.1021/la504652z.

141   J. C. Thomas, *J. Colloid Interface Sci.*, 1987, **117**, 187–192.

142   E. B. Mock, H. De Bruyn, B. S. Hawkett, R. G. Gilbert and C. F. Zukoski, *Langmuir*, 2006, **22**, 4037–4043.

143   E. D. Sudol and J. W. Vanderhoff, *J. Polym. Sci. A Polym. Chem*, 1986, **24**, 3515–3527.

144   C. J. Ferguson, G. T. Russell and R. G. Gilbert, *Polymer (Guildf).*, 2002, **43**, 6371–6382.

145   Y. Men, X. Li, J. Rieger, F. Reinhold, X. Chen, S. Fischer and V. Boyko, *Lnagmuir*, 2011, **27**, 8458–8463.

146   L. Malherbe and C. Mandin, *Atmos. Environ.*, 2007, **41**, 6322–6330.

147   G. J. Raw, S. K. D. Coward, V. M. Brown and D. R. Crump, *J. Expo. Anal. Environ. Epidemiol.*, , DOI:10.1038/sj.jea.7500363.

148   N. Santiago Sánchez, S. Tejada Alarcón, R. Tortajada Santonja and J. Llorca-Pórcel, *Sci. Total Environ.*, 2014, **485–486**, 720–725.

149   J. G. Vieira, G. D. C. Oliveira, G. R. Filho, R. M. N. De Assunção, C. D. S. Meireles, D. A. Cerqueira, W. G. Silva and L. A. D. C. Motta, *Carbohydr. Polym.*, 2009, **78**, 779–783.

150   J. George, R. Kumar, V. A. Sajeevkumar, K. V. Ramana, R. Rajamanickam, V. Abhishek, S. Nadanasabapathy and Siddaramaiah, *Carbohydr. Polym.*, , DOI:10.1016/j.carbpol.2014.01.057.

151   S. Hu, J. Rieger, Y. Lai, S. V. Roth, R. Gehrke and Y. Men, *Macromolecules*, 2008, **41**, 5073–5076.

152   J. L. Koenig and J. P. Bobiak, *Macromol. Mater. Eng.*, 2007, **292**, 801–816.

153   S. Cho, H. Chung, Y. A. Woo and H. J. Kim, *Bull. Korean Chem. Soc.*, 2005, **26**, 115–118.

154   V. M. Brown, D. R. Crump and P. T. C. Harrison, *Environ. Sci. Process. Impacts*, 2013, **15**, 2164–2171.

155   M. Hulin, D. Caillaud and I. Annesi-Maesano, *Indoor Air*, 2010, **20**, 502–514.

156   M. J. Mendell, *Indoor Air*, 2007, **17**, 259–277.